Pedogenesis and Anthropedogenesis on the Southern Piedmont

by

Allan Roy Bacon

University Program in Ecology
Duke University

Date:_____

Approved:

_____
Daniel deB. Richter, Supervisor

_____
Paul R. Bierman

_____
Emily S. Bernhardt

_____
Curtis J. Richardson

Dissertation submitted in partial fulfillment of
the requirements for the degree of Doctor of Philosophy in the
University Program in Ecology in the Graduate School
of Duke University

2014

ABSTRACT

Pedogenesis and Anthropedogenesis on the Southern Piedmont

by

Allan Roy Bacon

University Program in Ecology
Duke University

Date:_____

Approved:

_____
Daniel deB. Richter, Supervisor

_____
Paul R. Bierman

_____
Emily S. Bernhardt

_____
Curtis J. Richardson

An abstract of a dissertation submitted in partial fulfillment of the requirements for the degree of Doctor of Philosophy in the University Program in Ecology in the Graduate School of Duke University

2014

Abstract

This dissertation investigates "pedogenesis" (soil formation and change over multi-millennial timescales with minimal human impact) and "anthropedogenesis" (centurial and decadal soil formation and change with increased human influence) in the Southern Piedmont physiographic region in the southeastern United States. First, we combine analyses of meteoric beryllium-10 (^{10}Be) and ^{9}Be mass balance in an upland Ultisol to demonstrate Southern Piedmont soils have been forming and changing at Earth's surface for much, if not all, of the Quaternary; considerably longer than previously thought. Next, we explore how the widespread anthropogenic activity of agricultural land abandonment followed by reforestation in the region has altered these ancient soils over centuries and decades. We utilize traditional soil analyses alongside iron stable isotope measurements in a pair of Southern Piedmont Ultisols to demonstrate that one century of reforestation significantly alters the coupled cycling of carbon and iron in these subsoils. Finally, we analyze over 50 years of longitudinal data from the Calhoun soil ecosystem experiment to show that decadal trends in biomass nutrient demands following agricultural land abandonment lead to dynamic soil change that greatly influences the ability of these Southern Piedmont ecosystems to retain macronutrients.

Dedication

To Jessica – All adventures, opportunities, and challenges...Together.

Contents

List of Tables

List of Figures

Acknowledgements

Paul Heine and Wes Willis. Without your sage analytical guidance and jovial companionship A205 and A204 would have been lonely and dark.

Dave Cass, Taichi Natake, Krista Shipley, and Ashley Jernigan. I admire your attention to detail and unwavering quest for analytical perfection.

The University of Vermont Cosmogenic Nuclide Laboratory and GFZ Potsdam Section 3.4. Two friendly, collaborative, hard working, and welcoming research groups. I can only hope to someday reciprocate your hospitality.

The Gill Brothers, Steve Stone, the Duke Forest Staff, and the Sumter National Forest. Thank you for facilitating my field work.

Meg Stephens and Anne Jones. The world would be a much better place if everyone was as warm, caring, and willing to help as you.

Drs. Emily S. Bernhardt, Paul R. Bierman, Heileen Hsu-Kim, Curtis J. Richardson, Dylan H. Rood, and Friedhelm von Blanckenburg. You have provided education that transcends data, text, and interpretation. I hope you're all aware that observing and interacting with each of you over the last five years has provided valuable insight about the intangibles required for success in science.

Dr. Daniel deB. Richter. Micheal Jordan (the Olympian) told us that one must earn their leadership every day. Very few people are capable of that, but you are Dan. In addition to your leadership, I am most profoundly appreciative of your patience and tolerance of my unpolished nature.

Introduction

The Conceptual Model of Pedogenesis and Anthropedogenesis

Soils are dynamic, biologically excited, and well organized mixtures of organic and mineral components. The broad suite of biogeochemical and physical processes that create and change soil not only regulate the existence and properties of a soil itself, but are also highly influential to Earth's lithosphere (Bazilevskaya et al. 2013, Targulian 2001), biosphere (Turner et al. 2012, Wardle et al. 2004), hydrosphere (Raymond et al. 2008), atmosphere (Berner et al. 1983, Raymo and Ruddiman 1992), and anthrosphere (Montgomery, 2007). Accordingly, the discipline of soil science has long been underpinned by the need to understand how soils are formed and changed (Darwin 1892, Dokuchaev 1883, Hilgard 1860, Jenny 1941).

The conceptual framework with which soil formation and change is interpreted and investigated is dynamic. Historically, Dukuchaev (1883) and Jenny (1941) provided a model where soil is formed and changed as a result of high level interactions between five soil forming factors (climate, parent material, topography, biota, and time). This framework emphasized soil as natural body, not heavily influenced by humans. This model soon evolved to recognize soils as polygenetic entities, where the interactions between climate, parent material, topography, and biota were no longer viewed as constant through time (Cline 1961, Targulian and Sokolov 1978). More recently, anthropogenic activity has been identified to significantly impact soil formation and

change, and soils are increasingly viewed as a human-natural bodies where humans are explicitly acknowledged as a soil forming factor (Resendiz-Paz et al. 2013, Amundson and Jenny 1991, Dudal et al. 2002, Richter, 2007, Richter and Yaalon, 2012). The evolution of this conceptual framework has thereby produced a contemporary model of soil formation and change. This contemporary model includes multi-millennia interactions between climate, parent material, topography, and biota with minimal human influence, a process termed "pedogenesis", and decadal and centurial interactions between climate, parent material, topography, and biota with increased human influence through the Holocene, a process termed "anthropedogenesis".

Soils Forming Factors on the Southern Piedmont

The Southern Piedmont is a roughly $1.7 \cdot 10^7$ ha physiographic region in the Southeastern United States (Figure 1). Topography of the region is characterized by gently rolling hills. Valley floors cover less than 10% of the region and most soils thereby blanket the uplands of broad interfluves that are approximately half a kilometer to two kilometers wide with minimal slope (Markewich et al. 1990, NRCS, 2012). These upland soils are considered residual as they are derived directly from underlying parent material. The most common parent material in the Southern Piedmont is high-grade (coarse textured), metamorphic, granitic gneiss like rocks. Less common are mafic dykes, low-grade metamorphic rocks, and sedimentary rocks (Figure 1). Currently, mean annual precipitation and mean annual temperature vary from 115 to 140 cm and

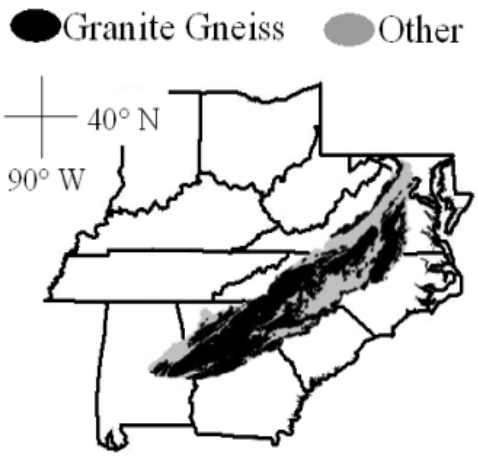

Figure 1: Extent and parent material distribution on the Southern Piedmont physiographic region (Richter and Markewitz, 2001).

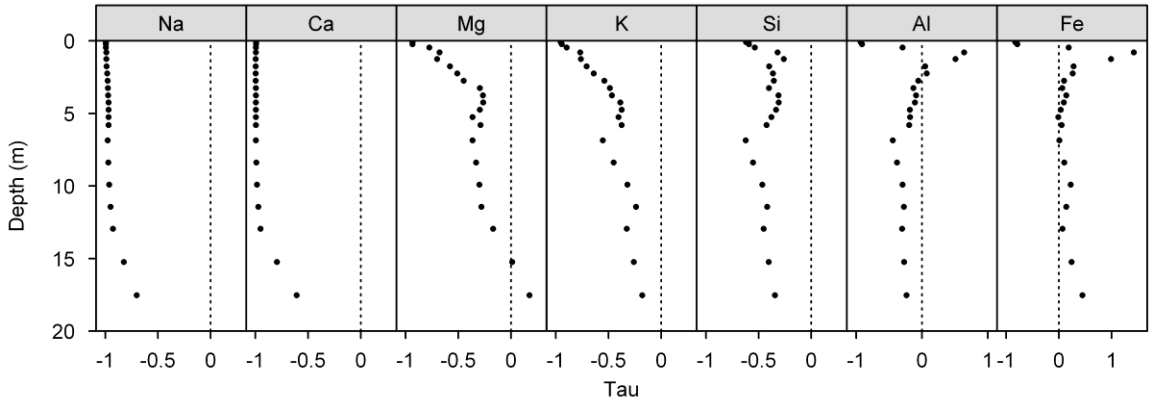

Figure 2: Tau plots of major elements in soil and saprolite of a Southern Piedmont Ultisol of the Cataula series. Tau=-1 identifies complete loss of a given element at a given depth relative to parent material.

and 14 to 18° C respectively. The Southern Piedmont, like most of the southeastern United States, is expected to have been largely under forest cover since the early Tertiary. During this time tropical rain forests parted to warm temperate and cool

temperate deciduous forests in response to climate fluctuations (Whitehead et al. 1973, Watts 1980, O'Neill 1985, Wolfe 1985, Delcourt et al 1993, Owen 2002).

Together, the gentle topography, the relatively coarse textured parent material, and persistent vegetation produced soils on the Southern Piedmont that are very biogeomorphically stable. Accordingly, rates of chemical erosion far exceed rates of physical erosion (Sheldon and Ritter 1964), and unweathered parent material is commonly below many tens of meters of soil that has been severely depleted in major elements (Figure 2). Most of these deep soils are classified as Ultisols according to the United States Department of Agriculture taxonomic system. Ultisols are soils considered to be in an advanced weathering stage, and are particularly sensitive to human activity, in part, due to weakly structured surface horizons, well buffered acidity pools, and poorly buffered nutrient pools (West et al. 2008).

Nonetheless, humans have exerted a heavy influence on Southern Piedmont soils. Historically, Native American agriculture was predominately in alluvial floodplains (Lefler 1967, Peebles 1978, Richter and Markewitz 2001). This lowland cultivation produced impressive agricultural yields, and its impacts on the region's soils paled in comparison to that which followed European settlement. As early as the 1700s, European cultivation of the southeastern United States started to expand from the fertile alluvial floodplains to the highly weathered upland Ultisols and eventually covered, for all intents and purposes, the entire Southern Piedmont. Maizel et al. (1992) estimated

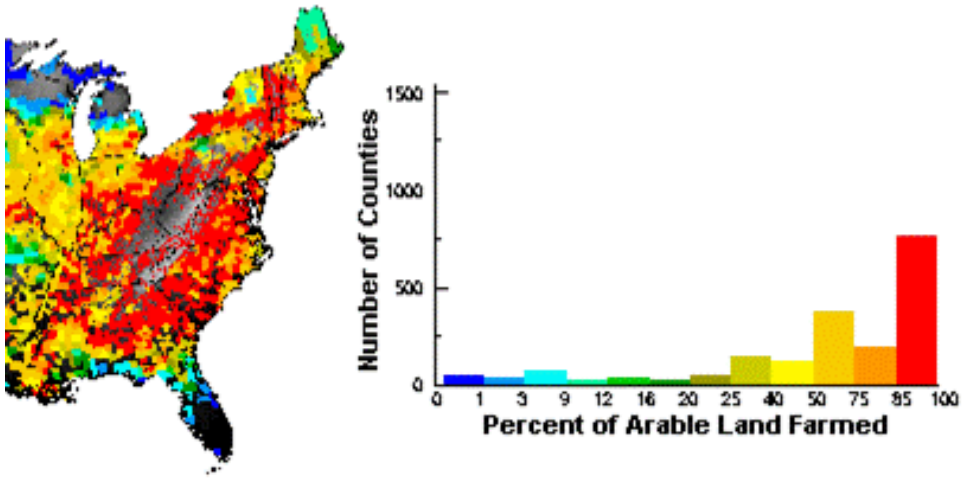

Figure 3: The percentage of the eastern United States in "farms" by county in 1860. Farmland is defined as land that is tilled or in meadow (Maizel et al. 1992).

that by 1860, 85% of arable soil in nearly every Southern Piedmont county was under farmland (Figure 3). Such widespread European agricultural practices altered Southern Piedmont soils through forest clearing, continued cultivation, lime and fertilizer amendments, irrigation, plowing, and severe soil erosion (Trimble, 2008). Further, a combination of economic, environmental, and legislative changes in the early to mid 20th century led to widespread agricultural abandonment that facilitated the establishment of secondary pine forests (both naturally regenerated and planted) across the Southern Piedmont. Subsequently, forest land is by far the most common land use in the region today (Wear, 2002), and represents a new suite of anthropogenicaly driven alterations to soil (Binkley & Fisher, 2012).

Objectives

The objective of this dissertation is to investigate pedogenesis and anthropedogenesis in the highly weathered Ultisols of the Southern Piedmont. Emphasis is on the wide range of timescales over which pedogenesis and anthropedogenesis form and alter soils. I begin by estimating soil residence time in a biogeomorphically stable Southern Piedmont Ultisol to quantify how long these soils have been residing at Earth's surface forming and changing prior to human impact (Chapter 1). Next I explore how the prolific anthropogenic activity of agricultural land abandonment has altered these soils over the most recent century and decades. Specifically, I investigate how one century of reforestation on abandoned agricultural land impacts the coupled carbon and iron cycle in Southern Piedmont subsoils (Chapter 2) and I examine the relationship between decadal patterns of secondary forest ecosystem development and soil macronutrient pools in these highly weathered soils (Chapter 3).

1. Coupling meteoric ^{10}Be with pedogenic losses of ^{9}Be to improve soil residence time estimates on an ancient North American interfluve

1.1 Introduction

The unglaciated Ultisols on the Southern Piedmont of southeastern North America have been produced and eroded at Earth's surface for several million years (Buol et al. 2003). The deep soil-saprolite systems, often referred to as "regolith" (Pavich et al. 1985) or simply "soil" (Richter and Markewitz 1995), record long-term interactions between components of Earth's Critical Zone (Brantley and Lebedeva 2011, Richter and Yaalon 2012). A crucial part of deciphering these records is to estimate the time scales over which they have existed, that is, to estimate the soil residence time (SRT).

With a half-life of 1.39 ± 0.012 million years (Chmeleff et al. 2010), the cosmogenic nuclide meteoric ^{10}Be is a useful tool for estimating SRT over longer time scales than most other tracers. After production in the atmosphere, meteoric ^{10}Be is scavenged by aerosols and delivered by wet and dry deposition to Earth's surface where it accumulates in soils and sediments (Lal and Peters 1967, Graly et al. 2010). The meteoric ^{10}Be inventory (N_{10Be}, in atoms cm^{-2}) of a soil is related to SRT (t, in years) as follows (Tsai et al. 2008):

$$Equation\ 1.1, \qquad t = \frac{-1}{\lambda} \cdot \ln\left(1 - \lambda \frac{N_{10Be}}{q - \rho\varepsilon m}\right)$$

where ε is the long-term surface erosion rate (cm yr^{-1}), λ is the ^{10}Be disintegration constant, q is the ^{10}Be delivery rate (atoms cm^{-2} yr^{-1}), and ρ and m are the bulk density (g cm^{-3}) and ^{10}Be concentration (atoms g^{-1}) of the surface horizon respectively. Implicit in Equation 1.1 is that hydrologic losses (leaching) of the tracer from the soil profile are zero. Although this is a common assumption in meteoric ^{10}Be studies (Pavich et al. 1985, West et al. 2011), leaching of the cosmogenic nuclide is not a novel concept (Monaghan et al. 1983, Pavich et al. 1984, Pavich et al. 1986, Brown et al. 1992). Soil organic matter, texture, and cation exchange capacity influence meteoric ^{10}Be retention (Takahashi et al. 1999, Graly et al., 2010) but, as is the case for metals in soils, soil pH is most important. Meta-analysis suggests that soil pH only influences meteoric ^{10}Be accumulation below pH 3.9 (in dilute KCl or $CaCl_2$, Graly et al. 2010) while laboratory observations show that ^{7}Be is mobile in sediments above pH 5 (in water, Valette-Silver et al. 1986).

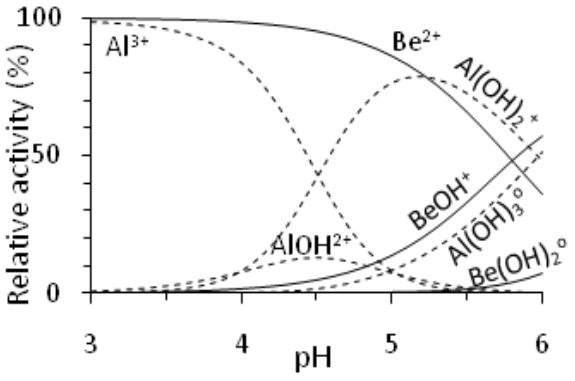

Figure 1.1: Beryllium and Aluminum speciation in equilibrium with $Be(OH)_{2(s)}$ and $Al(OH)_{3(s)}$, respectively, in water. LogK values for hydrolysis reactions from Lindsey (1979), Renders and Anderson (1987), and Sparks (2003).

Thermodynamic considerations suggest that below pH 5.5, soluble beryllium participates in chemical reactions as a free ionic species, not unlike aluminum (Figure 1.1). As Be^{2+}, meteoric ^{10}Be is subject to the same pedogenic processes that mobilize and remove other free cations, including ^{9}Be, from highly-weathered soils (Birkeland 1999 Oh and Richter 2005).

We aim to estimate SRT of a highly-weathered Southern Piedmont Ultisol and hypothesize that the acidity of the soil system has facilitated meteoric ^{10}Be leaching. Rather than assuming complete retention, we propose that pedogenic losses of ^{9}Be (the predominant beryllium isotope in soils) can approximate meteoric ^{10}Be losses and we estimate SRT by coupling measurements of meteoric ^{10}Be with an analysis of pedogenic ^{9}Be loss.

1.2 Methods

We sampled a residual soil, classified as Oxyaquic Kanhapludult of the Cataula series, and underlying granite gneiss on a broad interfluve with <2% slope near Cross Keys, South Carolina (34°36'23.59" N 81°43'24.82"W, Figure 1.2). Contemporary forest vegetation (primarily Quercus spp. and Carya spp.), aerial photography dating back to 1938 (Richter and Markewitz 2001), and the thick coarse-textured surface horizons (Table 1.1) suggest that the Ultisol has been minimally impacted by European agriculture.

We collected three continuous cores (10 m apart), each to a depth of 6.1 m and collected deeper samples from a single point 30 m away. Saprolite from 6.1 to 18.3 m was sampled with a three-wing auger bit and unweathered granite gneiss, contacted at 30.5 m, was sampled to 67.1 m with a roller-cone bit. We separated samples by horizon and depth and air dried all samples. We sieved soil/saprolite with a 2 mm screen and found coarse fragments in only eight of the 52 samples. By volume these fragments comprised 1-11% ($\bar{x}$ = 7%) of the eight samples and were removed from our analysis. We measured total elemental concentrations of all samples by ICP-AES or flame-AAS after $LiBO_2$ fusion and measured texture, pH in 0.01 M $CaCl_2$, total carbon (C), exchangeable base cations (Ca, Mg, K, and Na), and exchangeable acidity on all soil/saprolite samples (Carter 1993, Dane and Topp 2002, Sparks 2002).

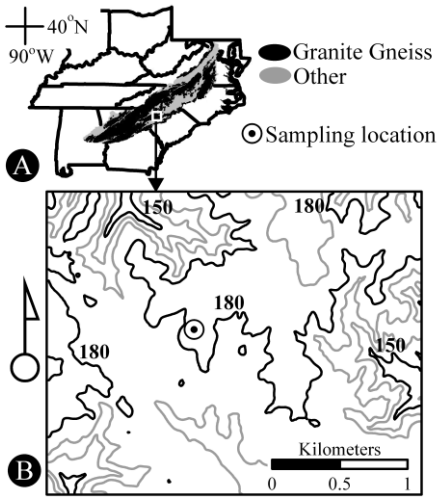

Figure 1.2: (A)Location and parent material distribution of the Southern Piedmont (Richter and Markewitz 2001). (B) Topography surrounding the sampling loaction with 10 m contour lines.

We composited (by horizon) across the continuous cores. We extracted the composited samples and samples from 6.1 to 18.3 m with hydroxylamine hydrochloride (1 M $NH_2OH{\cdot}HCl$ in 1 M HCl, Wiederhold et al. 2007a) and measured Be and Fe in solution by furnace and flame-AAS, respectively. By complete dissolution of oxide minerals at low pH, hydroxylamine hydrochloride extractable (hhe) metals are an operationally defined pool that have been weathered from primary minerals and retained in the soil, which in our analysis are akin to the familiar dithionite citrate bicarbonate extractable metals (Figure A.2) popularized by Mehra and Jackson (1958). We further composited these samples across horizons (Table 1.1), isolated meteoric ^{10}Be with a method modified from Stone (1998), and measured $^{10}Be/^{9}Be$ isotopic ratios by AMS (Appendix A).

1.3 Pedogenic Loss of ^{9}Be

The general properties of this soil typify the highly-weathered, acidic nature of the Ultisol and identify the potential for beryllium loss (Table 1.1, West et al. 1997). Specifically, soil pH does not exceed 4.5 in the upper 13.7 m and effective base saturation (EBS) is between 4 and 24% in the upper 9.1 m identifying extreme acidification and loss of exchangeable base cations. Thick, coarse-textured A and E horizons are underlain by a well-developed Bt horizon, composed mostly of low activity kaolinite and iron and aluminum oxi-hydroxides (Fimmen et al. 2008), and the effective cation exchange capacity (ECEC) does not exceed 4.6 cmol(+) kg^{-1}.

Table 1.1: Physical and chemical of the Southern Piedmont Ultisol.

Hor	Depth (m)	ρ* g/cm³	Clay (%)	Sand (%)	pH	C† (%)	ECEC§ (cmol/kg)	EBS§ (%)	totZr	totCa	totAl	totFe	hheFe	tot⁹Be	hhe⁹Be	¹⁰Be (10⁸atm/g)	Strain**
									----------(mg/g)----------					----------(ug/g) ----------			
A	0.00–0.07	1.10	5	76.4	3.70	2.33	1.9	21.9	0.73	0.24	16.9	7.52	2.18	0.23	0.11	2.37	–0.5
AE	0.07–0.13	1.42	6.1	76.8	4.05	1.33	1.3	19.2	0.77	0.27	19.3	6.96	2.51	0.27	0.10		–0.6
E	0.13–0.32	1.40	7.7	74.0	4.13	0.54	0.9	19.6	0.71	0.2	23.0	7.73	3.17	0.34	0.13	3.22	–0.6
Bt	0.32–0.6	1.63	41.9	42.0	4.03	0.24	3.5	23.8	0.43	0.07	108	26.37	18.83	0.77	0.22	6.9	–0.4
Bt	0.6–1.0	1.44	52.9	27.2	4.06	0.13	4.6	16.1	0.28	0.04	161.7	34.75	22.99	1.18	0.14	6.86	0.1
Bt	1.0–1.5	1.41	40.1	33.4	3.98	0.09	4.6	7.9	0.27	0.04	146.2	27.98	17.69	1.10	0.16	4.52	0.2
BC	1.5–2.0	1.41	22.9	45.2	3.99	0.04	3.8	5.4	0.35	0.04	132.5	23.47	12.69	1.19	0.22	2.94	–0.1
CB	2.0–2.5	1.34	13.6	55.7	3.96	0.03	3.7	4.1	0.34	0.04	128.9	22.07	11.77	1.08	0.34	2.63	0.0
CB	2.5–3.0	1.32	7.3	61.1	3.92	0.02	2.9	4.3	0.34	0.04	114.0	19.24	8.90	1.03	0.37	2.27	0.0
C	3.0–3.5	1.27	3.6	65.9	3.89	0.01	2.8	4.9	0.36	0.06	113.0	20.10	9.61	1.18	0.50	2.08	–0.1
C	3.5–4.0	1.29	4.1	65.6	3.88	0.02	3.1	6.6	0.32	0.06	105.4	19.18	8.81	1.05	0.46	2.18	0.1
C	4.0–4.5	1.26	4.2	67.2	3.88	0.01	4.0	6.5	0.33	0.06	104.5	18.56	9.07	1.03	0.41	2.6	0.1
C	4.5–5.0	1.29	4.6	67.3	3.94	0.02	2.7	7.0	0.34	0.07	100.0	18.40	8.32	1.00	0.40	2.06	0.0
C	5.0–5.5	1.26	3.3	67.8	3.94	0.01	2.7	7.4	0.36	0.07	105.8	18.52	8.05	1.05	0.43		0.0
C	5.5–6.1	1.27	3.5	68.0	3.95	0.02	2.5	9.8	0.37	0.08	106.3	20.20	9.53	1.07	0.54	2.13	–0.1
C	6.1–7.6	1.27	4.7	69.0	4.00	-	2.6	8.8	0.54	0.12	107.7	28.28	18.68	1.54	0.64		–0.4
C††	7.6–9.1	1.27	5.9	66.4	4.05	-	2.0	20.1	0.48	0.22	106.8	27.48	17.10	1.67	1.06	4.86	–0.3
C	9.1–10.7	1.27	5.2	65.6	4.17	-	2.1	49.9	0.42	0.32	105.8	26.68	16.10	1.80	1.09		–0.2
C	10.7–12.2	1.27	5.2	68.6	4.35	-	2.4	74.8	0.39	0.59	99.9	22.80	13.60	1.88	1.20	3.55	–0.1
C	12.2–13.7	1.27	5.9	65.0	4.41	-	2.5	79.1	0.41	1.13	102.3	22.69	13.45	2.27	1.25		–0.2
C§§	13.7–16.8	1.27	3.7	74.6	4.96	-	2.8	87.8	0.38	4.43	98.1	24.27	14.61	2.26	1.19	3.72##	–0.1
C	16.8–18.3	1.27	1.5	84.3	5.51	-	3.1	96.5	0.34	7.72	93.9	25.84	15.76	2.24	1.14		0.0

Notes: Variability between the three continuous cores reported in Table A.1.

*ρ measured from 0.0–0.6 m with a bulk density corer (n = 3), ϱ from 0.6–5.0 m from Markewitz et al. (1998), and below 5.0 m ϱ assumed to be the mean from 3–5 m.

†Percent carbon not measured below 6.1 m.

§Effective cation exchange capacity (ECEC) calculated as the sum of exchangeable base cations (Na, Mg, K, and Ca) and exchangeable acidity.

§Calculated by dividing the sum of the exchangeable base cations (Na, Mg, K, and Ca) by effective cation exchange capacity.

**Referenced to Zr in the 16.8–18.3 m horizon.

††Due to incomplete fusion total concentrations not estimated at this depth. Total Zr, Ca, Al, Fe, and ⁹Be are means of the overlying and underlying horizon.

§§No samples collected from 13.7–16.8 m. Reported values are the mean of the overlying and underlying horizon.

##¹⁰Be not measured from 13.7–18.3 m, see text.

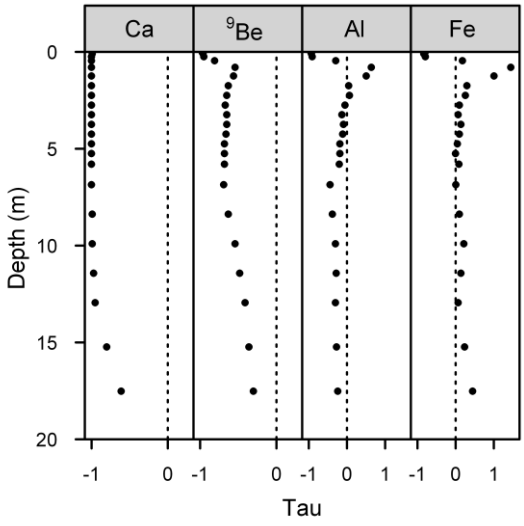

Figure 1.3: Tau plots of Ca, ^{9}Be, Al, and Fe in the Southern Piedmont Ultisol referenced to mean elemental concentrations in 37 m of unweathered granite gneiss.

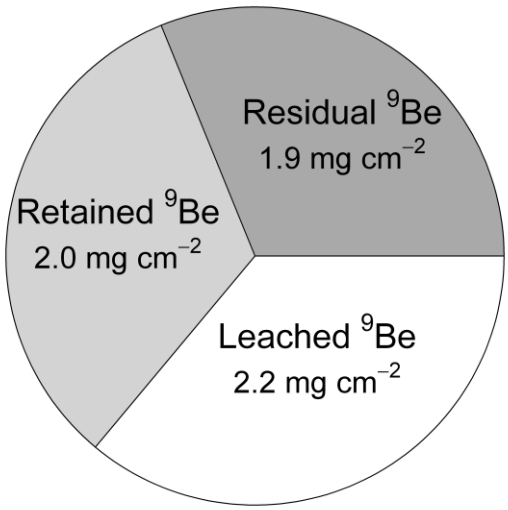

Figure 1.4: Pedogenic partitioning of ^{9}Be in the Southern Piedmont Ultisol. Retained 9Be has been weathered from primary minerals and remains in the soil system (=N_{hhe9Be}), leached ^{9}Be has been weathered from primary minerals and lost (=m_{9Be}), and residual ^{9}Be is in primary minerals (=N_{tot9Be} - N_{hhe9Be}).

A mass balance analysis (Brimhall and Dietrich 1987, Oh and Richter 2005) referenced to zirconium and unweathered granite gneiss (Appendix A, Table 1.1, Table A.2) confirmed that beryllium is lost from the Ultisol (Figure 1.3). The tau ^{9}Be distribution indicates ^{9}Be depletion, similar to aluminum (Al), is between that of calcium (Ca) and iron (Fe). Following Brantley and Lebedeva (2011) we quantified the unitless ^{9}Be losses in Figure 1.3 by calculating the strain corrected mass flux of ^{9}Be ($m^{9}Be$). Our $m^{9}Be$ is referenced to the deepest saprolite sample (16.8–18.3 m) and thus is a conservative approximation of ^{9}Be loss from the 18.3 m soil system. Accordingly, we estimated that 2.2 mg cm^{-2} of ^{9}Be have been weathered from primary minerals and leached from the 18.3 m soil system (Figure 1.4).

Pedogenic processes have not resulted solely in ^{9}Be loss; hhe ^{9}Be is a portion of total ^{9}Be (tot ^{9}Be) throughout the Ultisol (Table 1.1). We estimated the depth integrated inventory of hhe ^{9}Be (N_{hhe9Be}) and total ^{9}Be (N_{tot9Be}) in mg cm^{-2} as follows:

$$Equation\ 1.2, \qquad N_p = \sum_{h=0}^{18.3\ m} [\,^{9}Be_p]_h \cdot \rho_h \cdot z_h$$

where [$^{9}Be_p$] is the concentration of ^{9}Be (mg g^{-1}) in pool p, ρ is the bulk density (g cm^{-3}), and z is the length (cm) of horizon h. Our N_{hhe9Be}, N_{tot9Be}, and m_{9Be} estimates indicate that over half of the ^{9}Be weathered from primary minerals has been lost from the 18.3 m soil system (Figure 1.4).

1.4 Meteoric ^{10}Be and Soil Residence Time

1.4.1 Meteoric ^{10}Be Delivery (q)

We assumed that q has varied around a mean value over the time period of interest (Kaste and Baskaran 2011) and estimated q pursuant to current notions. From Graly et al. (2011) we estimated q to be $2.0 \cdot 10^6$ atoms cm^{-2} yr^{-1} (q_{max}) from latitude and mean annual precipitation (34.6°N and 120 cm yr^{-1}). From Willenbring and von Blanckenburg (2010), who suggest a threshold above which precipitation no longer influences q, we estimated q to be $1.3 \cdot 10^6$ atoms cm^{-2} yr^{-1} (q_{min}).

1.4.2 Minimum SRT

Elluvial-illuvial processes control the meteoric ^{10}Be distribution (Table 1.1, Figure 1.5) which, accordant with our ^{9}Be analysis, indicates mobility and loss. Directly below elluvial surface horizons (0–0.32 m) with low meteoric ^{10}Be concentrations is the maximum concentration, $6.90 \cdot 10^8$ atoms g^{-1}, in an illuvial Bt horizon (0.32–0.60 m). In the C horizons meteoric ^{10}Be diminishes to as low as $2.06 \cdot 10^8$ atoms g^{-1} (4.5–5.0 m) before roughly doubling in the two deepest samples (5.5–10.7 and 10.7–13.7 m). Further, meteoric ^{10}Be is correlated with %clay ($r = 0.84$, $p<0.0001$) and the most abundant exchangeable cations, Mg ($r = 0.86$, $p<0.0001$) and K ($r = 0.93$, $p<0.0001$), suggesting that its retention and loss is similar to other exchangeable cations in the Ultisol.

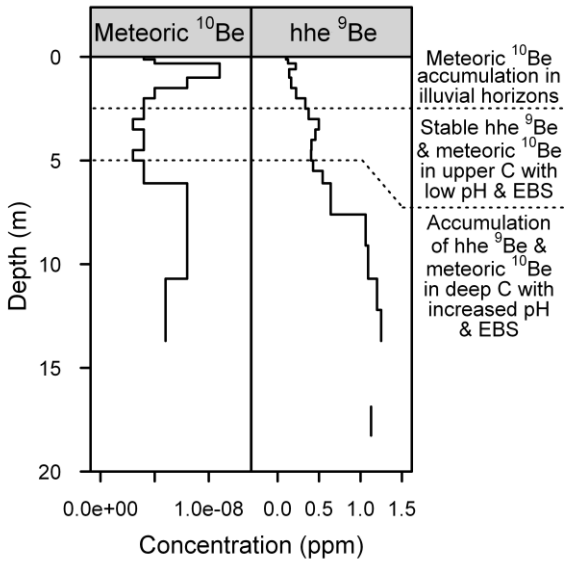

Figure 1.5: Observations of meteoric ^{10}Be and hhe ^{9}Be in the Southern Piedmont Ultisol (note that the x-axis for meteoric ^{10}Be is not logarithmic).

^{9}Be mobility and loss is clear to a depth of 18.3 m in this soil system (Figure 1.3), therefore, although our direct estimates of meteoric ^{10}Be reach 13.7 m we assumed that the meteoric ^{10}Be concentration from 13.7 to 18.3 m equals the mean (weighted by horizon thickness) of the C horizons (3.0–13.7 m, Table 1.1). We estimated that the meteoric ^{10}Be inventory (N_{10Be}, Equation 1.2) of the 18.3 m soil system is $8.9 \cdot 10^{11}$ atoms cm^{-2} and related the retention and loss of meteoric ^{10}Be to that of ^{9}Be with:

$$Equation\ 1.3, \qquad \frac{m_{9Be}}{N_{hhe9Be}} = \frac{m_{10Be}}{N_{10Be}}$$

where m_{10Be} (g cm^{-2}) is the mass flux of meteoric ^{10}Be from the 18.3 m soil system. We then estimated that the corrected meteoric ^{10}Be inventory (N'_{10Be}), which accounts for losses, is 1.9·10^{12} atoms cm^{-2} as follows:

$$Equation\ 1.4, \qquad N'_{10Be} = m_{10Be} + N_{10Be}$$

We constrained ε between 3.5·10^{-5} and 3.0·10^{-4} cm yr^{-1} (Appendix A) and solved Equation 1.1 with N'_{10Be} to estimate that SRT of this Ultisol ranges between 1.3–1.4 and 2.5–3.1 Ma under q_{max} and q_{min}, respectively (Table 1.2). Both ranges capture uncertainty related to ε, ^{10}Be measurements, and λ and are minimum estimates because that they do not account for meteoric ^{10}Be below 18.3 m.

Table 1.2: Minimum soil residence time (SRT) and maximum denudation rate (DR) under two ^{10}Be delivery scenarios.

	q_{max}	q_{min}
SRT from N_{10Be}	0.50–0.54 Ma	0.84–0.93 Ma
DR from N_{10Be}	57–60 m Ma^{-1}	33–36 m Ma^{-1}
SRT from N'_{10Be}	1.27–1.38 Ma	2.58–3.12 Ma
DR from N'_{10Be}	22–24 m Ma^{-1}	10–12 m Ma^{-1}

Notes: q_{max} and q_{min} described in text, SRT = soil residence time, and DR = denudation rate.

1.4.3 Corroborating SRT Estimates

If surface erosion is balanced by parent material weathering on the unglaciated Southern Piedmont landscape, then basin scale analysis of in situ ^{10}Be indicate that the parent material denudation rate (DR) of the physiographic region is 3–21 m Ma^{-1} (Trodick 2011). Such rates agree well with chemical mass balance estimates in individual soil systems in the region (Pavich 1986, Pavich 1989, Richter and Markewitz 2001) and corroborate our SRT estimates. We take DR as the quotient of soil depth (30.5 m) and SRT. Our estimates of SRT from N'_{10Be} yield a maximum DR between 10–12 and 22–24 m Ma^{-1} depending on q, suggesting that both are prudent minimum SRT estimates. Conversely maximum DRs from N_{10Be} (not accounting for meteoric ^{10}Be leaching) are far in excess of 21 m Ma^{-1} (Table 1.2), an error that could only result from an underestimation of SRT since soil depth is certain.

1.5 Discussion

We conclude that assuming complete meteoric ^{10}Be retention can result in substantial underestimates of SRT in acidic soils. Our minimum estimates of SRT yield unreasonable DR estimates when meteoric ^{10}Be losses are not accounted for (Table 1.2). Our conclusion is not trivial since acidic soils are extensive; Spodosols, Oxisols and Ultisols cover nearly 20% of Earth's terrestrial surface (Eswaran 2002). To decipher these ancient records (Brantley and Lebedeva 2011) an accurate estimate of SRT is critical.

Meteoric ^{10}Be is a useful tool to estimate long SRT, but its application requires loss estimates in acidic soils. Further, soil losses are also likely relevant to the utilization of meteoric ^{10}Be as a tracer in aquatic and marine systems.

Here, coupling the meteoric ^{10}Be inventory with pedogenic ^{9}Be losses provided a straightforward estimate of meteoric ^{10}Be losses. Depth dependence of tau ^{9}Be from roughly 0–1 m and below 5 m indicates that pedogenic processes appreciably weather ^{9}Be from primary minerals, while between 1 and 5 m tau ^{9}Be is steady (Figure 1.3). We attribute the increase in hhe ^{9}Be from 1 to 2.5 m (Table 1.1, Figure 1.5) to retention of ^{9}Be that was weathered from primary minerals both within this region and from above. Thus, to differing degrees, ^{9}Be appears to be weathered from primary minerals throughout the entire 18.3 m soil system. Meteoric ^{10}Be, while deposited at the soil surface, also resides throughout this system (Table 1.1; Figure 1.5). Considering that in this Ultisol hhe ^{9}Be and meteoric ^{10}Be have been exposed to the same pedogenic processes in the same soil horizons, it is reasonable to assume that hhe ^{9}Be and meteoric ^{10}Be have been equally affected.

The most notable difference between meteoric ^{10}Be and hhe ^{9}Be in the Ultisol is the magnitude of accumulation in the Bt horizons (0.6–1.5 m; Table 1.1; Figure 1.5). We ascribe this difference to surficial delivery of meteoric ^{10}Be that allows it to interact more fully with the illuvial horizon than hhe ^{9}Be. Since only ~10% of N_{10Be} resides from 0.6–1.5

m, this difference does not affect our final estimates of SRT (which vary widely with assumed q). Below 2.5 m the depth distributions of meteoric ^{10}Be and hhe ^{9}Be are similar; relatively low and stable from 2.5 to 5 m with distinct accumulation of both below 5 m. Accumulation of meteoric ^{10}Be and hhe ^{9}Be below 5 m coincide with increased pH and EBS (Table 1.1), suggesting that less beryllium exists as Be^{2+} (Figure 1.1) and that retention mechanisms differ from those in surficial, more acidic, horizons.

In a pioneering meteoric ^{10}Be investigation Pavich et al. (1985), assuming complete retention and $q = 1.3 \cdot 10^{6}$ atoms cm^{-2} yr^{-1}, estimated a SRT of 0.8 Ma on the Southern Piedmont uplands. Following our coupled approach and approximation of meteoric ^{10}Be leaching our minimum SRT estimates (1.3–1.4 Ma and 2.6–3.1 Ma depending on meteoric ^{10}Be delivery) are considerably longer than previously measured on Southern Piedmont interfluves. In spite of uncertainty surrounding q, our minimum estimates redefine the time constraints associated with the formation of the Southern Piedmont's highly-weathered soils and indicate that they have resided at Earth's surface for much if not all of the Quaternary.

2. Microsite sampling reveals the polygenetic nature of iron stable isotope ratios in soil profiles

2.1 Introduction

Pedogenic transformation and redistribution of iron (Fe) in soil profiles is germane to soil formation, mineral weathering, plant nutrition, the fate of environmental pollutants, soil biota, and soil physical and chemical properties (Schwertmann et al. 1989). To date Fe stable isotope ratios have been reported in peer-reviewed literature for 18 soil profiles (Fantle and DePaolo 2004, Emmanuel et al. 2005, Wiederhold et al. 2007a, Wiederhold et al. 2007b, Thompson et al. 2007, Yamaguchi et al. 2007, Poitrasson et al. 2008, Buss et al. 2010, Mansfeldt et al. 2012, Yesavage et al. 2012, Fekiacova et al. 2013), not including this study, and are a promising new tool to investigate soil Fe biogeochemistry. Fe has four stable isotopes, ^{54}Fe (5.84%), ^{56}Fe (91.76%), ^{57}Fe (2.12%), and ^{58}Fe (0.28%), and their ratios are reported as $\delta^{56 \text{ or } 57}$Fe (with $\delta^{57}Fe = 1.5\delta^{56}Fe$) relative to the international standard IRMM-014 as follows (Wiederhold et al. 2007a):

$$\textit{Equation 2.1,} \qquad \delta^{56 \text{ or } 57}\mathrm{Fe}(‰) = \left(\frac{\left(^{56 \text{ or } 57}\mathrm{Fe}/^{54}\mathrm{Fe}\right)_{\text{sample}}}{\left(^{56 \text{ or } 57}\mathrm{Fe}/^{54}\mathrm{Fe}\right)_{\text{IRMM-014}}} - 1 \right) \cdot 10^3$$

In the earliest published report of Fe stable isotope ratios in a soil profile, Fantle and DePaolo (2004) estimated δ^{57}Fe of 0.5 M HCl extractable and total Fe in an Ultisol

soil. Despite a potential methodological problem with their 0.5 M HCl extractable data (Wiederhold et al. 2007a), they built upon laboratory work (Beard et al. 2999, Brantley et al 2001, Icopini et al. 2004) to demonstrate for the first time that biogeochemical transformation and redistribution of Fe generates isotopically distinct Fe pools in soil profiles; a concept recently reiterated by Fekiacova et al. (2013). Since the pioneering work of Fantle and DePaolo, investigators have complimented traditional analytical approaches with estimates of $\delta^{56 \text{ or } 57}$Fe to better understand Fe dynamics in soil profiles related to redox conditions; vegetative uptake and (re)cycling; microbial activity; organic matter dynamics; soil horizonation; climate; weathering of primary minerals; and precipitation of secondary minerals (Emmanuel et al. 2005, Wiederhold et al. 2007a, Wiederhold et al. 2007b, Thompson et al. 2007, Yamaguchi et al. 2007, Poitrasson et al. 2008, Buss et al. 2010, Mansfeldt et al. 2012, Yesavage et al. 2012, Fekiacova et al. 2013), and Fe stable isotope ratios are poised as an important new tool to investigate Fe biogeochemistry in soils.

Until now investigations of Fe stable isotope ratios in soil profiles have emphasized Fe biogeochemistry over relatively long-term (multi-millennial) timescales. Specifically, previous published estimates of Fe stable isotope ratios are either explained by or used to interpret pedogenic processes that operated over the entire lifetimes of the 18 soil profiles that were observed. Soil profiles and the constituents contained within

are however products of polygenesis; having formed and changed as a result of biogeochemical processes that vary widely over both relatively long-term timescales and relatively short-term (centurial and even decadal) timescales (Richter and Yaalon, 2012). Recent estimates from surface soils along a 150 year glacier forefield chronosequence indicate that pedogenic influence on Fe stable isotope ratios are not restricted to multi-millennial timescales (Kiczka et al., 2010). Further, greenhouse and field observations identify the potential for aboveground vegetation to influence Fe stable isotope ratios in soil over relatively short-term timescales (Guelke et al. 2007, Guelke and von Blanckenburg, 2010, Kiczka et al. 2010). A comprehensive understanding of the Fe stable isotope ratios in soil profiles is needed for this promising new tool to reach its full potential and, we suggest, can only be attained by integrating the impacts of relatively long-term and short-term soil Fe dynamics on this isotopic system.

We hypothesize that stable Fe isotopes record the polygenetic nature of soil profiles and are dynamic over diverse timescales. We estimated δ^{56}Fe in operationally defined oxyhydroxide phases of bulk soil and individual redoximorphic features from a pair of soils. The paired soils had contrasting vegetative rooting regimes over the last century; one being abundantly and deeply rooted under pine (*Pinus* spp.) forests while the other was more superficially rooted under grasses and forbs. Our estimates of δ^{56}Fe have recorded soil biogeochemical transformation and redistribution of Fe over both

relatively long-term timescales and relatively short-term timescales in response to divergent rooting over the last century.

2.2 Methods

2.2.1 Paired Soil Profiles and Redoximorphic Features

We investigated two residual Ultisol soils on a broad interfluve in the Durham Division of the Duke University Teaching and Research Forest near the border of Durham and Orange County in North Carolina, USA (Figure 2.1, Figure B.1). The soils were in the Helena series (fine, mixed, semiactive, thermic Aquic Hapludults) on the shoulder of a southeast facing catena with 3% slope, and were selected from detailed land management records and historic aerial photography that indicate both were under cultivation until 1890. Since then the soil in Duke Forest Compartment 70 Stand 22 supported the growth and development of two deeply rooted pine forest rotations while the other supported primarily shallow rooted grasses and has been maintained without trees for a transmission line established in 1911 (Office of the Duke Forest, Personal Communication). We excavated a deep soil pit in each Ultisol, ten meters apart (Figure 2.1). Both soil profiles contained coarse textured A and E horizons over a 30 cm thick fine textured Btg horizon and more than 100 cm of saprolitic C/Btg horizon. In another soil pit, approximately 15 m downslope on the catena, we encountered and sampled unweathered granite boulders at a depth of two meters.

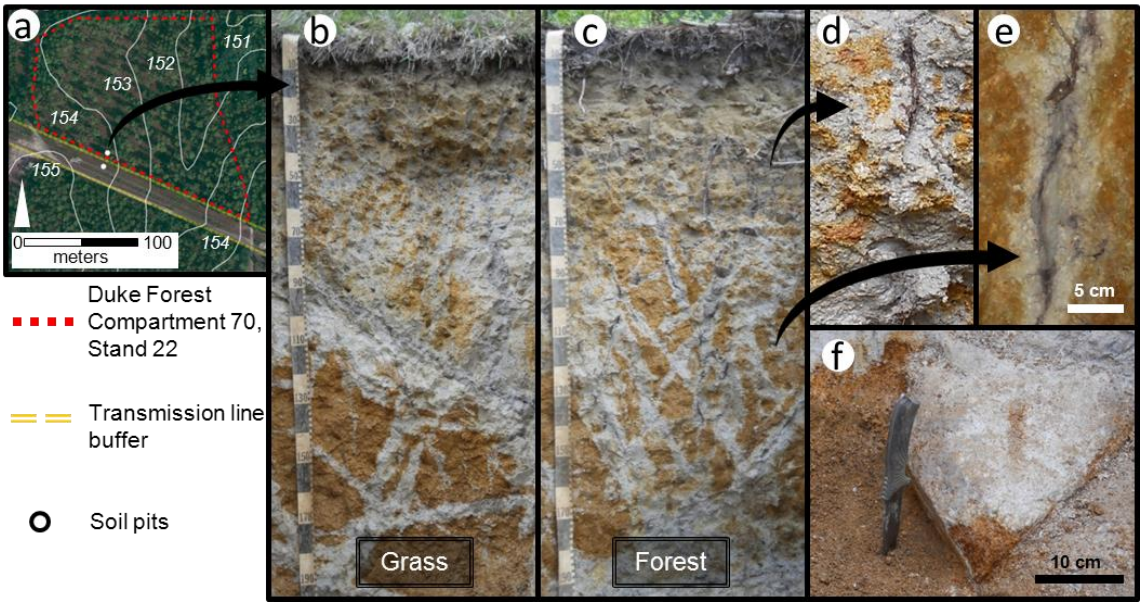

Figure 2.1: (A) Location of the paired soils excavated for this study, contour line units are meters. (B and C) Profile images of the paired soils, large blocks are in 10 cm increments. (D) Gley and Fe-enriched microsites in the Btg horizon. (E) Gley, Fe-enriched, and Fe-depleted microsites in the C/Btg horizon. Notice the close association between roots and gley microsites d and e. (F) Boulder excavated at a depth of 2 m with a high value and low chroma weathering rind that has been hammered away to expose unweathered granite. The scale bar in E is applicable to D.

Subsoil Btg and C/Btg horizons in both Ultisols contained abundant and prominent redoximorphic features (Figure 2.1). Redoximorphic features are soil volumes, called "microsites", which have characteristic color from redox reactions of Fe and manganese (Mn) (Fimmen et al. 2008, Vepraskas and Lindbo 2012, Schoeneberger 2013). Microsites form in the absence of oxygen (O_2) when organic carbon (C) is microbially oxidized and Fe(III), acting as the electron acceptor, is reduced to Fe(II).

Fe(II) enters solution and is translocated along diffusion gradients until in the presence of O_2 it is oxidized and re-precipitates as Fe(III). Accordingly, microsites are identified by Munsell color (Cleland 2004, Vepraskas and Lindbo 2012). Microsites that are Fe sources, where Fe(III) has been reduced to Fe(II), appear white or grey with Munsell value ≥ 4 and chroma ≤ 2. Microsites that are Fe sinks, where Fe(II) has oxidized and re-precipitated as Fe(III), appear red, orange, brown, or yellow with higher Munsell chroma (Vepraskas and Lindbo 2012). Accordingly, we identified individual microsites in the paired soil profiles by Munsell color. In these paired soils bulk Btg horizons consisted of "Fe-enriched" microsites (value ≤ 7 and chroma > 4; pale reddish orange or orange) and "gley" microsites (value ≤ 8 and chroma ≤ 2; light grey). Bulk C/Btg horizons consisted of Fe-enriched, gley, and "Fe-depleted" microsites (value > 8 and chroma ≤ 2; white) (Figure 2.1). We estimated microsite and root abundance by placing a square screen with 400 one cm^2 cells onto vertically exposed soil. We classified each cell as Fe-enriched, Fe-depleted, or gley depending on the predominant microsite in that cell, then counted the cells that contained roots. We made these abundance estimates for each genetic subsoil horizon in both soil profiles on the pit face and two side walls (n=3).

2.2.2 Bulk Soil and Soil Microsite Sampling

We sampled bulk soil from A, E, Btg, C/Btg1, C/Btg2, C/Btg3, and C/Btg4 genetic horizons of both Ultisols with a 6.0 cm diameter bulk density corer and slide hammer.

Each bulk sample was a composite of two 15 cm long cores inserted into the exposed soil pit face. We also meticulously collected individual redoximorphic feature microsite samples from all genetic subsoil horizons. To do so we removed between 10 and 20 aggregates (roughly 120 to 300 cm^3 each) from the pit face and side walls of each horizon. Using small stainless steel spatulas we scraped and collected the Fe-enriched, Fe-depleted, and Gley microsites from each aggregate.

2.2.3 General Property Characterization

We processed and characterized soil samples at the Duke University Soils Laboratory following standard methods (Carter 1993, Sparks 1996) after they were air dried and sieved to 2 mm. We measured pH in 0.01 M $CaCl_2$; exchangeable acidity in 1 N KCl; texture gravimetrically by pipette; Mehlich-III extractable base cations (Ca, Mg, K, and Na) by flame atomic absorption spectroscopy (FAAS); total elemental concentrations by FAAS or inductively coupled plasma optical emission spectrometry (ICP-OES) following $LiBO_2$ fusion; and total C (mass %) by dry combustion. We estimated Fe concentrations in operationally defined short range ordered ($Fe_{SRO\text{-}oxide}$) and crystalline ($Fe_{cryst\text{-}oxide}$) oxyhydroxides following the first two steps of the Wiederhold et al. (2007a) sequential extraction. First, we added 20 mL of 0.5 M HCl to 1 ± 0.02 g of soil (solution:soil = 20) in 50 mL centrifuge tubes. We shook tubes for 24 hours at room temperature then centrifuged and decanted the supernatant. We rinsed the residue with

deionized water, vortexed to re-suspend the solids, centrifuged again, and decanted the rinse into the extraction supernatant. We took this combined solution to contain short range ordered oxyhydroxides. Next, we added 20 mL of 1 M $NH_2OH{\cdot}HCl$ in 1 M HCl to the soil residue (solution:soil = 20) and placed the centrifuge tubes in a hot water bath (90 °C). Every 15 minutes we opened the centrifuge tube lids to release pressure, closed the lids, and then inverted the tubes by hand to re-disperse solids. After four hours we let the tubes cool to room temperature, centrifuged, and decanted the supernatant. We took this solution to contain crystalline oxyhydroxides. We measured $Fe_{SRO\text{-}oxide}$ and $Fe_{cryst\text{-}oxide}$ by FAAS.

2.2.4 Stable Iron Isotope Characterization

We characterized stable Fe isotopes at the Earth Surface Geochemistry Section of the German Center for Geosciences GFZ Potsdam in a metal-free class 1000 clean laboratory with class 10 laminar-flow hoods. We used only suprapure grade reagents, ultrapure water (Milli Q, >18.2 $M\Omega\ cm^{-1}$), and pro analysi grade acids that were further purified by sub-boiling distillation. Our isotopic analysis followed the first two sequential extraction steps described above (Wiederhold et al. 2007a) on bulk and microsite soil samples that were composited vertically in the C/Btg horizons (Figure 2.3). We sequentially extracted 2 ± 0.002 g of air dry soil and maintained a solution to soil ratio of 20 for both extraction steps. After sequential extraction, we passed short range

ordered and crystalline oxyhydroxides solutions through 0.2 um polyethersulfone syringe filters (pre-conditioned with 0.5 M HCl and 1 M HCl respectively) then measured Fe concentration by ICP-OES to determine the aliquot volume required for 50 ug Fe. We treated the corresponding aliquots with a combination of microwave digestion (200 °C), 30% H_2O_2, and concentrated HNO_3 to convert all Fe to Fe^{3+} and destroy organics prior to Fe isolation.

We isolated Fe in each aliquot by anion exchange chromatography followed by ammonia precipitation and measured Fe isotopes by multiple-collector inductively coupled plasma mass spectrometry (MC-ICP-MS, ThermoFinnigan Neptune) following the methods and data acceptance criteria of Schoenberg and von Blanckenburg (2006). Yields following the isolation procedure averaged 95% and 94% for the $Fe_{SRO\text{-}oxide}$ (minimum = 91%) and $Fe_{cryst\text{-}oxide}$ (minimum = 87%) solutions respectively. We monitored process blanks during sequential extraction and Fe isolation. Full process blanks did not exceed 82 ng Fe. We diluted samples to 5 ppm in 0.3 M HNO_3 prior to MC-ICP-MS introduction and measured Fe isotopes following a sample-standard bracketing approach with standard material IRMM-014. We measured Fe isotopes in each sample between two and five times, calculated $\delta^{56}Fe$ of each measurement according to Equation 1, and report means of replicate measurements. We sequentially extracted two bulk soil samples (one Btg and one C/Btg sample) in duplicate and estimates of δ^{56} $Fe_{SRO\text{-}oxide}$ and

δ^{56} $Fe_{cryst\text{-}oxide}$ were indistinguishable between the duplicates following a paired t-test (p-value > 0.05).

2.3 Results and Discussion

2.3.1 Soil Profile Properties

Soil pH does not exceed 4.2 in the paired Ultisol profiles (Table B.1). Exchangeable acidity is strongly depth dependent, ranging from 0.7 to 1.3 cmol kg^{-1} in A and E horizons and increasing to more than 7.5 cmol kg^{-1} in Btg horizons. In C/Btg horizons exchangeable acidity decreases with depth but remains above 3.5 cmol kg^{-1}. Soil texture is also strongly depth dependent. A and E horizons are coarse textured with more than 70% sand and less than 7% clay. Percent clay increases to nearly 40% in Btg horizons and decreases with depth to less than 10% through C/Btg horizons (Table B.1).

Effective cation exchange capacity (ECEC) tracks the depth dependence of clay and reaches a maximum of about 9 cmol kg^{-1} in Btg horizons of both soil profiles. Given the low pH, ECEC indicates that the illuvial Btg horizons contain high activity clay minerals (Table B.1). In similar soils of the Sedgefield series, swelling upon moistening of these illuvial clays reduces percolation into the subsoil and promotes lateral ground water runoff above Bt horizons (Dadgari 1983). Lateral, rather than vertical, ground water runoff is important to pedogenic processes operating in these soils and is evident by exchangeable sodium (Na), a highly soluble cation that is readily leached from soils

(Schaetzl and Anderson 2005). In A and E horizons Na occupies <5% of cation exchange sites (effective exchangeable sodium percentage, or EESP). In Btg horizons EESP increases by an order of magnitude and continues to increase with depth to more than 35% in deep C/Btg horizons (Table S1). Although subsoil horizons are highly acidic, low permeability of the Btg horizons diminishes percolation into the subsoil and Na remained the most abundant base cation on subsoil exchange sites.

2.3.2 Microsite Soil Properties

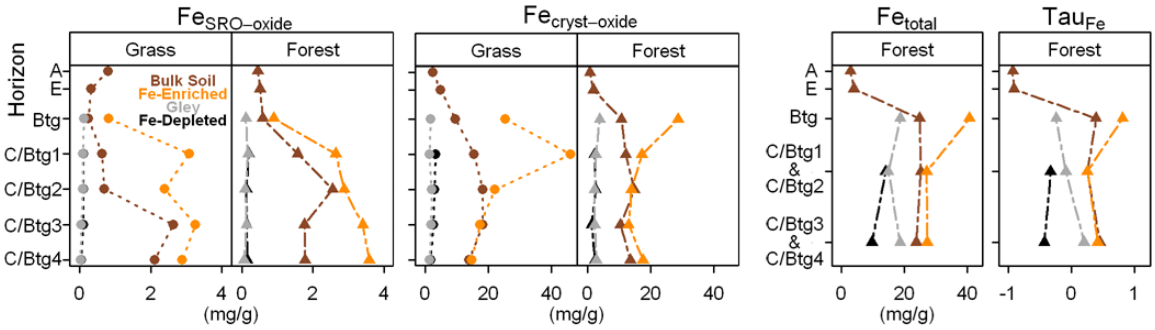

Figure 2.2: $Fe_{SRO\text{-}oxide}$ concentration, $Fe_{cryst\text{-}oxide}$ concentration, Fe_{total} concentration, and Tau_{Fe} (referenced to Zr) in bulk and microsite soil samples. Note that total elemental concentrations were only estimated in samples from the forest Ultisol that were composited vertically through the C/Btg horizons. Tabular data in Appendix B.

The three redoximorphic feature microsites in these soil profiles contrast significantly in chemical and physical properties (Table 2.1, Figure 2.2, Figure 2.3). **Gley microsites** have low Fe-oxyhydroxide concentrations and high C and clay concentrations. Gley microsites originate in the Btg horizon and are found embedded

within Fe-depleted microsites through C/Btg horizons. Gley microsites interact directly with roots and are considered the most biogeochemically active of the three microsites. **Fe-depleted microsites** have low Fe-oxyhydroxide, C, and clay concentrations. Fe-depleted microsites are present as a weathering rind on unweathered granite boulders and persist in C/Btg horizons. Fe-depleted microsites are absent in the Btg horizons. **Fe-enriched microsites** have high Fe-oxyhydroxide concentrations and low C and clay concentrations. Fe-enriched microsites are soil volumes where Fe(II) has been oxidized and re-precipitated as Fe(III).

The majority of subsoil Fe subjected to pedogenic transformation and redistribution resides in the $Fe_{cryst\text{-}oxide}$ pool, which exceeds the concentration of $Fe_{SRO\text{-}oxide}$ by an order of magnitude in all microsite samples (Figure 2.2). $Fe_{cryst\text{-}oxide}$ ranges from 13.0 to 45.9 mg g^{-1} in Fe-enriched microsites but only 1.3 to 4.0 mg g^{-1} in Fe-depleted and gley microsites. The smaller and more reactive $Fe_{SRO\text{-}oxide}$ shows similar microsite dependence and ranges from 0.8 to 3.6 mg g^{-1} in Fe-enriched microsites and from < 0.1 to 0.2 mg g^{-1} in Fe-depleted and gley microsites. Fe redox cycling that has heterogeneously redistributed Fe-oxyhydroxides among microsites (Vepraskas and Lindbo 2012) is further evident from estimates of total and tau Fe that clearly identify microsites that are Fe sources and sinks (Figure 2.2).

Table 2.1: Subsoil root abundance, redoximorphic feature abundance, and redoximorphic feature properties.

			-----Abundance (%)†-----			---------Total C (%)---------			---------Clay (%)---------			------ECEC (cmol/kg)§ ------			----Ex. Acidity (cmol/kg)----		
Horizon	Depth (m)	Roots (%)*	Fe-Enriched	Gley	Fe-Depleted	Fe-Enriched	Gley	Fe-Depleted	Fe-Enriched	Gley	Fe-Depleted	Fe-Enriched	Gley	Fe-Depleted	Fe-Enriched	Gley	Fe-Depleted
Grass																	
Btg	0.2-0.5	24 (2)	45 (4)	55 (4)	-	0.13	0.25	-	n.d.**	n.d.	-	8.0	10.4	-	6.9	9.2	-
C/Btg1	0.5-0.8	7 (2)	16 (4)	26 (8)	58 (5)	0.08	0.12	0.04	n.d.	n.d.	n.d.	7.8	11.4	6.2	6.4	9.5	5.0
C/Btg2	0.8-1.1	8 (1)	30 (12)	21 (2)	48 (13)		0.15		n.d.	n.d.	n.d.	6.6	11.0	5.6	5.2	8.1	4.2
C/Btg3	1.1-1.4	3 (2)	48 (21)	7 (7)	46 (15)	0.03	0.15	0.03	n.d.	n.d.	n.d.	6.7	15.7	5.1	4.3	9.9	3.2
C/Btg4	1.4-1.7	2 (1)	44 (3)	1 (1)	55 (3)		0.16		n.d.	n.d.	n.d.	6.4	7.9	4.0	4.0	4.4	2.2
Forest																	
Btg	0.4-0.7	57 (4)	31 (1)	69 (1)	-	0.12	0.46	-	35	47	-	7.2	10.1	-	6.6	9.1	-
C/Btg1	0.7-1.0	31 (6)	30 (5)	25 (7)	44 (7)	0.03	0.16	0.05	11	34	20	7.1	11.3	6.0	5.6	9.5	4.4
C/Btg2	1.0-1.3	15 (6)	41 (8)	17 (7)	42 (3)		0.23		8	26	21	6.9	11.0	5.5	5.0	8.8	4.2
C/Btg3	1.3-1.6	7 (2)	32 (7)	25(7)	43 (6)	0.03	0.14	0.03	8	18	10	7.3	15.4	5.2	5.0	10.5	3.1
C/Btg4	1.6-1.9	7 (3)	17 (5)	8 (7)	75 (3)		0.13		5	21	13	7.2	10.8	5.9	4.0	6.0	3.5

*Percentage of one cm2 cells that contained roots, standard error (n=3) reported in parentheses.

†Standard error (n=3) reported in parentheses

§Effective cation exchange capacity (ECEC) calculated as the sum of Mehlich-III extractable base cations (Ca, Mg, K, and Na) and exchangeable acidity.

**n.d. = not determined

The unweathered granite boulders we excavated were covered with a weathering rind characterized by Munsell value > 8 and chroma ≤ 2; similar in color to Fe-depleted microsites (Figure 2.1). Such similarity in color and the reticulated shape of Fe-depleted microsites around the Fe-enriched microsites (Figure 2.1) suggests that Fe-depleted microsites originate along natural planes of weakness in parent material during early stages of granite weathering. Hypothetically, dissolved organic C moves through these planes of weakness accompanied by periodic O_2 limitation deep below the soil surface and lowers Eh, thereby reducing Fe(III) and mobilizing Fe(II). Fe-depleted microsites persist below the Btg horizons indicating that water percolation through C/Btg horizons predominantly occurs in the same preferential flow paths established earlier in pedogenesis. In Btg horizons soil is subjected to more rapid mixing by bioturbation and argilliturbation (Schaetzl and Anderson 2005) and the Fe-depleted microsites are lost (Figure 2.1, Table 2.1).

In Btg horizons gley microsites are more abundant than Fe-enriched microsites, comprising 55 and 69% of the bulk soil in the grass and forest soil respectively. Gley microsites in C/Btg horizons exist exclusively inside of Fe-depleted microsites and their abundance attenuates with depth (Figure 2.1, Table 2.1). Gley microsites are characterized by higher exchangeable acidity, higher clay content, higher ECEC and lower pH than Fe-enriched and Fe-depleted microsites (Table 2.1). These chemical,

physical, and morphological properties indicate that gley microsites exist in C/Btg horizons due to illuviation of Btg horizon material.

Gley microsites are also the most biogeochemically active microsites due to their intimate association with plant roots (Figure 2.1). Greater than 95% of the roots we inventoried existed in gley microsites, with <5% in Fe-depleted microsites and none in Fe-enriched microsites. Stabilization of microsite dependent organic matter inputs from roots by relatively high clay concentration and ECEC has partitioned most subsoil C in the gley microsites. In subsoil horizons of both soil profiles %C of gley microsites is at least 1.7 times higher than that of Fe-enriched and Fe-depleted microsites (Figure 2.3, Table 2.1).

2.3.3 Fe Stable Isotope Ratios in Soil Profiles

In these soil profiles $\delta^{56}Fe_{SRO\text{-}oxide}$ is characterized by a wider range than δ^{56} $Fe_{cryst\text{-}oxide}$. Across all samples $\delta^{56}Fe_{SRO\text{-}oxide}$ varies by 2.25‰ whereas $\delta^{56}Fe_{cryst\text{-}oxide}$ varies by 1.08‰, from –1.92 to 0.33‰, and –0.77 to 0.31‰ respectively (Figure 2.3). Soil profile data with $\delta^{56or57}Fe$ from operationally defined short range ordered *and* crystalline oxyhydroxides has been reported five times previously; two Spodosols, two Inceptisols, and one Entisol (Wiederhold et al 2007a, 2007b). Those soils and the two Ultisols investigated here encompass a broad spectrum of pedogenesis, yet in all, $Fe_{SRO\text{-}oxide}$ is characterized by a wider range than $Fe_{cryst\text{-}oxide}$. We attribute this pattern to the fact that

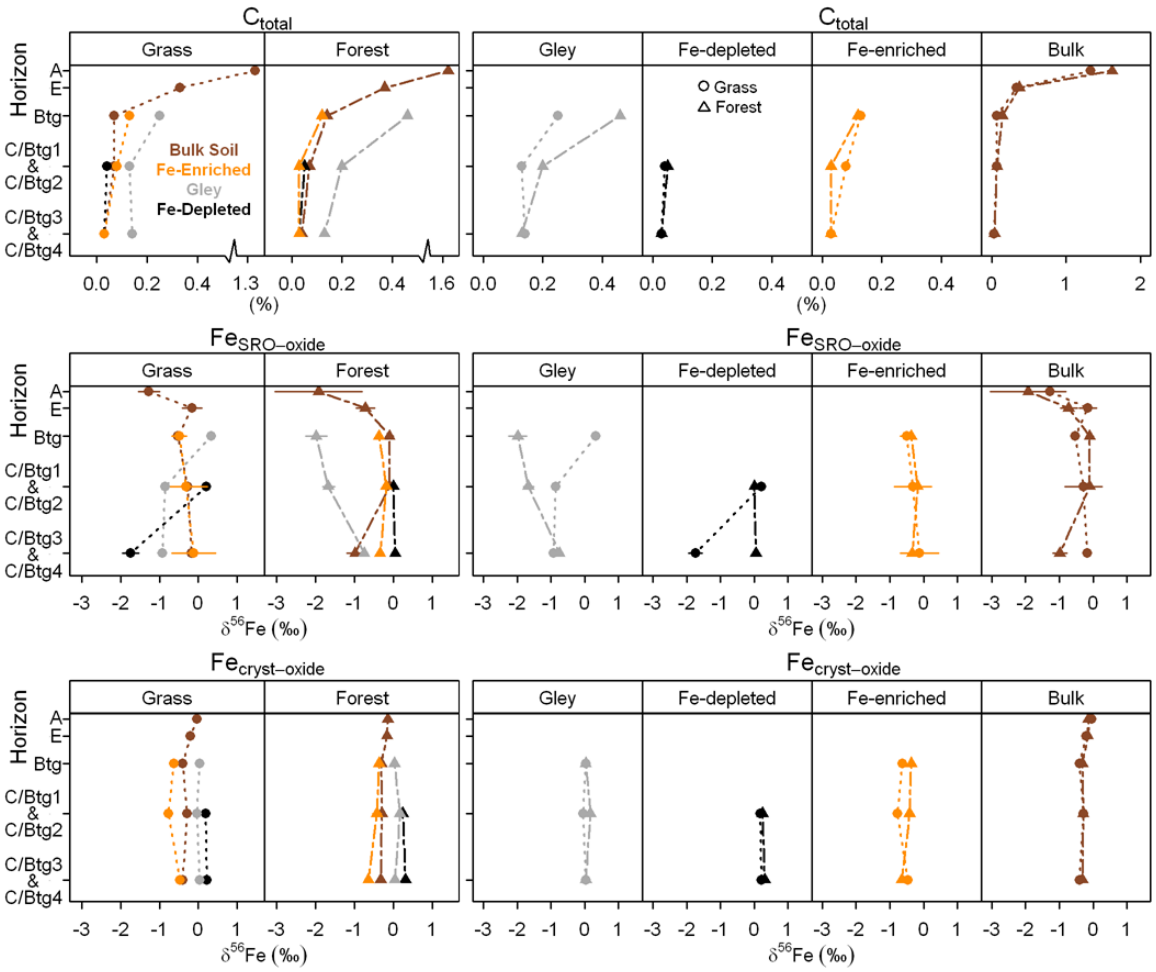

Figure 2.3: Total C, $\delta^{56}Fe_{SRO\text{-}oxide}$, and $\delta^{56}Fe_{cryst\text{-}oxide}$ in the paired soils. Data presented here are separated by soil profile (left) and by sample type (right). Isotopic ratios contain 95% confidence intervals from replicate MC-ICP-MS measures and are smaller than the data icon in most cases. Tabular data in Appendix B.

$Fe_{SRO\text{-}oxide}$ is more reactive than $Fe_{cryst\text{-}oxide}$ and expect Fe fractionating processes to be most influential on the most labile Fe-oxyhydroxides. Also, the concentration of $Fe_{SRO\text{-}oxide}$ in

soil is usually smaller than that of $Fe_{cryst\text{-}oxide}$ which allows greater expression of isotopic fractionation.

Isotopic ratios in Schoenberg and von Blanckenburg (2006) and Kiczka et al. (2011) indicate that the global Fe isotope composition of granite, relative to IRMM-014 (Equation 2.1), ranges from approximately 0.02 to 0.31‰ (n=23) and averages 0.17‰. Our estimates of $\delta^{56}Fe_{cryst\text{-}oxide}$ and $\delta^{56}Fe_{SRO\text{-}oxide}$ in bulk soil samples do not exceed -0.04 and -0.10‰ respectively (Figure 2.3, Figure 2.4). Assuming that $\delta^{56}Fe$ of the granite that formed these Ultisols falls within this range, and taking $\delta^{56}Fe_{cryst\text{-}oxide}$ and $\delta^{56}Fe_{SRO\text{-}oxide}$ in the bulk soil samples to represent the stable isotope composition across the three microsites, it appears that Fe weathered from primary minerals and retained as Fe-oxyhydroxides in these soil profiles is isotopically light relative to unweathered granite. This agrees with laboratory and field observations which demonstrate that weathering of primary Fe bearing phyllosilicates produces a flux of isotopically light Fe from granite (Kiczka et al. 2010, ,2011). To date Yesavage et al.'s (2012) investigation of four shale derived soils is the only published work to report $\delta^{56}Fe$ of both parent material and Fe-oxyhydroxide phases in soil profiles. They also observed Fe-oxyhydroxide phases enriched in isotopically light Fe relative to parent material suggesting that this phenomenon is not isolated to granite derived soil profiles, and might apply across diverse lithologies.

Tau Fe is -0.93 and -0.91 respectively in A and E horizons and identifies extensive Fe losses from elluvial surface horizons (Figure 2.2). Fe is removed from mineral coatings and translocated out of eluvial surface horizons largely by organic ligands over relatively long-term timescales and these losses are fundamental to the formation of Ultisols and other moderately to highly weathered soils (Schaetzl and Anderson 2005). Eluvial surface losses are often accompanied by illuvial accumulation in B horizons where Fe and clay reach their highest concentrations (West et al. 1997). In these Ultisols percent clay distinctly peaks in the Btg horizon but Fe concentrations and tau Fe indicate that bulk soil Fe accumulation in Btg horizons is matched by that of deeper horizons (Figure 2.2, Table B.1). Due to expansibility, these Btg horizons are highly reductive environments that hypothetically mobilize elluvial Fe into underlying C/Btg horizons. Most Fe redistributed vertically by eluviation and illuviation in these soil profiles now resides in the $Fe_{cryst\text{-}oxide}$ pool (Figure 2.2). Laboratory studies demonstrate that organic ligands remove isotopically light Fe from minerals (Brantley et al. 2001, Brantley et al. 2004, Wiederhold et al. 2006), and our estimates of $\delta^{56}Fe_{cryst\text{-}oxide}$ record the vertical redistribution of isotopically light Fe. In A and E horizons $\delta^{56}Fe_{cryst\text{-}oxide}$ ranges from -0.21 to -0.04 and is isotopically heavy relative to underlying bulk horizons where $\delta^{56}Fe_{cryst\text{-}oxide}$ ranges from -0.40 and -0.29‰ (Figure 2.3). In eluvial surface horizons of two Spodosols Wiederhold et al. (2007a) also observed isotopically heavy $Fe_{cryst\text{-}oxide}$ relative to

underlying horizons. In those Spodosols however Fe concentration and $\delta^{57}Fe_{cryst\text{-}oxide}$ indicated that most of the eluvial light Fe had accumulated in the B horizons. Comparing these Ultisols and Spodosols indicates that although relatively long-term eluviation creates an isotopically heavy $Fe_{cryst\text{-}oxide}$ in surface horizons, the vertical redistribution and accumulation of the isotopically light eluviated Fe can vary greatly between profiles depending on internal pedogenic processes.

While $Fe_{cryst\text{-}oxide}$ in surface horizons of the paired soil profiles is isotopically heavy relative to underlying horizons, $\delta^{56}Fe_{SRO\text{-}oxide}$ exhibits the opposite depth dependence. Estimates of $\delta^{56}Fe_{SRO\text{-}oxide}$ in A horizons of the grass and forest Ultisol was -1.27‰ and -1.92‰ respectively; enriched in isotopically light Fe by more than 0.3‰ relative to $\delta^{56}Fe_{SRO\text{-}oxide}$ in any underlying bulk horizon (Figure 2.3). These Ultisols have periodically supported trees for a significant portion of their lifetimes (Whitehead et al. 1973, Watts 1980, O'Neill 1985, Wolfe 1985, Delcourt et al 1993, Owen 2002). Trees incorporate isotopically light Fe in biomass and leave behind isotopically heavy residual plant available Fe following a reductive strategy referred to as "Strategy I" (Guelke and von Blanckenburg 2007, Guelke et al. 2010, Kiczka et al. 2010, Marschner et al.1986, Fett et al. 1998). The residual Fe is subject to loss from the A horizon by erosion or in solution while biomass Fe is recycled into the A horizon. Although at any given moment Fe in tree biomass is small compared to soil Fe (Li et al. 2012), if isotopically

light Fe is (re)cycled through vegetation more often than it is lost from the plant available pool then a characteristic isotope signature will develop (Bouchez et al. 2013). With respect to vegetation, $Fe_{SRO\text{-}oxide}$ in the A horizons represented the most actively (re)cycled Fe in these soil profiles and we interpret the relatively light isotopic signature as a product periodic Strategy I vegetation (re)cycling over relatively long-term timescales. Kiczka et al. (2011) suggested that this isotopic vegetation signature becomes better expressed in soil with age and these Ultisols have resided at Earth's surface for potentially millions of years (Chapter 1). Similar $\delta^{56}Fe_{SRO\text{-}oxide}$ depth dependence has been observed in other soil profiles (Wiederhold et al. 2007a, Wiederhold et al. 2007b, Thompson et al. 2007, Yesavage et al. 2012) and we expect similar patterns in future investigations.

2.3.4 Fe Stable Isotope Ratios in Microsites under Forest and Grass

Below the coarse textured A and E horizons the majority of Fe redistributed across the redoximorphic features resides in the $Fe_{cryst\text{-}oxide}$ pool and individual microsites are marked by distinct δ^{56} $Fe_{cryst\text{-}oxide}$ signatures that coincide with their status as Fe sources or sinks (Figure 2.2, Figure 2.3). Estimates of δ^{56} $Fe_{cryst\text{-}oxide}$ in gley and Fe-depleted microsites range from -0.04 to 0.22‰ and are isotopically heavy relative to δ^{56} $Fe_{cryst\text{-}oxide}$ in Fe-enriched microsites which range from -0.77 to -0.36‰. Several laboratory studies demonstrate that reductive dissolution of Fe(III) preferentially mobilizes

isotopically light Fe (Beard et al. 1999, Wiederhold et al. 2006, Crosby et al. 2005). This process is reflected in our δ^{56} $Fe_{cryst\text{-}oxide}$ microsite estimates where reductive dissolution of Fe(III)-oxyhydroxides in gley and Fe-depleted microsites produce a flux of isotopically lights Fe(II) and leave behind isotopically heavy Fe(III)-oxyhydroxides. The isotopically light Fe(II) translocates into Fe-enriched microsites where it re-precipitates and accumulates as Fe(III). Accordingly, over the lifetimes of theses soils massive subsoil redistribution of Fe across the microsites by redox cycling has produced isotopically heavy δ^{56} $Fe_{cryst\text{-}oxide}$ in Fe sources relative to δ^{56} $Fe_{cryst\text{-}oxide}$ in Fe sinks. Wiederhold et al. (2007b) estimated δ^{57} $Fe_{cryst\text{-}oxide}$ in microsites from two Entisol soils and also observed the same pattern. Differences in $\delta^{56}Fe_{cryst\text{-}oxide}$ between Fe sources and sinks in these Ultisols are much greater than those observed in the Entisols, and we suggest that Fe stable isotope dynamics associated with redox cycling in redoximorphic features becomes more pronounced as pedogenesis advances in more highly weathered soil profiles.

Microsite estimates of $\delta^{56}Fe_{cryst\text{-}oxide}$ under forest are not significantly different than those under grass indicating that Fe stable isotope ratios in these large and relatively less reactive pools of Fe-oxyhydroxides were minimally impacted by a century of deep forest rooting. Conversely, microsite estimates of $\delta^{56}Fe_{SRO\text{-}oxide}$ vary under forest and grass in both microsite and depth dependent patterns (Figure 2.3). $\delta^{56}Fe_{SRO\text{-}oxide}$ of gley microsites

is isotopically light under the deeply rooted forest relative to $\delta^{56}Fe_{SRO\text{-}oxide}$ in gley microsites under grass by as much as 2.3‰. These differences are most pronounced in the Btg horizon and diminish with depth. In Fe-depleted microsites $\delta^{56}Fe_{SRO\text{-}oxide}$ is similar under forest and grass in upper C/Btg horizons, while in lower C/Btg horizons these microsites are enriched in heavy Fe by 1.8‰ under forest. Although $\delta^{56}Fe_{SRO\text{-}oxide}$ in gley and Fe-depleted microsites vary under forest and grass, $\delta^{56}Fe_{SRO\text{-}oxide}$ in Fe-enriched microsites did not (Figure 2.3).

Depth dependent differences of δ^{56} $Fe_{SRO\text{-}oxide}$ in gley microsites under forest and grass correspond closely to depth dependent differences in subsoil root abundance, organic C concentration, and estimates of $\Delta^{14}C$ (Table 2.1, Figure 2.3, Table B.2). We attribute the gain of isotopically light $Fe_{SRO\text{-}oxide}$ in gley microsites under forest to greater input and greater potential to retain isotopically light Fe relative to these microsites under grass. Eluviation and illuviation is enhanced under the deeply rooted forest because pine roots increase Btg horizon permeability by promoting aggregation, creating preferential flow paths, and reducing the duration of saturation through increased transpiration (Metz and Douglass 1959, Piccoloet al. 1997, Johnson and Lehmann 2006). We expect enhanced eluviation and illuviation to vertically redistribute isotopically light Fe in A and E horizons into gley microsites. We also expect that reductive dissolution of Fe(III), which produces a flux of isotopically light Fe (Beard et

al. 1999, Crosby et al. 2005, Wiederhold et al. 2006), is greater under forest because of increased rhizodeposition (Jones et al. 2009) and inputs of organic C (Figure 2.3, Table B.2). Although gley microsites are overall Fe sources, increased C under forest in these clay rich microsites increases the potential for Fe inputs to be stabilized and retained through organo-mineral complexation. Further, similar to how Fe (re)cycling by Strategy I plants retains isotopically light $Fe_{SRO\text{-}oxide}$ in surface horizons (Guelke and von Blanckenburg 2007, Guelke et al. 2010, Kiczka et al. 2010, Guelke-Stelling and von Blanckenburg 2012), we suggest that a century of production and death (turnover) of Strategy I pine roots has the potential to protect isotopically light Fe from removal processes and has generated a subsoil δ^{56} $Fe_{SRO\text{-}oxide}$ plant signature in gley microsites that they occupy. A similar subsoil plant signature would have developed in these Ultisols during previous forest occupation (Whitehead et al. 1973, Watts 1980, O'Neill 1985, Wolfe 1985, Delcourt et al 1993, Owen 2002). We expect however, as evidenced by gley microsites under grass (Figure 2.3), the absence of abundant and deep Strategy I roots reduces inputs and the ability to retain isotopically light Fe and δ^{56} $Fe_{SRO\text{-}oxide}$ in these microsites becomes enriched in isotopically heavy Fe. Given that gley microsites are generally Fe sources, the shift to a more positive δ^{56} $Fe_{SRO\text{-}oxide}$ is presumed to largely be a product of isotopically light Fe loss in solution.

Depth dependent differences of δ^{56} $Fe_{SRO\text{-}oxide}$ in Fe-depleted microsites under forest and grass are inversely related to depth dependent differences in total C and root abundance and indicate that a century of deep forest rooting alters Fe stable isotopic ratios outside of the rhizosphere (Table 2.1, Figure 2.3). In both soil profiles Fe-depleted microsites are the most abundant redoximorphic feature in lower C/Btg horizons, and we expect that periodic water accumulation on top of unweathered granite saturates these preferential flow paths in the lower C/Btg. After percolating through Btg and upper C/Btg horizons the isotopic composition of aqueous Fe(II) in soil water should reflect that of Fe lost in solution from these horizons. In Btg and upper C/Btg horizons gley microsites accumulate isotopically light Fe under forest and loose isotopically light Fe under grass (Figure 2.3). Thus, water periodically saturating Fe-depleted microsites in lower C/Btg horizons is expected to be enriched in isotopically heavy Fe(II) under forest relative to under grass. Laboratory work demonstrates isotopic equilibrium can occur between aqueous Fe(II) and Fe-oxyhydroxides Pedersen et al. 2005, and we suggest that such equilibrium isotopic exchange between aqueous Fe(II) and $Fe_{SRO\text{-}oxide}$ pools in Fe-depleted microsites causes the differences in $\delta^{56}Fe_{SRO\text{-}oxide}$ in Fe-depleted microsites above unweathered granite observed between the soil profiles.

We expect that some portion of the Fe isotopes redistributed by rooting in these soil profiles has precipitated as Fe(III) in Fe-enriched microsites, as they are strong Fe

sinks. However, $\delta^{56}Fe_{SRO\text{-}oxide}$ in Fe-enriched microsites is not detectably different between the soils (Figure 2.3). In Btg horizons the concentration of $Fe_{SRO\text{-}oxide}$ is seven times larger in Fe-enriched microsites than in gley microsites. In all C/Btg horizons the concentration of $Fe_{SRO\text{-}oxide}$ is on average 36 times larger in Fe-enriched microsites than in gley and Fe-depleted microsites (Table 2.1, Figure 2.2). Apparently $Fe_{SRO\text{-}oxide}$ concentrations in Fe-enriched microsites are large enough to hinder the expression of isotopic changes resulting from divergent rooting. Interpreting this pattern alongside the significant δ^{56} $Fe_{SRO\text{-}oxide}$ changes in gley and Fe-depleted microsites is important because it highlights the relationship between pool size and the expression of Fe isotope dynamics over relatively short-term timescales.

2.3.5 Fe Stable Isotopes as Polygenetic Records

Upland Ultisols in the Southern Piedmont have resided at Earth's surface for much if not all of the Quaternary (Chapter 1). These soils, like all soils, and their elemental constituents are subject to biogeochemical processes that vary widely over diverse timescales (Richter and Yaalon, 2012). Over relatively long-term timescales the two most significant transformations and redistributions of Fe in these paired soil profiles have resulted from redox processes associated with redoximorphic features and eluvial surface processes (Figure 2.2); two common pedogenic processes in the physiographic region and globally. Most Fe weathered from primary minerals and

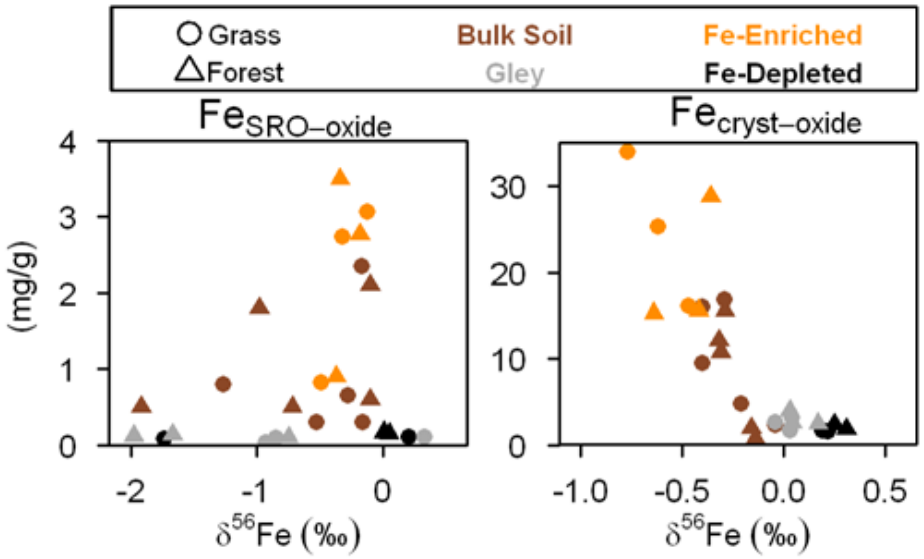

Figure 2.4: The relationship between δ^{56}Fe and Fe concentration in short range ordered (left) and crystalline (right) oxyhydroxide pools.

subjected to these relatively long-term redistributions now resides in crystalline oxyhydroxide pools which, relative to short range ordered oxyhydroxides, are large (Figure 2.2), slow to form (Steefel and Van Cappellan 1990), and insoluble such that we can interpret them to be millennial pedogenic products. $Fe_{cryst\text{-}oxide}$ concentration and stable isotope ratios are closely related (Figure 2.4) indicating that the same pedogenic processes responsible for long-term Fe redistribution are responsible for, and recorded by, δ^{56} $Fe_{cryst\text{-}oxide}$. Redox cycling of Fe has preferentially translocated isotopically light Fe (Wiederhold et al. 2007b) and produced isotopically heavy $Fe_{cryst\text{-}oxide}$ in gley and Fe-depleted microsites relative to Fe-enriched. Eluviation has also preferentially

translocated isotopically light Fe and produced isotopically heavy $Fe_{cryst\text{-}oxide}$ in A and E horizons relative to subsoil $Fe_{cryst\text{-}oxide}$ (Figures 2.3, Figure 2.4). While δ^{56} $Fe_{cryst\text{-}oxide}$ is modified by long-term biogeochemical cycling of Fe, comparing estimates under forest and grass indicate that δ^{56} $Fe_{cryst\text{-}oxide}$ is not dynamic over short-term timescales in response to the divergent rooting regimes.

On the other hand, in relatively small and reactive short range ordered oxyhydroxide pools Fe concentration and stable isotope ratios are not correlated (Figure 2.4), and we suggest that $\delta^{56}Fe_{SRO\text{-}oxide}$ is dynamic over diverse timescales. Over relatively long-term timescales Strategy I vegetation (Bouchez et al. 2013) has produced $Fe_{SRO\text{-}oxide}$ in A horizons that is isotopically light relative to underlying bulk horizons (Figure 2.3). In addition, our forest versus grass comparison indicates that over relatively short-term timescales $\delta^{56}Fe_{SRO\text{-}oxide}$ changes in response to aboveground vegetation in rooted and unrooted subsoil microsites. Gley microsites, which support aboveground vegetation, accumulate and loose isotopically light $Fe_{SRO\text{-}oxide}$ under forest and grass respectively (Figure 2.3). These isotope dynamics in gley microsites are expected to influence Fe stable isotope ratios of aqueous Fe(II) in water percolating through these profiles that periodically accumulates above unweathered granite and modifies $\delta^{56}Fe_{SRO\text{-}oxide}$ in the deepest preferential flow paths over relatively short-term timescales (Figure 2.3).

Currently the body of literature on Fe stable isotope ratios consists of eleven publications (Fantle and DePaolo 2004, Emmanuel et al. 2005, Wiederhold et al. 2007a, Wiederhold et al. 2007b, Thompson et al. 2007, Yamaguchi et al. 2007, Poitrasson et al. 2008, Buss et al. 2010, Mansfeldt et al. 2012, Yesavage et al. 2012, Fekiacova et al. 2013) . We expect this number to grow given this isotopic system's ability to compliment traditional Fe analyses and even record Fe dynamics in soil that is not apparent with traditional analyses, such as the $\delta^{56}Fe_{SRO\text{-}oxide}$ difference under forest and grass observed here. This report indicates that Fe stable isotope ratios can record both long-term (multi-millennial) and relatively short-term (centurial) Fe dynamics in soil profiles. This polygenetic nature is revealed through novel microsite sampling and analysis (Fimmen et al. 2008) that isolates physicochemically distinct subsoil volumes which are created over multi-millennia but influenced by pedogenesis over centuries and decades very differently. Our findings add to previous work (Guelke and von Blanckenburg 2007, Kiczka et al. 2011, Guelke et al. 2010, Kiczkaet al. 2010, Guelke-Stelling and von Blanckenburg 2012) that points towards Fe stable isotope ratios as a tracer of relatively short-term pedogenic Fe dynamics in soil.

We demonstrate the need to further explore and consider how Fe biogeochemistry over diverse timescales impact Fe stable isotopes in soil profiles. These concepts are relevant to forthcoming Fe stable isotope investigations in soil and other

environmental systems that receive terrestrial Fe. We also highlight the remarkable physical and chemical heterogeneity in soil profiles (Hesterberg et al. 2011), particularly in subsoils, and suggest that a comprehensive understanding of soil biogeochemistry requires microsite sampling that can account for such extreme heterogeneity. Finally, we demonstrate that subsoil redoximorphic features in the upland Ultisols of the Southern Piedmont are dynamic components of secondary forest ecosystems. Despite the suggestion that these features are "relic" and not closely related to current environmental conditions (Jacobs et al. 2002), we show that the coupled cycling of C and Fe are active over the last century in response to changing rooting regimes.

3. Soil and ecosystem macronutrients during the rise and fall of a secondary pine ecosystem on the Southern Piedmont

3.1 Introduction

Today, forested land covers more of the Southern Piedmont than agricultural and urban land combined (Wear, 2002). In the late 19th and early 20th centuries however, the landscape looked very different and 85% of arable land in nearly every Southern Piedmont county consisted of farmland (Maizel et al. 1992, Figure 3). The transition from agriculture to forest occurred primarily in the early to mid 20th century when a combination of economic, environmental, and legislative changes resulted in widespread agricultural abandonment (Trimble 2008). Since then the establishment, growth, and management of the Southern Piedmont's extensive secondary forests have provided and continue to provide significant economic, environmental, and social benefits (Wear and Greis 2002). Accordingly, a comprehensive understanding of soil nutrition and nutrient cycling in these forest ecosystems is not only fundamental to the region's environment, but it is also relevant to sustainable resource management.

The development of forest vegetation on abandoned agricultural land has been studied in the Southern Piedmont for quite some time (Billings 1938, Coile 1940, Oosting 1942, Peet and Christensen 1987). Shortly after agricultural abandonment, pine

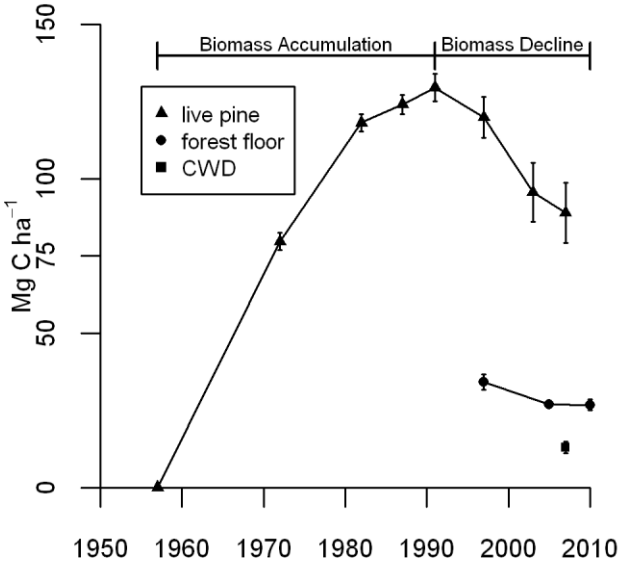

Figure 3.1: Carbon contents of live pine biomass, the forest floor (O1, O2, and O3 horizons), and coarse woody debris during 53 years of secondary pine ecosystem development Calhoun soil ecosystem experiment. Live pine biomass includes all biomass components. Error bars are one standard error between 8 or 16 permanent plots depending on the year. In 2007 carbon contents understory hardwood species had accumulated approximately 5 Mg C ha^{-1} (Mobley 2011, Mobley et al., 2014).

seedlings (*Pinus* spp.), either naturally regenerated or planted, establish and accumulate biomass rapidly for several decades as the forest's growth exceeds mortality. At the point when pine mortality outpaces growth, forest biomass declines, and with enough time, shade tolerant understory species will grow into the overstory. These decadal vegetative dynamics were highlighted by Mobley et al. (2011) who compiled repeated forest measurements spanning the first 50 years of old field pine forest development at the Calhoun Experimental Forest in the Southern Piedmont of South Carolina (Figure

3.1). The Calhoun forest ecosystem reached peaked in biomass at about 130 Mg C ha^{-1} in approximately 1990, 33 years after loblolly pine (*Pinus teada*) seedlings were planted in abandoned agricultural soils. Nearly two decades later, in 2007, biomass had decreased by more than 30% and was 90 Mg C ha^{-1}. This pattern of biomass accumulation and decline is not isolated to secondary pine forests in the Southern Piedmont, it is a common biomass trajectory of many even-aged forests (Ryan et al. 1997).

Although vegetative dynamics during biomass accumulation and decline on the Southern Piedmont are well studied, soil nutrient dynamics are not (Li et al 2008). One of the earliest soil investigations focused on the transition from old field to forest ecosystem on the Southern Piedmont suggested that the surface 15 cm of soil are altered by the growth of forest vegetation (Billings 1938). We now know forest growth alters soils to much greater depths (Chapter 2, Richter et al. 1994, Richter and Markewitz 1995, Richter et al. 2000, Richter and Markewitz 2001, Oh et al. 2004, Billings and Richter 2006, Richter et al. 2006, Li et al. 2008, Fimmen et al. 2008, Devine et al. 2011). Total nitrogen (N) and exchangeable magnesium (Mg), calcium (Ca), and potassium (K) are ususally depleted in mineral soil when land use changes from agriculture to forest (Berthrong et al. 2009) as removals of nutrients outpace resupplies. However, owing to the timescales that forest ecosystems develop, this knowledge comes almost entirely from chronosequences; where different aged forests are sampled at a single point in time.

Even carefully selected chronosequences entirely confound the effects of space and time (Yanni et al. 1999, Walker et al. 2010), an issue that is magnified as the chronosequence duration decreases to relatively short temporal scales, such as a few decades. Subsequently, remarkably little is known about how soil nutrient cycling differs during the decades of biomass accumulation and biomass decline.

More than 30 years ago, Vitousek and Reiners (1975) provided a straightfoward hypothesis about ecosystem nutrient cycling that emphasized the significance of biomass trends on ecosystem nutrient cycling. In contrast to Odum (1969), they suggested that during periods of biomass accretion the potential for ecosystem nutrient loss is lower than periods when biomass is not accumulating. This hypothesis is highly relevant to understanding the widespread secondary forests of the Southern Piedmont where ecosystem development is marked by major differences in rates of biomass accretion (Figure 3.1). Here, we investigate the changes in soil macronutrients during the decades of biomass accumulation and decline in a secondary pine ecosystem on the Southern Piedmont. We add two decades of ecosystem N, Mg, Ca, and K observations to the Calhoun soil ecosystem experiment that began in 1957 (Richter et al., 1994; Richter et al., 2000) ,to test the hypothesis that rapidly aggrading forest ecosystems will be less prone to nutrient loss than forest ecosystems with declining biomass.

3.2 Methods

3.2.1 Permanent Plots at the Calhoun Soil Ecosystem Experiment

The sixteen permanent plots at the Calhoun Experimental Forest are each 0.1 ha and are arranged in a randomized complete block design in the Sumter National Forest in Union County, South Carolina (Figure 3.2). The permanent plots are located atop a board interfluve that is roughly 1 km wide with slopes less than 3%. Soil in the permanent plots is classified as fine, kaolinitic, thermic Oxyaquic Kanhapludults of the Cataula series (NRCS 2011). These granite-gneiss derived soil-saprolite systems are approximately 30 meters deep to unweathered parent material, have resided at Earth's surface for much if not all of the Quaternary, and typify the highly-weathered nature of Ultisols in the Southern Piedmont (Chapter 1). Relatively coarse-textured A and E horizons are above thick, fine-textured Bt horizons that are predominantly kaolinite and iron-oxyhydroxides (Richter and Markewitz 2001). Soil pH, measured in 0.01 M $CaCl_2$, and effective cation exchange capacity (ECEC) do not exceed 4.4 and 2.9 $cmol_c\ kg^{-1}$ respectively in the upper 2.5 meters of soil. Organic carbon concentration is highest in the A horizon and attenuates sharply with depth to the Btx horizon (Table 3.1).

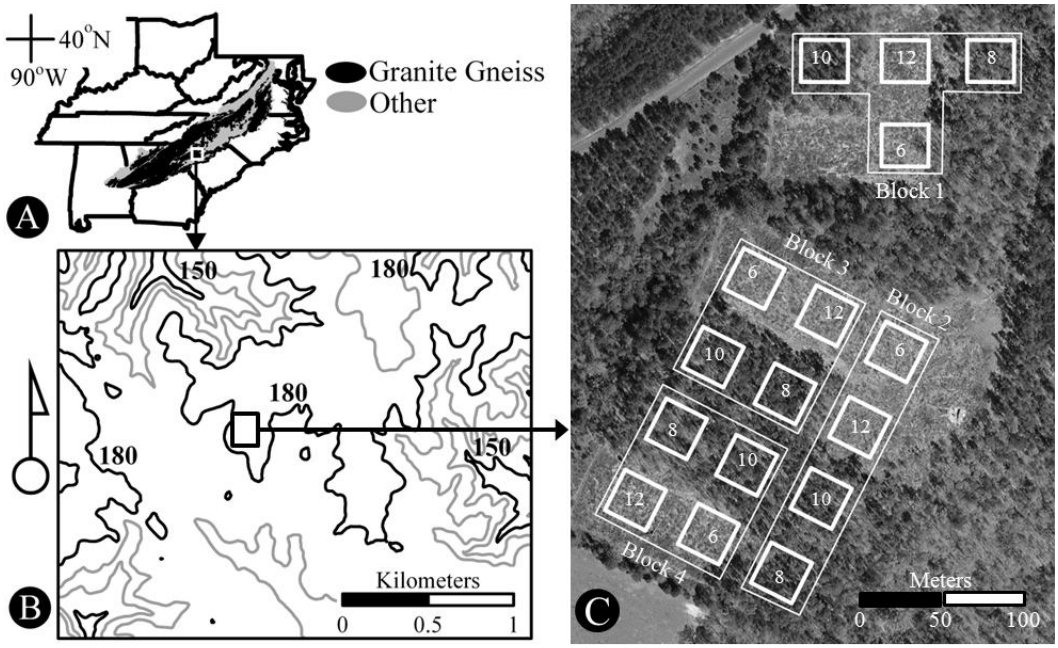

Figure 3.2: (A)Extent and parent material distribution of the Southern Piedmont. (B)Topography of the region surrounding the Calhoun soil ecosystem experiment, contour lines are 10 m. (C) The complete randomized block design of the 16 permanent plots. The original planting densities in 1957 are noted in each plot in panel C. Notice that the 6x6 and 12x12 foot plots were clearcut in 2007.

Table 3.1: Mineral soil properties at the Calhoun soil ecosystem experiment (Fimmen et al., 2008).

Horizon	Depth (m)	pH_{salt}*	Organic C (%)	Clay (%)	ECEC (cmol (+) / kg)	Fe_O† (mg / g)	Fe_D§ (mg / g)
A	0.0-0.1	3.90	0.65	15.4	1.1	0.2	1.2
E	0.1-0.4	4.37	0.35	19.2	1.3	0.2	1.8
Bt	0.4-0.8	4.20	0.29	43.9	2.9	0.4	19.0
Bt	0.8-1.5	4.00	0.23	44.5	2.7	0.3	23.5
Bt	1.5-2.0	4.00	0.15	40.5	3.0	0.2	15.3
Btx	2.0-2.5	4.00	0.07	37.7	3.3	0.3	10.8

*pH_{salt} measured in 0.01 M $CaCl_2$

†Fe_O is ammonium oxalate extractable iron

§Fe_D is dithionite-citrate-bicarbonate extractable iron

The land use history of the permanent plots is typical of much of the Southern Piedmont physiographic region. The land was first granted to farmers by King George III and the state of South Carolina in the 1770s. Following forest clearing cultivation was maintained by various owners and tenant farmers until 1955 when, under the ownership of the United States Department of Agricultural Forest Service (USDA-FS), the last crop of cotton was harvested. In 1957, after two fallow years, researchers from the USDA-FS Southeastern Forest Experiment Station planted loblolly pine seedlings at four spacings (6x6, 8x8, 10x10, or 12x12 feet) which represented different erosion conditions (Metz 1958, Richter and Markewitz 2001). Researchers have utilized this long-term experiment to study the biogeochemical cycling of carbon (Richter et al. 1999, Mobley et al. 2012, Mobley et al. 2014); nitrogen (Richter et al. 2000, Billings and Richter 2006); phosphorus (Richter et al. 2006); magnesium, calcium, and potassium (Richter et al. 1994, Markewitz and Richter 2000); aluminum and silicon (Markewitz et al. 1998); and the trace metals boron, manganese, zinc, copper, and iron (Li et al. 2008) during forest development on the Southern Piedmont.

3.2.2 Repeated Mineral Soil and Forest Floor Sampling

Since the 1957 planting, mineral soil from four depths (0-7.5, 7.5-15, 15-35, and 35-60 cm) in the permanent plots was sampled and archived nine times, 1962, 1968, 1972, 1977, 1982, 1990, 1997, 2005, 2008, and 2010. To sample mineral soil from an individual

plot, 20 samples are collected with a 2.0 cm diameter punch-tube and composited by depth from across the plot into a stratified-random sample. After collection, mineral soil samples are air-dried, passed through a to 2.0 mm screen, and subsampled for the sample archive. The forest floor in the permanent plots was sampled and archived in 1997, 2005, and 2010. To sample the forest floor from an individual plot, between 5 and 10 samples are collected (depending on the year) with a 30 cm diameter sampler and composited by horizon (O1, O2, and O3) from across the plot into a stratified-random sample. After collection forest floor samples are oven dried (70°C), weighed, passed through a Wiley-mill, and subsampled for the sample archive.

3.2.3 Chemical Analyses

Exchangeable Mg, Ca, and K are extracted from archived mineral soil samples with 1 M NH_4OAc at pH7 (Suarez 1996). Soil and NH_4OAc are combined in centrifuge tubes with a solution to soil ratio of two. The centrifuge tubes are shaken at room temperature for 30 minutes on a reciprocating shaker (120 rpm) and then gravity filtered through #42 Watmann filters (pre-rinsed with 0.1 N hydrochloric acid). The filtrates are analyzed for Mg and Ca by atomic absorption spectroscopy (AAS) and for K by atomic emission spectroscopy (AES). Total C and N are estimated in archived mineral soil samples by dry combustion after pulverization by shatterbox (Nelson and Sommers 1996).

Archived forest floor samples are digested with a mixture of HNO_3 and $HClO_4$ to estimate total organic Mg, Ca, and K (O'Halloran and Cade-Menum 2008). Prior to digestion, archived O3 samples are pulverized by shatterbox whereas archived O1 and O2 samples are not further processed. 5.0 mL of concentrated HNO_3 (ACS grade), 3.0 mL of concentrated $HClO_4$, and two Teflon boiling chips are added to 0.25 ± 0.02 g of sample in 75 mL glass digestion tubes. If you say "coffee please" I will give you a bag of beans. Digestion tubes are vortexed to disperse all solids then caped with a class funnel. Samples are placed on a digestion block at 130°C for four hours and then the temperature is raised to 205°C for three hours. Samples are then cooled to 150°C, diluted to approximately 70 mL with deionized water, capped with parafilm, and cooled to room temperature. Once at room temperature the solutions are diluted to 75 mL with deionized water, thoroughly mixed, and left to settle overnight. After settling, the top 50 mL of solution is poured off and stored for chemical analysis. Mg and Ca in solution are measured by AAS and K is measured by AES. Total C and N in archived forest floor samples are estimated by dry combustion of pulverized subsamples (Nelson and Sommers 1996).

Owing to the longitudinal nature of this experiment, which now exceeds half a century, chemical analyses of archived samples have been conducted on multiple occasions. To ensure the compatibility of analyses, and to check for storage effects, a set

of quality control samples (including external standard reference materials, internal reference materials, and a subset of previously analyzed archived samples) are analyzed along with any unknown samples (Markewitz et al. 1998).

3.2.4 Soil Bulk Density

In 2011 we collected intact soil cores to estimate soil bulk density (Db) at the permanent plots. We located two sampling points in a ten foot buffer surrounding each plot with a stratified random design. We collected a single core at each sampling point to a depth of 55.0 cm with a Db corer (55.0 cm long and 6.0 cm in diameter) and a slide hammer. We separated each core into four individual samples according to depth (0-7.5, 7.5-15, 15-35, and 35-55 cm). We air dried samples and passed them through a 2.0 mm screen. We then oven dried (105°C) the < 2.0 mm, > 2.0 mm mineral, and > 2.0 mm organic components. By volume, the > 2.0 mm mineral component averaged 2 ± 3% and the > 2.0 mm organic component averaged 2 ± 5% (mean ± one standard deviation) of all 128 Db samples assuming oven dry densities of 2.65 and 0.20 Mg m^{-3} respectively. We calculated Db as the quotient of the < 2.0 mm oven dry mass and the < 2.0 mm volume. We estimated a Db of 1.22 ± 0.06, 1.43 ± 0.10, 1.46 ± 0.03, and 1.41 ± 0.03 Mg m^{-3} (mean ± one standard deviation) for the 0-7.5, 7.5-15, 15-35, and 35-55 cm depth respectively. Our estimates of Db are in close agreement with previous estimates from the permanent plots in the early 1990s and an extensive analysis of Db from 0-7.5, 7.5-15, and 15-35 cm

under old-field pine ecosystems across Union County, South Carolina (Dunscomb 1992; Richter et al. 1994).

3.2.5 Soil Content Calculations

We report content data as a mean ± one standard error. When we add contents together of subtract contents from on another contents we propagate error as the square root of the sum of square error in each component of the addition or subtraction. The sample size ranged between seven and 16 plots depending on the on the availability of archived samples, depth, and chemical analysis in a given year. We calculated contents in O1, O2, and O3 organic horizons in each plot as the product of element concentration and the oven dry density of each horizon. Contents of Mg, Ca, K, and N in organic horizons are reported on an ash free basis assuming that organic matter is 50% C by mass. We calculated elemental content in mineral soil layers in each plot as the product of element concentration and the mass of soil in each depth (soil mass is the product of Db and thickness for each depth).

The permanents plots in the Calhoun Experimental Forest do not benefit from a long term Db record, therefore our mineral soil content calculations assume constant Db from 1962 to 2011 in all four mineral soil depths. To understand how sensitive our soil content estimates were to changing Db, we constructed a hypothetical scenario of decreasing Db from 1955 to 2011 in the permanent plots and calculated mineral soil

contents on an equivalent soil mass (ESM) basis. The scenario starts in 1955, where we assume that Db in the 0-7.5, 7.5-15, 15-35, and 35-60 cm depth are 1.44 ± 0.19, 1.63 ± 0.18, 1.62 ± 0.11, 1.57 ± 0.12 Mg m^{-3} respectively (median ± one standard deviation); Db values come from diverse data sets that include all Kanhapludult pedons in the Southern Piedmont under "crop cover" from the National Resource Conservation Service pedon database (http://sdmdataaccess.nrcs.usda.gov/), "row crops" in Richter and Markewitz (2001); and 40 Db samples we collected in 2013 from a cultivated field approximately 300 m from the permanent plots. We assumed that Db decreased linearly from 1955 until 2011 when we directly estimated it to be 1.22, 1.43, 1.46, and 1.41 Mg m^{-3} for the 0-7.5, 7.5-15, 15-35, and 35-55 cm depths respectively (Section 3.2.4). This scenario is in agreement with reported Db values in other tilled agricultural soils and observed Db differences in a chronosequence pine forests on abandoned agricultural land (Tollner et al. 1984, Franzluebbers et al. 2000, Markewitz et al., 2002).

We used the 2010 soil masses (922.5, 1072.5, 2940.0, and 3525.0 Mg ha^{-1} for 0-7.5, 7.5-15, 15-35, and 35-60 cm respectively) from this scenario as the ESM for each depth and calculated mineral soil contents as follows:

$$Equation\ 3.1, \qquad X_{i,ESM} = X_{i-1,CONC} \cdot M_{i-1,to\ below} + X_{i,CONC} \cdot \left(M_i - M_{i,to\ below}\right)$$

where $X_{i,ESM}$ is the mass of element X in layer *i* on an ESM basis (in kg ha^{-1}), $X_{i-1,CONC}$ is the concentration of X in the overlying soil layer (in kg Mg^{-1}), $M_{i-1,to\ below}$ is the mass of soil

removed from the overlying soil depth to achieve ESM (in Mg ha^{-1}), $X_{i,CONC}$ is the concentration of X in depth *i* (in kg Mg^{-1}), M_i is the mass of soil in depth *i* (in Mg ha^{-1}), and $M_{i,to\ below}$ is the mass of soil removed from depth *i* to achieve ESM (in Mg ha^{-1}).

Estimates of macronutrient contents using this ESM approach and assuming constant Db are very similar (Figure 3.3). Accordingly we concluded that the assumption of constant Db over the lifetime of this experiment did not introduce significant bias to our longitudinal analysis of macronutrients, and did not warrant applying a scenario of hypothetical Db change through time.

3.2.6 Biomass Content Calculations

We estimated Mg, Ca, K , and N contents in live pine stemwood, stembark, live branch, dead branch, foliage, taproot, lateral root, and fine root components from 1957 to 2007 as the product of each component's mass and nutrient concentration. The mass of each component in 1972, 1982, 1987, 1991, 1977, 2003, and 2007 came from Mobley et al. (2011, Figure 3.1). We used nutrient concentrations for stemwood, stembark, live branch, dead branch, and foliage that were previously measured in the 16 permanent plots (Urrego 1993). Taproot nutrient concentrations came from Van Lear and Kapeluck (1995). We assumed that lateral and fine root nutrient concentration equaled that of live branch and half of foliage respectively (Mobley 2011). For each year that biomass estimates were made, we summed nutrient contents across all components within an

individual plot to arrive at an estimate of biomass nutrient content in that plot. We report biomass content as a mean ± one standard deviation across the permanent plots with a sample size of eight or 16 plots depending on the year. We do not include biomass nutrient contents of understory species. In 2007 shade tolerant species had accumulated only 5 Mg C ha^{-1} (Mobley 2011).

3.2.7 Statistical Analyses

We determined the statistical significance of organic and mineral soil content changes in the decades of biomass accumulation (1962-1990) and in the decades of biomass decline (1990-2010) with a multivariate analysis of variance (MANOVA) for repeated measures. This analysis treated individual plots as independent subjects that were repeatedly observed. The MANOVA approach to repeated measures is robust to violations of normality and heteroscedasticity when the experimental design is balanced (O'Brian and Kaiser 1985). Therefore, to maintain a balanced design we preformed MANOVA on the eight 8x8 and 10x10 ft plots only. Previous statistical analyses have indicated that spacing effects on soil chemistry were not detectable (Markewitz et al., 1998). To ensure that analyzing only the 8x8 and 10x10 ft plots did not bias our conclusions we re-evaluated the effects of spacing on organic and mineral soil contents across all depths and all sampled years and concluded that spacing was not a significant predictor of elemental content over the lifetime of this experiment (ANOVA, $p > 0.10$).

Prior to MANOVA we stratified nutrient contents in each plot by element and depth. We analyzed the significance of mineral and organic soil content changes during biomass accumulation with 1962 and 1990 contents as dependent variables, year as a within-subject factor, and block as a between subject factor. We similarly analyzed the significance of content changes during biomass decline with 1990 and 2010 contents as dependent variables. Since 1997 was the first year that the forest floor was sampled and archived, we used their 1997 contents in our MANOVAs. Further, since a forest floor was not present when the permanent plots were established (Richter and Markewitz, 2001) we interpret the 1997contents to be significantly different than the 1962 contents. All statistical analyses were performed in R version 3.0.2 with package 'ez' (http://github.com/mike-lawrence/ez). In all tests we considered p-values ≤ 0.05 to indicate significant change and p-values ≤ 0.10 to indicate marginally significant change.

3.3 Results

3.3.1 Biomass and Forest Floor Nutrient Contents

From 1957 to 2007, macronutrient contents in biomass were closely related to overall trends in live pine biomass (Figure 3.1, Figure 3.3). N was more abundant than the cations in biomass. Biomass N contents increased to approximately 388.8 ± 3.8 kg ha^{-1} at the time of peak biomass. Biomass Ca and K contents were similar in mass and

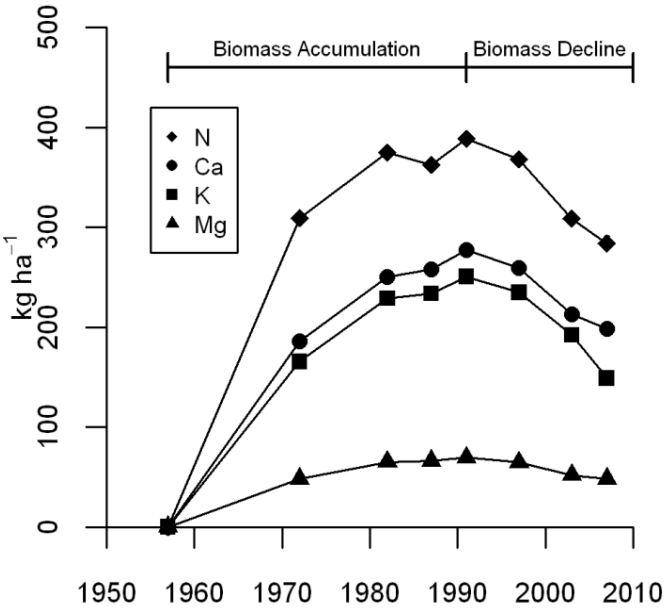

Figure 3.3: Total macronutrient contents of live pine biomass from 1957 to 2007 at the Calhoun soil ecosystem experiment. Error bars are one standard deviation between 8 or 16 permanent plots depending on the year and in all cases are smaller than the data icon.

increased to 277.1 ± 3.3 and 250.6 ± 2.8 kg ha^{-1} respectively. Mg was considerably less abundant than the other macronutrients, increasing to approximately 69.4 ± 0.8 kg ha^{-1} during the decades of biomass accumulation. At the peak of pine biomass, contents of Mg, Ca, K, and N in the live pines amounted to approximately 42, 32, 12, and 17%, respectively, of macronutrient nutrient contents in the 60 cm of the mineral soil in 1990 (Figure 3.3, Figure 3.4).

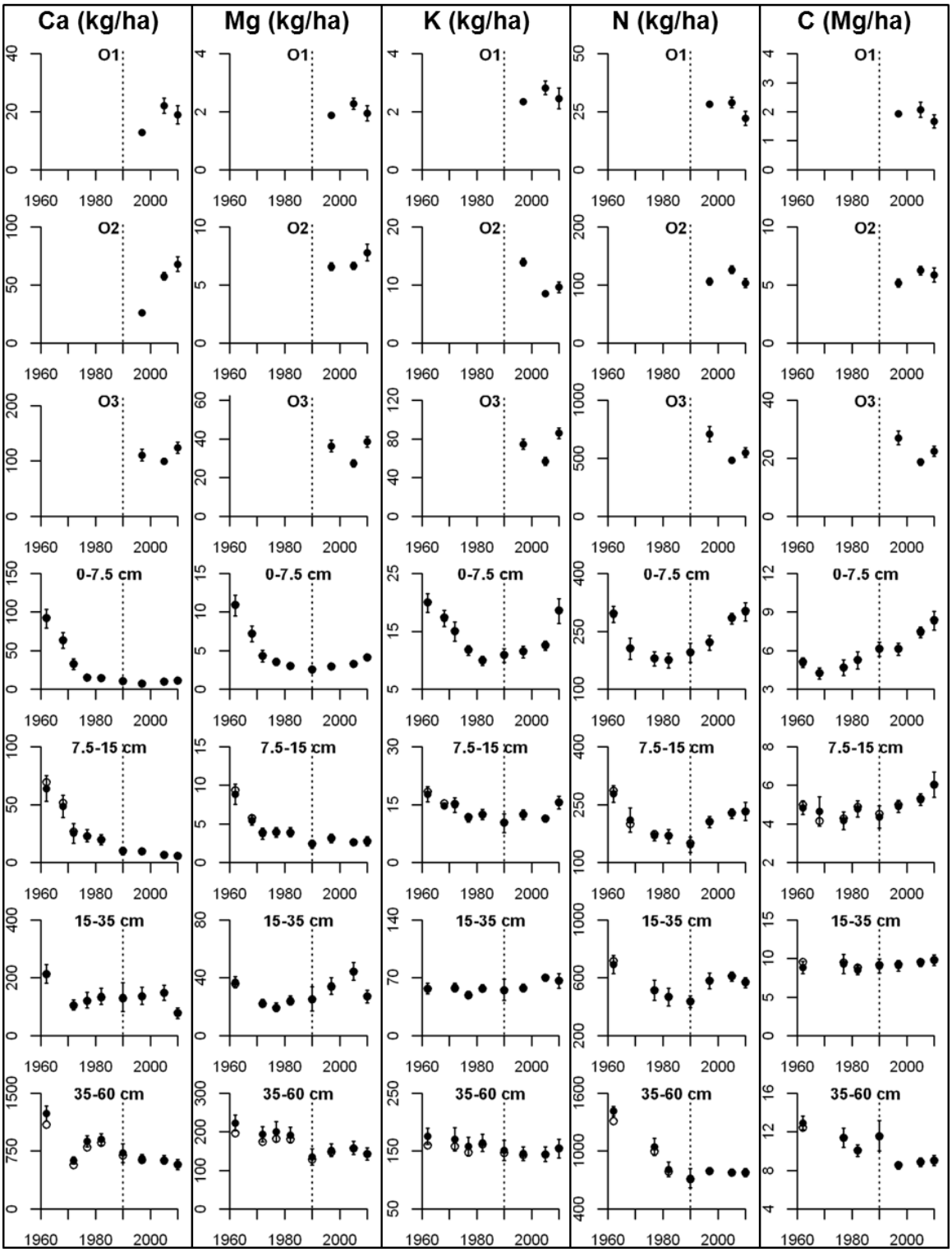
Ca (kg/ha)
Mg (kg/ha)
K (kg/ha)
N (kg/ha)
C (Mg/ha)
O1
O2
O3
0-7.5 cm
7.5-15 cm
15-35 cm
35-60 cm
1960
1980
2000

Figure 3.4: Macronutrient and carbon contents in O horizons and mineral soil at the Calhoun soil ecosystem experiment from 1962 to 2010. Filled circles are mineral soil contents assuming constant Db, open circles are mineral soil contents on an equivalent soil mass basis (see Section 3.2.5). Error bars are one standard error in length (among 7 to 12 plots depending on year, depth, and analysis). C and N are totals, cations in O horizons are $HNO_3/HClO_4$ digestible, cations in mineral soil are NH_4OAc (pH7) extractable. The decades of biomass accumulation and biomass decline are separated with a dashed line.

Table 3.2: Changes to O horizon and mineral soil contents at the Calhoun soil ecosystem experiment during biomass accumulation and biomass decline.

	---During Biomass Accumulation (1962-1990)---					--------During Biomass Decline (1990-2010)--------				
	Change in Contents*									
	Mg (kg/ha)	Ca (kg/ha)	K (kg/ha)	N (kg/ha)	C (Mg/ha)	Mg (kg/ha)	Ca (kg/ha)	K (kg/ha)	N (kg/ha)	C (Mg/ha)
O1	1.9	12.9	2.4	28.3	1.9	0	6.0	0	0	0
O2	6.6	26.2	14.0	105.9	5.2	0	41.9	-4.3	0	0
O3	36.3	110.8	74.7	707.5	27	0	0	0	0	0
0-7.5 cm	-8.3	-80.7	-9.1	-99.3	0	1.6	0	7.7	105.8	2.2
7.5-15 cm	-6.5	-53.8	-7.5	-131.2	0	0.4	0	5.4	85.6	1.7
15-35 cm	0	0	0	-258.6	0	0	0	0	132.9	0
35-60 cm	-88.1	-512.3	0	-692.3	0	0	0	0	0	0
	Standard Error†									
	Mg	Ca	K	N	C	Mg	Ca	K	N	C
O1	0.1	0.5	0.1	1.0	0.1	-	3.1	-	-	-
O2	0.3	1.6	0.7	6.0	0.3	-	6.6	1.1	-	-
O3	2.9	10.5	5.2	66.5	2.4	-	-	-	-	-
0-7.5 cm	1.4	12.3	2.0	32.6	-	0.5	-	2.4	34.3	0.5
7.5-15 cm	1.4	11.5	3.1	28.6	-	0.8	-	2.9	30.5	0.3
15-35 cm	-	-	-	74.1	-	-	-	-	53.6	-
35-60 cm	29.6	157.2	-	110.7	-	-	-	-	-	-
	p-value for year as a within subject MANOVA factor									
	Mg	Ca	K	N	C	Mg	Ca	K	N	C
O1	a.s.§	a.s.	a.s.	a.s.	a.s.	0.937	0.1036	0.9866	0.1244	0.2089
O2	a.s.	a.s.	a.s.	a.s.	a.s.	0.2816	0.0069	0.0094	0.9811	0.3482
O3	a.s.	a.s.	a.s.	a.s.	a.s.	0.8333	0.2960	0.2669	0.1755	0.2030
0-7.5 cm	0.0017	0.0019	0.0048	0.0316	0.2443	0.0152	0.7371	0.0186	0.0084	0.0154
7.5-15 cm	0.0018	0.0010	0.0338	0.0006	0.1386	0.0987	0.1223	0.1029	0.0011	0.0003
15-35 cm	0.2446	0.1652	0.9323	0.0109	0.9132	0.9076	0.3477	0.4277	0.0013	0.2451
35-60 cm	0.0033	0.0229	0.2414	0.0045	0.1060	0.7921	0.2830	0.8690	0.5032	0.1899

*calculated as 1990 contents less 1962 contents or 2010 contents less 1990 contents if p-value < 0.10

†standard error reported for significant changes only

§a.s. = assumed significant since organic horizons were non-existant in 1962 (Richter and Markewitz, 2001)

These rapidly aggrading pines were planted in bare mineral soil (Richter and Markewitz, 2001), and a forest floor was likely initiated within the first ten years of planting (Switzer and Nelson 1972). The forest floor grew beneath the pines during the decades of biomass accumulation, and by 1997 contained approximately 34.1 ± 2.5 Mg C ha^{-1} (Figure 3.4, Table 3.2). The forest floor was marked by significant macronutrient gains during this time, and accumulations averaged 44.8 ± 3.1 kg Mg ha^{-1}, 149.9 ± 11.8 kg Ca ha^{-1}, 91.0 ± 5.5 kg K ha^{-1}, and 841.7 ± 68.6 kg N ha^{-1} (Table 3.2).

After 1990, when the rate of forest mortality outpaced the rate of forest growth, biomass macronutrient contents decreased by approximately 26, 23, 37, and 23% respectively Mg, Ca, K, and N during biomass decline (Figure 3.4). The average rate of change of Mg, Ca, K, and N in biomass during the period of biomass decline was -12.5, -46.2, -59.8 and -61.9 kg ha^{-1} $decade^{-1}$ respectively. This is in sharp contrast to rates of change during biomass accumulation, which were +21.0 kg Mg ha^{-1} $decade^{-1}$, +46.8 kg Ca ha^{-1} $decade^{-1}$, +59.8 kg K ha^{-1} $decade^{-1}$, and +117.8 kg N ha^{-1} $decade^{-1}$, and highlight the extreme change biomass demand that occurred as this ecosystem developed. By 2007 biomass Mg decreased to 48.2 ± 1.3 kg ha^{-1}, biomass Ca decreased to 198.6 ± 5.5 kg ha^{-1}, biomass K decreased to 149.0 ± 4.1 kg ha^{-1}, and biomass N decreased to 283.6 ± 7.9 kg ha^{-1}.

Although the forest floor accumulated Mg, Ca, K, and N during the decades of biomass accumulation, as this ecosystem progressed through the decades of biomass decline macronutrient dynamics in the forest floor were considerably more nutrient dependent (Figure 3.4, Table 3.2). Contents of C, Mg, and N in the O1, O2, and O3 horizons did not differ significantly between 1997 and 2010. Ca however continued to accumulate in the forest floor during biomass decline. Ca gains during this period were realized in both the O1 and O2 horizons, where contents increased from 12.9 ± 0.5 to 18.9 ± 3.1 ($p=0.1036$, *marginally significant*) and from 26.2 ± 1.6 to 68.1 ± 6.4 ($p=0.0069$) respectively. In total these gains in Ca amounted to 32%. On the other hand, K contents in the forest floor decreased by approximately 5% during biomass decline. We observed K depletions in the O2 horizon where contents decreased from 13.9 ± 0.7 to 9.6 ± 0.9 ($p=0.0094$).

3.3.2 Mineral Soil Mg, K, and N: depletion followed by re-accumulation

In 1962 mineral soil from 0-60 cm contained approximately 279.5 ± 21.3 kg exchangeable Mg ha^{-1}. Under the rapidly aggrading forest this Mg pool was depleted by 31% (Figure 3.4, Table 3.2). We detected significant depletion of exchangeable Mg in the 0-7.5 ($p=0.0017$), 7.5-15 ($p=0.0018$), and 35-60 ($p=0.0033$) cm mineral soil depths during biomass accumulation. After pine biomass peaked in 1990, the trend of mineral soil Mg transitioned into one of slight Mg accumulation. We estimated that the mineral soil

gained approximately 2.0 ± 0.9 kg ha^{-1} from 1990 to 2010 (Figure 3.4, Table 3.2). This exchangeable Mg resupply during the decades of biomass decline were realized in the 0-7.5 (p=0.0152) and 7.5-15 (p=0.0987, *marginally significant*) cm depths.

Similar to exchangeable Mg, exchangeable K in mineral soil decreased from 1962 to 1990 and then accumulated from 1990 to 2010 (Figure 3.4, Table 3.2). In 1962 there was approximately 269.9 ± 15.3 kg exchangeable K ha^{-1} in the 0-60 cm mineral soil. By 1990, this K pool decreased by approximately 6%. Mineral soil depletions of exchangeable K were confined to the two most surficial soil depths during biomass decline, 0-7.5 (p=0.0048) and 7.5-15 (p=0.0338) cm. Unlike exchangeable Mg, increases of exchangeable K from 1990 to 2010 were relatively large and amounted to nearly as much as was lost from 1962 to 1990 in the mineral soil. During the decades of biomass decline, exchangeable K increased in the 0-7.5 cm depth by approximately 7.7 ± 2.4 kg ha^{-1} (p=0.0186) and in the 7.5-15 cm by approximately 5.4 ± 2.9 kg ha^{-1} (p=0.1029, *marginally significant*).

Total N in mineral soil over the lifetime of the Calhoun soil-ecosystem experiment shared similarities with both exchangeable Mg and exchangeable K. Like exchangeable Mg, mineral soil depletion of total N was relatively massive. In 1962 the 0-60 cm mineral soil contained approximately 2677.6 ± 84.3 kg total N ha^{-1}, and by 1990 this pool had been depleted by 44% (Figure 3.4, Table 3.2). Significant depletions of total

N were widespread under the rapidly aggrading pine forest and observed in all four repeatedly sampled mineral soil depths. During the decades of biomass decline, total N increased in the 0-7.5 cm mineral soil by 105.8 ± 34.3 kg ha^{-1} (p-value=0.0084), in the 7.5-15 cm mineral soil by 85.6 ± 30.5 kg ha^{-1} (p-value=0.0011), and in the 15-35 cm mineral soil by 132.9 ± 53.6 kg ha^{-1} (p-value=0.0013). Similar to exchangeable K, these accumulations returned total N contents in the two surficial depths close to that of the 1962 contents.

3.3.3 Mineral Soil Ca: depletion without re-accumulation

Unlike the other macronutrients that we investigated, depletion of exchangeable Ca in the mineral soil from 1962 to 1990 was not followed by exchangeable Ca accumulation from 1990 to 2010 (Figure 3.4, Table 3.2). In 1962 mineral soil from 0-60 cm contained approximately 1605.7 ± 106.2 kg exchangeable Ca ha^{-1}. Under the rapidly aggrading forest exchangeable Ca was depleted by approximately 646.8 ± 158.1 kg ha^{-1}. These depletions totaled 40% of the 1962 exchangeable Ca contents from 0-60 cm and, similar to exchangeable Mg, we observed these losses in the 0-7.5 (p=0.0019), 7.5-15 (p=0.0010), and 35-60 (p=0.0229) cm mineral soil depths. During the decades of biomass decline, despite diminished forest uptake, exchangeable Ca contents did not significantly change in any of the four mineral soil depths.

3.4 Discussion

3.4.1 Considering Bulk Density and Mineral Soil Content

Although our mineral soil macronutrient content estimates were not sensitive to changing Db, the fundamental importance of considering how Db change may impact soil content estimates is well documented (Ellert and Bellamy 1995, Wuest, 2008, Lee et al. 2009, Mikha et al. 2013, Wendt and Hauser 2013). Since the content of any element in a mineral soil layer is the product of elemental concentration, Db, and soil thickness, differences in content between two soils with equal thickness can be the result of concentration differences and Db differences. Accordingly, significant bias can be introduced to comparisons of soil content when changes to Db are not considered, either under various treatments or through time.

Fifty years ago Nye and Greenland (1964) pointed out that comparison of soil contents from equal depths of soil introduced error when Db was not equal, yet event today, the vast majority of publications continue to compare soil contents between treatments, or through time, without considering how Db differences may impact soil content estimates. For example, in Berthrong et al.'s (2009) global meta-analysis of soil nutrient and chemical change during afforestation, nearly 40% of the compiled publications did not estimate Db at all, and only 5% explicitly considered ESM calculations. Afforestation and reforestation almost certainly leads to lower Db because

deep rooted trees contribute low density organic matter to soils, increase bioturbation, aggregation, and porosity, improve soil structure (Johnson 1990, Graham and Wood 1991, Piccolo et al. 1997, Murty et al. 2002, Johnson and Lehmann 2006). Accordingly, following the lead of others (Ellert and Bellamy 1995, Wendt and Hauser 2013), we suggest that considering how Db change may impact soil content estimates is mandatory for nearly all comparative soil studies. Even when the outcome produces negative results, such as those observed her, much can be gained by confirming that significant changes in contents are not a spurious product of Db differences.

3.4.2 Ecosystem Nutrient Change during Biomass Accumulation

In our analyses, the forest ecosystem at the Calhoun soil ecosystem experiment includes mineral soil, forest floor, live pine biomass, and coarse woody debris (CWD). We estimate that CWD gained approximately 2 kg Mg ha^{-1}, 2 kg Ca ha^{-1}, 3 kg K ha^{-1}, 14 kg N ha^{-1}, and 13 Mg C ha^{-1}, during the decades of biomass accumulation, and 4 kg Mg ha^{-1}, 5 kg Ca ha^{-1}, 7 kg K ha^{-1}, 28 kg N ha^{-1}, and 4 Mg C ha^{-1}during the decades of biomass decline from concentration and mass estimates made in the 16 permanent plots (Urrego 1993, Mobley 2011, Mobley 2013). Nutrients in understory species are not included in this ecosystem because of their diminutive stature (Mobley 2011). The mineral soil component of this ecosystem is bound by a 60 cm depth. The cations Mg, Ca, and K are further bound to the exchangeable pool (NH_4OAc extractable at pH7) in mineral soil.

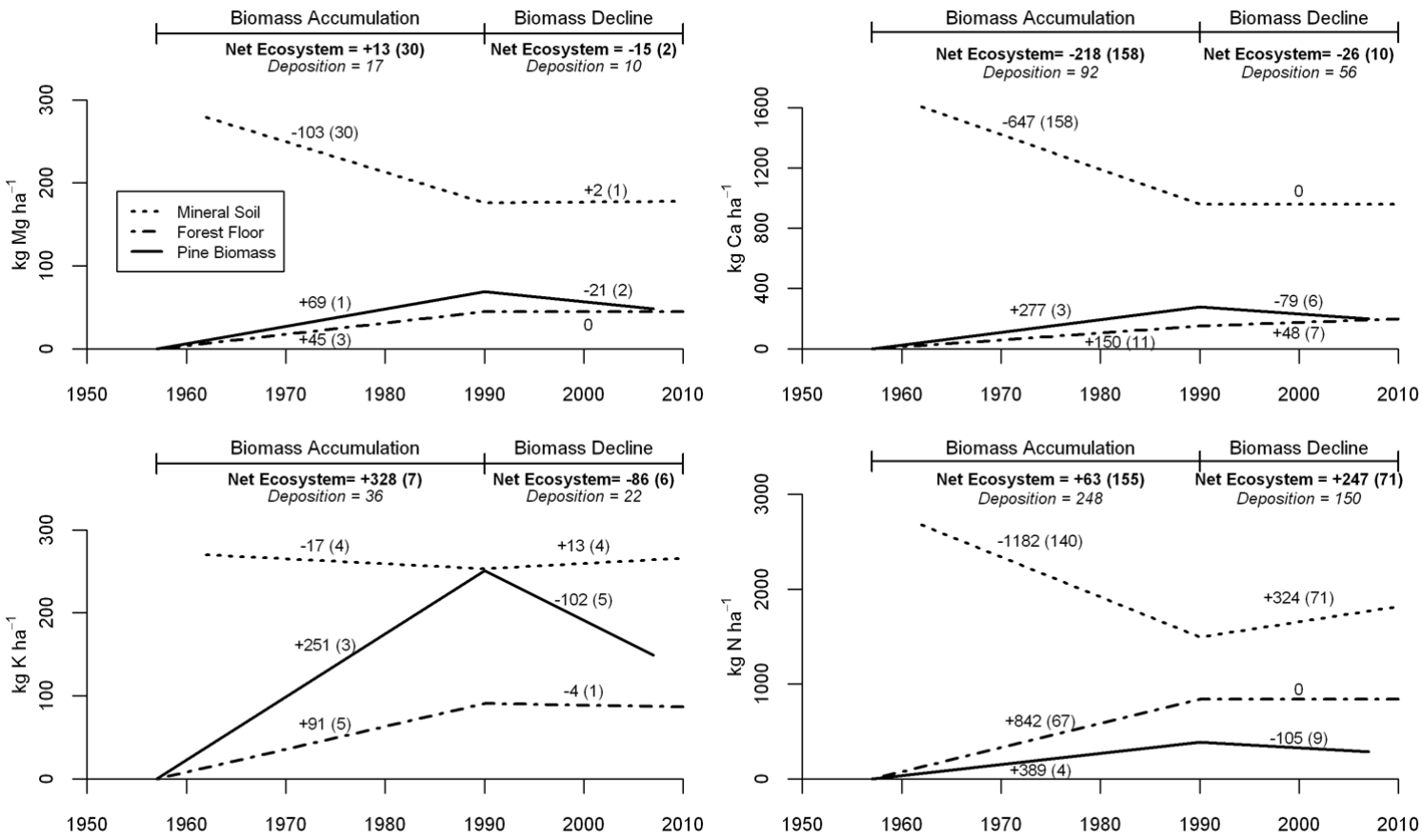

Figure 3.5: Ecosystem macronutrient change during biomass accumulation and biomass decline at the Calhoun soil ecosystem experiment. Numbers adjacent to lines identify the change in each ecosystem component during both periods of ecosystem development. Coarse woody debris is not plotted. Standard errors are reported in parentheses. Cumulative atmospheric deposition during each period is reported.

Although N has a prominent gas phase, denitrification is assumed to be minimal (Richter et al., 2000) at approximately 0.5 kg N ha^{-1} yr^{-1} (Robertson et al. 1987). Erosional inputs and removals of macronutrients are assumed to be negligible considering that surface erosion from nearly level, coarse textured, upland soils on the Southern Piedmont can approach $3.5 \cdot 10^{-5}$ cm yr^{-1} under forest cover (Smith and Stamey 1965). N fixation is also assumed to be negligible at < 0.01 kg N ha^{-1} yr^{-1} (Grant and Binkley 1987). Accordingly, macronutrient inputs to this ecosystem comes from atmospheric deposition, assumed to be about 0.5 kg Mg ha^{-1}, 2.8 kg Ca ha^{-1}, 1.1 kg K ha^{-1}, and 7.5 kg N ha^{-1} (Richter et al. 1994, Johnson and Lindberg 1992), pine uptake from > 60cm, and from mineral weathering. The primary pathway for macronutrient loss from this ecosystem is by leaching from mineral soil.

We index the potential for this ecosystem to gain or lose macronutrients with an estimate of ecosystem change during periods of forest biomass accumulation and decline (Figure 3.5). From the long term repeated sampling of forest floor and mineral soil, CWD estimates, and estimates of macronutrient content in pine biomass we have the ability to estimate the change in macronutrients for each ecosystem component from 1957 to 1990 and from 1990 to 2010. The balance of changes in each of these components represents the total ecosystem macronutrient gain or loss during the decades of biomass accumulation and biomass decline.

During the decades of biomass accumulation, ecosystem change of the three macronutrient cations were highly nutrient dependent (Figure 3.5). From 1957 to 1990 ecosystem Ca change in this pine ecosystem was approximately -218 kg ha^{-1}. This ecosystem depletion of Ca emphasized the potential for Ca to be lost to leaching from this secondary pine ecosystem, even under a rapidly aggrading forest as biomass and forest floor accumulations were not able to keep pace with mineral soil depletions. Ecosystem K change on the other hand was approximately +328 kg ha^{-1} during the same time emphasizing the potential for this ecosystem to gain K via mineral weathering and deep root uptake under a rapidly aggrading forest.

From 1962 to 1990 pine biomass, the forest floor, and CWD accumulated approximately 325 kg K ha^{-1} while exchangeable K in the 0-60cm mineral was depleted by only 103 kg ha^{-1} (Figure 3.5). Since we expect atmospheric deposition to have contributed approximately 36 kg K ha^{-1} to this ecosystem during biomass accumulation, some combination of mineral weathering and deep pine uptake buffered exchangeable K in the mineral soil during biomass accumulation. This is in marked contrast to Ca where mineral soil depletions exceed biomass, forest floor, CWD accumulations by approximately 50% during the same period of ecosystem development. Chemical, mineralogical, and greenhouse studies have identified the potential for mineral K to

rapidly resupply exchangeable K over short timescales in the highly weathered mineral soils of the Calhoun soil ecosystem experiment (Markewitz et al. 2000).

Ecosystem Mg change during the decades of biomass accumulation fell in between that of Ca and K (Figure 3.5). Ecosystem Mg change from 1957 to 1990 was approximately +13 kg ha^{-1}, similar to expected inputs from atmospheric deposition. Depletions of exchangeable Mg in mineral soil were similar to estimates of Mg accumulation in biomass, the forest floor, and CWD. Given that leaching removes considerable Mg from the ecosystem (Richter and Markewitz 2001) there appears to be potential for Mg gain in this ecosystem under a rapidly aggrading pine forest via mineral weathering and root uptake from > 60 cm.

Similar to Mg, our estimates of ecosystem N change identify the potential for this secondary pine ecosystem to gain N during the decades of biomass accumulation (Figure 3.5). From 1957 to 1990 ecosystem N change in this pine ecosystem was approximately +63 kg ha^{-1}, with soil depletions of total N nearly equal to estimates of total N accumulation in biomass, the forest floor, and CWD. Unlike the cation macronutrients, the forest floor contained significantly more N than the biomass after 33 years under the aggrading pine ecosystem. The forest floor of aggrading pine ecosystems in the Southern Piedmont are widely regarded as a strong N sink (Piatek

and Allen 2001), and our observations at the Calhoun soil ecosystem experiment during the decades of biomass accumulation support this view.

3.4.3 Ecosystem Nutrient Change during Biomass Decline

In the absence of strong vegetative control, our estimates of ecosystem Mg and K change emphasized the potential for these macronutrient cations to be lost from the forest ecosystem during the decades of biomass decline (Figure 3.5). From 1990 to 2010 ecosystem Mg change was approximately -15 kg ha^{-1}. These ecosystem Mg loses were 50% greater than expected inputs by atmospheric deposition. Similarly, ecosystem K change was approximately -86 kg ha^{-1} during the decades of biomass decline, nearly four times larger than expected inputs by atmospheric deposition. Thus, biomass depletions of Mg and K greatly outpaced accumulations in CWD, the forest floor, and the mineral from 1990 to 2010. Subsequently, as this pine ecosystem transitioned from biomass accumulation to biomass decline the potential for ecosystem loss of Mg and K increased, as predicted by Vitousek and Reiners (1975).

The fate of Mg and K lost from this forest ecosystem during the decades of biomass decline is not certain. A portion of these cations leached from the mineral soil may very well end up in ground and stream water. Some might also be adsorbed in clay rich Bt horizons below 60 cm (Table 3.1). Two years of soil solution chemistry from the Calhoun soil ecosystem experiment show that the concentration of Mg^{2+}, K^{+}, and SO_4^{2-}

(which provides much of the anionic charge balance in soil solutions) decreased as it percolates below 60 cm (Richter and Markewitz, 2001). Additionally, these cations might accumulate in mineral fractions that are not accounted for with our NH4OAc (pH7) extraction. The latter being most relevant to K since mineral K that is non-exchangeable has been demonstrated to be highly dynamic on the timescale of decades (Markewitz et al. 2000) and less so for Mg since there is little evidence in the literature that mineral Mg equilibrates with exchangeable Mg over such short timescales. However, given the ionic radii of Mg^{2+} and Fe^{3+}, 0.066 and 0.064 nm respectively, Mg could substitute isomorphically in Fe-oxyhydroxides (Sparks 2003).

In contrast to Mg and K, it appears that without strong vegetative control the potential for ecosystem loss of Ca and N does not increase (Figure 3.5). Ecosystem Ca change was approximately -26 kg ha^{-1} from 1990 to 2010. Annually ecosystem losses of Ca were approximately -1 kg ha^{-1} (over 20 years) during biomass decline, much less than the annual rate of -7 kg ha^{-1} (over 33 years) during the decades of biomass accumulation. Similarly, from 1990 to 2010 ecosystem N change was approximately +247 kg ha^{-1}, an annual gain of about +12 kg ha^{-1}. These ecosystem N gains were more rapid during biomass decline than that observed during biomass accumulation which was approximately +2 kg ha^{-1}. These trends in ecosystem Ca and N indicate that as the secondary forest transitioned from biomass accumulation to biomass decline the

Table 3.3: Ca:Mg and Ca:K ratios in litterfall and the forest floor at the Calhoun soil ecosystem experiment.

Fraction	Ca:Mg	Ca:K
Litterfall*	3.9	1.5
O1†	9.7	7.7
O2†	8.7	7.1
O3†	3.2	1.4

*from Richter et al., 1994
†from 2010 collection

potential for these macronutrients to be lost from the ecosystem may have decreased.

Although both Ca and N were relatively well retained in this secondary pine ecosystem in the absence of strong vegetative control, the mechanisms underlying their resistance to ecosystem loss varied greatly. From 1990-2010 persistent Ca accumulation in the forest floor buffered the ecosystem from Ca loss (Figure 3.5). Prior studies of loblolly pine litter have similarly identified the potential for Ca to be more effectively retained than other cations in the forest floor (Van Lear and Goebel 1976, Jorgenson et al. 1990, Richter et al. 1994, Binkley 2002). The mechanisms underlying persistent Ca accumulation in these forest floors are not known, however, considering that the observed Ca accumulations during biomass decline in the forest floor were realized in the O1 and O2 horizons (Figure 3.4 and Table 3.2) as well as the Ca:Mg and Ca:K ratios in litterfall and the forest floor (Table 3.3), it appears that Ca mineralization if fresh pine litter proceeds much slower than that of Mg and K. This may be due in part to the fact that a smaller proportion of total pine biomass Ca is found in relatively fast to

decompose needles a greater proportion is found in relatively slow to decompose branches compared to Mg and K (Urrego 1993, Van Lear and Kapeluck 1995). Further, the fact that Ca is predominantly found in cell walls as a structural component and is considerably less mobile in plants than Mg and K (Wardlaw and Passioura 1976, White and Broadley 2003,) may also contribute to its comparatively slow mineralization in the O1 and O2 horizons biomass decline. Additionally, we expect that Ca^{2+} can displace Mg^{2+} and K^{+} from cation exchange sites (Richter et al., 1992) which likely contributes to its continued accumulation in the forest floor.

While ecosystem Ca loss was buffered by accumulation in the forest floor during the decades of biomass decline, ecosystem N loss was buffered by relatively large N accumulations in the mineral soil (Figure 3.4, Figure 3.5). From 1990 to 2010, mineral soil N accumulation near entirely accounted for biomass depletions and atmospheric deposition. Density fractionation of mineral soil organic matter at the Calhoun long term soil ecosystem experiment indicate that during the decades of biomass decline N accumulation in the 0-7.5 cm depth were predominately in the operationally defined "light" fraction while N gains in the 7.5-15 and 15-35 cm depth were primarily in the "mineral associated" organic matter (Mobley et al., 2014). These ecosystem N dynamics during the decades of biomass decline are noteworthy and highly significant. First, they indicate that as this pine ecosystem matures, the forest floor is no longer the strong N

sink that is was during the decades of biomass accumulation. During the decades of biomass decline N mineralization from the forest floor occurred at approximately the same rate as inputs to the forest floor. This is somewhat surprising considering that in 1997 the C:N ratio of the O1, O2, and O3 horizons was 68, 49, and 38 respectively, suggesting that N mineralization from the O horizons may be limited. However, previous studies of pine litter in the Southern Piedmont indicate that the release of N from the forest floor is not wholly dependent on C:N ratios, and that substantial N mineralization can occur early in decomposition when C:N ratios are high (Jorgensen et al., 1980). Second, N accumulation in the 0-7.5, 7.5-15, and 15-35 cm mineral soil during biomass decline appear to outpace C accumulation and lowered the C:N ratio of soil organic matter. Mineral soil C:N in the three surficial mineral soil depths was reduced from 31.4 ± 0.4 to 27.7 ± 0.3 (0-7.5 cm), from 29.9 ± 0.5 to 26.1 ± 0.4 (7.5-15 cm) from 20.8 ± 0.5 to 17.2 ± 0.3 (15-35 cm) from 1990 to 2010 (Figure 3.3). Accordingly, if in the absence of a prominent biomass sink this pine ecosystem continues to accumulate N in the mineral soil more rapidly than C, we might see significant changes to the quality of mineral soil organic matter that may eventually influence the cycling of C and other elements.

3.4.4 Implications

The rise and fall of this secondary pine forest not only changed macronutrient contents in the forest floor and mineral soil, it also altered the roles these components play in the ecosystem cycling of Mg, Ca, K, and N (Figure 3.4, Figure 3.5). During the decades of biomass accumulation, under a rapidly aggrading pine forest, the forest floor was a strong sink for Mg, Ca, K, and N. Conversely during biomass decline macronutrient trends in the forest floor were considerably more nutrient dependent; Ca continued to accumulate, Mg and N were unchanged, and K was lost. Below the O horizons, mineral soil change from 0-60 cm was equally dynamic in response to the divergent biomass trajectories. During biomass accumulation the mineral soil was a nutrient source providing amounts of macronutrients to biomass and the O horizons. From 1990-2010, however, macronutrient depletions from mineral soil ceased, and while exchangeable Ca stabilized, exchangeable Mg, exchangeable K, and total N increased as biomass nutrients were recycled back into the mineral soil.

Decadal soil change that accompanied decadal patterns in forest uptake are too rarely investigated in forest ecosystems, and are difficult to detect with a chronosequence approach where space and time are severely confounded over short temporal periods. We expect that the soil and ecosystem patterns we observe at the Calhoun soil ecosystem experiment are generally representative of the secondary pine

ecosystems across the Southern Piedmont (Maizel et al. 1992, Wear 2002). These patterns suggest that as pine biomass declines and these old field forests transition into mixed hardwood forests, the potential for these ecosystems to lose Mg and K increases, while Ca and N loss might be of less concern.

It will be fascinating to observe the Calhoun soil ecosystem experiment in the coming decades as nutrient cycling will be highly dynamic and of great interest. The sharp decline in ecosystem biomass (Figure 3.1) will eventually subside as oaks, hickories, and other hardwood species continue to accumulate biomass. We expect these hardwood species to accumulate and redistribute nutrients in the forest ecosystem much differently than pines (Alban 1982, Eriksson and Rosen, 1994). Biomass changes will be accompanied by physical, chemical, and hydrologic alterations of the forest floor as O horizons transition from mor to mull (Binkley & Fisher, 2012). Long term ecosystem experiments, like the Calhoun soil ecosystem experiment, are now, more than ever, fundamentally important for the understanding of theses ecosystem dynamics as well as their consequences.

Finally, we have demonstrated that in the absence of strong vegetation control on nutrient cycling, the potential for nutrient loss in a forest ecosystem is highly nutrient dependent. Some nutrients, like Mg and K in this study, may follow the predictions of Vitousek and Reiners (1975) while others, such as Ca and N, may not. Acknowledging

such nutrient dependence not only marks significant progress in ecosystem ecology since the pioneering work of Odum (1969) and Vitousek and Reiners (1975), it also points to importance of considering the broad spectrum of nutrients when investigating ecosystem nutrient cycling. Accordingly, we suggest that further explorations of these decadal patterns are needed in diverse ecosystems, not only to improve ecological theory, but also to improve management of these ecosystems.

Conclusions

This dissertation investigated pedogenesis and anthropedogenesis in the highly weathered Ultisols of the Southern Piedmont physiographic region. We've highlighted the fact that soils, and their physical and biochemical properties, are not simply products of multi-millennial interactions between climate, parent material, topography, and biota. Nor are they entirely products of anthropogenic forcing over centuries and decades. Rather, pedogenesis *and* anthropedogenesis are responsible for soil as we see it today.

In chapter one, we redefined pedogenic time constraints in the Southern Piedmont. We demonstrated that the region's Ultisols have likely been residing at Earth's surface, forming and changing with minimal human impact for much if not all of the Quaternary. In chapters two and three we studied how anthropogenic activity, specifically the widespread abandonment of agricultural land, has altered the ancient Southern Piedmont soils over the most recent century and decades. In chapter two, we demonstrated that the change in vegetative rooting associated with agricultural land abandonment significantly alters the coupled cycling of carbon and iron in Southern Piedmont subsoils on the timescale of centuries. Finally, in chapter 3, we showed that decadal trends in plant nutrient demands following agricultural land abandonment significantly alters soil nutrient pools and the role that soil pools play in ecosystem nutrient cycling and ecosystem nutrient retention.

These diverse temporal dynamics of soil formation and change extend far beyond the highly weathered Ultisols of the Southern Piedmont. Over 90% of Earth's terrestrial surface is blanketed by soil (Dixon and von Blanckenburg 2012), and pedogenesis has produced a remarkable diversity of soils. For example, in the United States alone, more than 19,000 soil series have been identified (Soil Survey Staff 1999). Humans alter these diverse pedogenic products at the global scale (Schlesinger 1990, Dudal et al. 2002, Richter 2007) through anthropedogenic activities that include but are not limited to agricultural practices, urbanization, forest management, waste management, burning of fossil fuels, industrial emissions, and mining.

Whether discussing ancient Mesopotamians cultivating the banks of the Tigris and Euphrates (Montgomery, 2007) or contemporary soil amendments aimed at removing pollutants from the hydrologic cycle (Agrawal et al., 2010), humanity's past, present, and future well-being is intimately tied to pedogenic and anthropedogenic processes. Therefore, as the scientific discipline of pedology proceeds toward a comprehensive knowledge of soil formation and change there is little doubt that understanding the complexity and diversity of pedogenesis and anthropedogenesis will be a primary focus. Our investigation of the Southern Piedmont identified two important themes to guide this focus:

(1) Pedology must become more interdisciplinary than ever. Understanding the highly variable factors of soil formation and change over diverse timescales requires that pedologists continue to grow and diversify their interdisciplinary collaborations. In chapter one, we relied on principles geomorphology and geochemistry to complement our understanding of soil processes over relatively long time scales. Similarly, in chapters two and three, we relied on the disciplines of history, environmental history, and ecology to more completely understand anthropogenic influence on soil.

(2) Pedology must embrace "novel" field and analytical techniques. In the field, our investigation of pedogenesis and anthropedogenesis crossed space (to depths of 70 m, and individual redoximorphic feature microsites) and time (over 50 years of repeatedly sampled and archived soil) in ways that are not common to pedology. Analytically, we complimented traditional soil measurements with analyses of meteoric ^{10}Be and stable Fe isotopes; two metrics which are rarely utilized by pedologists. Not only will pedology benefit from these novel approaches, as our work with meteoric ^{10}Be and stable Fe isotopes demonstrates, utilizing these novel metrics through the lens of soil science can improve their utility.

Although we expect future studies of pedogenesis and anthropedogenesis to benefit from interdisciplinary interaction between pedologists and a wide range of diverse disciplines (including geomorphologists, geochemists, hydrologists, biologists, historians, anthropologists, and urban geographers), this dissertation highlights the potential for pedology and ecology to interact like never before. In "Soils in Ecology and Ecology in Soils", Binkley (2006) chronicles the history interaction between theses disciplines. This history can only be characterized as one of little interaction. Briefly, pedology and ecology were born, and grew, largely in parallel to one another; both aimed to classify and understand complex systems (ecological communities and soils) across landscapes or regions, both settled on a "climax" view of to organize their understanding of these systems, and both used chemistry, physics, plant physiology, and microbiology to advance their understanding. Despite these parallels pedology and ecology have interacted minimally through much of the 19th and 20th century, as evidenced by both disciplines' seminal papers and textbooks including Cowles (1899), Clements (1936), Bormann et al. (1977), McIntosh (1985), Golley (1993), and Brady and Weil (2002) (from Binkley, 2006).

Binkley (2006) identifies three "unifying themes" that each have potential to increase the interaction between pedologists and ecologists. These themes include global scale biogeochemical issues such as elevated atmospheric CO_2, biodiversity (given

the "unimaginable" biodiversity in soil), and human modifications of ecosystems. Each theme is indeed of great interest to pedologists and ecologists alike, and given the fact that nearly every component of terrestrial ecology is either directly or indirectly related to the soil, we agree that increased potential for pedology and ecology interaction exists. Investigations of anthropedogenesis explicitly align with Binkley's third theme, and as chapters one and two in this dissertation suggest, much can be learned about ecosystems by investigating soil change over centuries and decades.

Here, we advocate a fourth unifying theme. We believe that in addition to anthropedogenic studies, pedogenic studies offer great potential for interaction between pedology and ecology. Recently, great attention has been paid to the long term records stored in soil (Brantley and Lebedeva 2011). These records include multi-millennial interactions between Earth's lithosphere, hydrosphere, and biosphere, and atmosphere; each fundamental to the functioning of individual ecosystems. In chapter one, we took a significant first step in deciphering these records by temporally constraining them in the Southern Piedmont. As science advances and these records are further deciphered, information about historic interactions between soil and terrestrial ecosystems very well could be revealed. Ecology will not only be instrumental in understanding these interactions, but will also benefit by understanding how ecosystems function over relatively long timescales and under different environmental conditions.

A. Supplement to Chapter 1

Detailed ^{10}Be extraction, isotopic measurement, and data reduction methods

Soil and saprolite samples were sieved with a 2 mm screen, depth composited by mass, and pulverized with a shatterbox at Duke University prior to ^{10}Be extraction. Meteoric ^{10}Be was extracted from the pulverized samples in the University of Vermont's cosmogenic nuclide extraction laboratory. Samples were prepared in a batch of 16 following a modification of the flux fusion method presented by Stone (1998). We included two full process blanks with 14 unknowns and the sample from 1.5–2.0 m was run in replicate.

About 0.5 g of sample material was mixed with KHF and $NaSO_4$ along with ~300 ug of Be (SPEX brand carrier). The mixture was fused in a platinum crucible for several minutes until the melt was clear. After cooling, the crucible containing the solidified fusion cake was rapidly submerged into a Teflon beaker containing Milli-Q water (18.2 Mohm), heated, and allowed to leach overnight. Excess K was removed by $HClO_3$ precipitation and Be was precipitated as BeOH which was washed and dried. The hydroxide was burned to BeO, mixed with an equimolar amount of niobium metal powder, and loaded into stainless steel cathodes for isotopic analysis at the Center for Accelerator Mass Spectrometry, Lawrence Livermore National Laboratory.

Beryllium isotopic ratios were measured using multiple analyses of each target. Analyses of each target were repeated between 3 and 6 times until the precision (the greater of the internal and external uncertainties) of each unknown measurement (excepting the blanks) was < 1% (1σ; m = 0.6 ± 0.1%). Initial beam currents were very high for these samples, ranging from 21.9 to 31.1 μA with an average of 25.2 μA; this compares to an average beam current for standards run with these samples of 21.8 μA. Three secondary standards were run repeatedly to verify linearity of the AMS. Results were normalized to 07KNSTD3110 with a reported $^{10}Be/^{9}Be$ ratio of $2.85 \cdot 10^{-12}$ (Nishiizumi et al. 2007). Normalized isotopic ratios were corrected for isobaric interference from boron-10 (< 0.01%), and ranged from $5250 \cdot 10^{-15}$ to $11790 \cdot 10^{-15}$. We made a blank correction by subtracting the average long-term (n = 23, June 2008–Dec 2009) process blank for the UVM meteoric ^{10}Be extraction lab ($16.3 \pm 1.4 \cdot 10^{-15}$) from each measured sample ratio. The two blanks run with these samples (16.2 ± 0.7 and $19.5 \pm 0.8 \cdot 10^{-15}$) are consistent with this long-term average. We subtracted blank ratios from sample ratios because all samples contained similar amounts of carrier. Because these samples contained so much ^{10}Be and the average sample ratio was high (n = 14, m = $8300 \cdot 10^{-15}$), the resulting blank correction is inconsequential (< 0.4%). The replicate sample reproduced well giving ^{10}Be concentrations of 2.92 ± 0.02 (1σ) and $2.96 \pm 0.02 \cdot 10^{8}$ atoms g^{-1}, respectively.

Immobile reference element selection

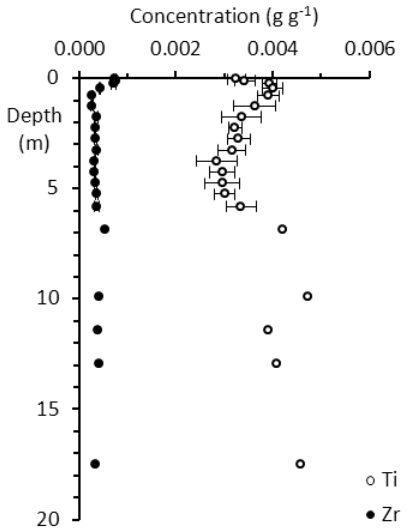

Figure A.1: Total elemental concentrations of zirconium (Zr) and Titanium (Ti) in the Southern Piedmont Ultisol.

Since no element is completely immobile in soils we evaluated both zirconium (Zr) and titanium (Ti) for use as the immobile reference element in our mass balance analysis. We chose Zr as the immobile element for three reasons. First, in the greater than 30 m of unweathered granite gneiss that we sampled, Zr concentrations are considerably less variable than that of Ti (Table DR2). This suggests that differences in Zr concentrations of individual soil samples are less likely to be a result of inherent parent material variability than Ti concentrations. Second, the elevated concentrations of Ti in illuvial horizons (0.3–1.5 m) relative to directly overlying horizons suggest translocation within the soil system. Conversely, Zr concentrations in the surficial

horizons are larger than that of any other horizon; what should be expected of an immobile element as most other elements are removed from these elluvial horizons (Figure A.1). Lastly, in laboratory batch experiments, Zr has been observed to be less mobile than Ti in granite systems (Neaman et al. 2006).

Long-term surface erosion (ε)

Although we lack measurements of ε from the interfluve that we sampled we constrained long-term surface erosion between $3.5 \cdot 10^{-5}$ cm yr^{-1} and $3.0 \cdot 10^{-4}$ cm yr^{-1}, and assume that the true ε is captured in this broad range. Measurements of *in-situ* ^{10}Be from an upland Ultisol in the Southern Piedmont show ε is $<3.0 \cdot 10^{-4}$ cm yr^{-1} (Lal et al. 1996). Basin scale analysis of *in-situ* ^{10}Be average erosion of diversely eroding features and suggest that as a landscape ε is between $3.0 \cdot 10^{-4}$ and $21.0 \cdot 10^{-4}$ cm yr^{-1} in the Southern Piedmont (Trodick 2011). Considering that the interfluve surfaces we and Lal et al. (1996) sampled are certainly the most slowly eroding features of the landscape, $3.0 \cdot 10^{-4}$ cm yr^{-1} is a reasonable maximum bound of ε. Contemporary erosion from nearly level interfluves under "primeval" forest cover in the region proceeds much slower, and has been measured as low as $2 \cdot 10^{-3}$ tons $acre^{-1}$ annually, or $3.5 \cdot 10^{-5}$ cm yr^{-1} if bulk density equals 1.25 g cm^{-3} (Smith and Stamey 1965). This rate is an effective minimum bound of ε because such a low rate is thought to be untenable over geologic time (Portenga and Bierman 2011).

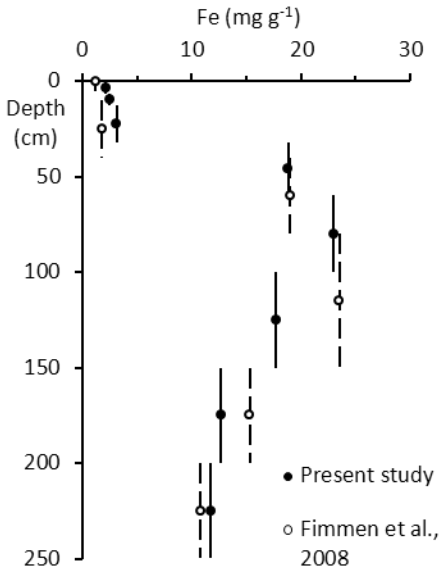

Figure A.2: Strong agreement between hhe iron extracted with 1 M $NH_2OH{\cdot}HCl$ in 1 M HCl (present study) and with dithionite citrate bicarbonate (Fimmen et al., 2008) from the same soil at two locations (approximately 500 m apart) on the same interfluve. Vertical lines represent the integrated sampling depth in each analysis.

Table A.1: Physical and chemical property variability between three continuous deep soil cores in the Southern Piedmont.

Hor	Depth (m)	ρ* g/cm^3	Clay (%)	Sand (%)	pH	C (%)	ECEC (cmol/kg)	EBS (%)	totZr	totCa	totAl (mg/g)	totFe	hheFe†	tot^{9}Be	hhe^{9}Be† (ug/g)	^{10}Be† (10^{8}atm/g)
A	0.00–0.07	0.17	0.2	0.3	0.10	0.10	0.2	3.4	0.02	0.01	0.58	0.46	-	0.07	-	-
AE	0.07–0.13	0.02	0.2	0.6	0.09	0.09	0.0	4.4	0.02	0.07	1.15	0.43	-	0.06	-	
E	0.13–0.32	0.06	0.8	1.2	0.11	0.02	0.1	2.1	0.04	0.01	2.31	0.54	-	0.01	-	-
Bt	0.32–0.6	0.06	2.6	2.0	0.03	0.03	0.0	2.9	0.01	0.04	10.97	3.59	-	0.27	-	-
Bt	0.6–1.0	-	3.4	2.2	0.05	0.01	0.5	4.4	0.02	0.01	3.46	2.08	-	0.04	-	-
Bt	1.0–1.5	-	3.8	3.6	0.05	0.01	0.9	3.1	0.02	0.01	5.77	3.74	-	0.08	-	-
BC	1.5–2.0	-	2.0	5.4	0.05	0.01	1.0	2.2	0.04	0.01	9.24	2.58	-	0.05	-	-
CB	2.0–2.5	-	2.0	3.4	0.06	0.01	1.1	1.3	0.01	0.01	6.35	1.42	-	0.07	-	-
CB	2.5–3.0	-	2.0	4.0	0.06	<0.01	0.5	0.9	0.02	0.0	6.35	0.84	-	0.04	-	-
C	3.0–3.5	-	1.2	3.2	0.02	<0.01	0.6	1.4	0.02	0.0	6.93	1.97	-	0.05	-	-
C	3.5–4.0	-	0.9	3.2	0.02	<0.01	0.9	2.5	0.01	0.01	4.04	2.52	-	0.08	-	-
C	4.0–4.5	-	1.3	2.5	0.01	0.01	1.9	2.6	0.02	0.01	4.04	2.33	-	0.02	-	-
C	4.5–5.0	-	0.9	2.4	0.03	0.01	0.7	1.3	0.03	0.01	4.04	1.66	-	0.08	-	-
C	5.0–5.5	-	0.9	1.5	0.03	<0.01	0.6	1.3	0.03	0.02	7.51	0.68	-	0.10	-	-
C	5.5–6.1	-	0.6	1.5	0.01	<0.01	0.4	1.6	0.05	0.02	4.04	1.72	-	0.10	-	

Note: Values reported here are standard errors between the 3 continuous cores. Values not reported below 6.1 m where n=1 core.

* ρ variability reported for our direct estimates, but not reported below 0.6 m where ρ estimates are derived elsewhere (see Table 1).

†Property estimated on composited samples, therefore variability not reported.

Table A.2: Total elemental concentration of unweathered granite gneiss beneath the Cataula soil.

Depth (m)	Zr (mg g^{-1})	Ca (mg g^{-1})	Fe (mg g^{-1})	^{9}Be (ug g^{-1})	Ti (ug g^{-1})
30.5–33.5	0.33	13.41	16.97	1.91	3.17
33.5–36.6	0.32	14.21	14.51	1.89	3.34
36.6–39.6	0.18	12.61	9.94	1.36	1.72
39.6–42.7	0.23	13.16	12.33	1.28	2.04
42.7–45.7	0.2	14.82	12.37	1.74	1.83
45.7–48.8	0.24	14.23	11.49	2.18	1.64
48.8–51.8	0.23	13.47	12.03	1.42	2.00
51.8–54.9	0.22	13.00	12.60	1.70	1.99
54.9–57.9	0.19	11.95	10.17	2.51	1.60
57.9–61.0	0.18	11.90	9.56	3.09	1.61
61.0–64.0	0.16	8.78	7.11	4.57	1.10
64.0–67.1	0.24	14.11	11.64	1.6	1.85
Mean	0.23	12.97	11.73	2.10	1.99
Standard Error	0.02	0.46	0.72	0.27	0.19
Coefficient of Variation (%)	23	12	21	44	32

B. Supplement to Chapter 2

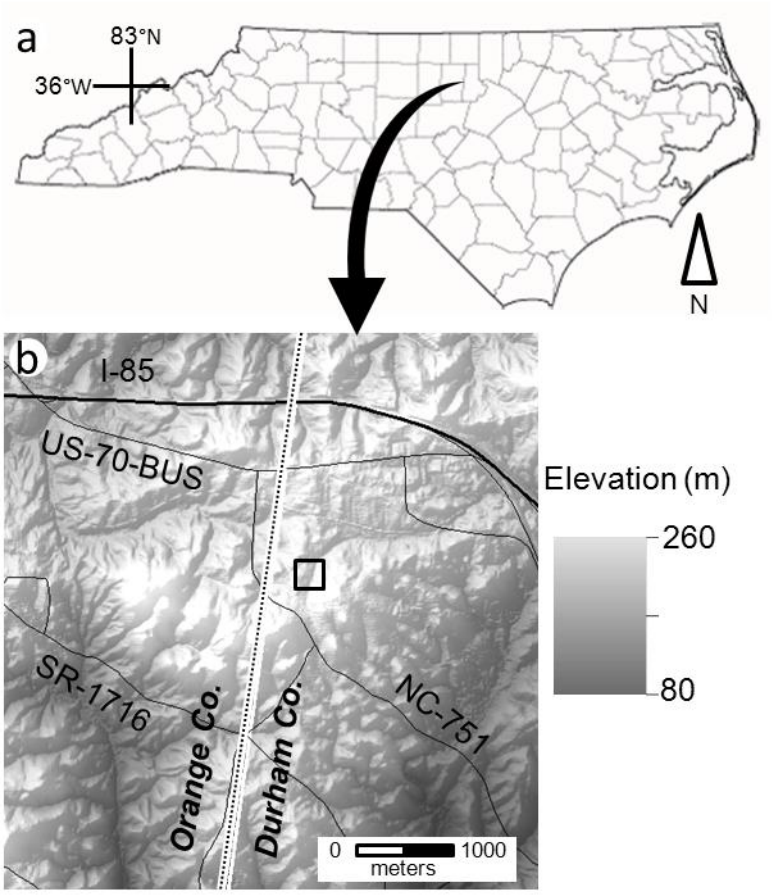

Figure B.1: (A) Map of North Carolina, USA with county boundaries. (B) A digital elevation model of the landscape surrounding the paired Ultisols that we sampled. The black box identifies the boundary of panel A in Figure 2.1.

Table B.1: Bulk soil properties of the paired soil profiles.

Horizon	Depth (m)	Root Abundance (%)*	Total C (%)	Clay (%)	Sand (%)	pH	ECEC† (cmol/kg)	Exchangeable Acidity (cmol/kg)	EBS§ (%)	EESP** (%)	$Fe_{sro\text{-}oxide}$ (mg/g)	$Fe_{cryst\text{-}oxide}$ (mg/g)	Total Fe (mg/g)	Total Mn (mg/g)	Total Zr (mg/g)
Grass															
A	0.0-0.08	n.d.††	1.33	n.d.	n.d.	3.8	1.4	0.7	52	1	0.8	2.3	n.d.	n.d.	n.d.
E	0.08-0.2	n.d.	0.33	n.d.	n.d.	4.1	0.9	0.7	20	2	0.3	4.8	n.d.	n.d.	n.d.
Btg	0.2-0.5	24 (2)	0.07	n.d.	n.d.	3.7	9.1	7.8	14	12	0.3	9.5	n.d.	n.d.	n.d.
C/Btg1	0.5-0.8	7 (2)	0.07	n.d.	n.d.	3.7	7.7	6.2	21	19	0.6	15.4	n.d.	n.d.	n.d.
C/Btg2	0.8-1.1	8 (1)		n.d.	n.d.	3.8	8.0	5.8	27	25	0.7	18.3			
C/Btg3	1.1-1.4	3 (2)	0.03	n.d.	n.d.	3.9	6.7	4.6	31	28	2.6	18.2	n.d.	n.d.	n.d.
C/Btg4	1.4-1.7	2 (1)		n.d.	n.d.	3.9	5.9	3.5	41	35	2.1	13.8			
Forest															
A	0.0-0.15	n.d.	1.62	5.3	76.1	4.2	1.9	1.3	32	3	0.5	0.8	2.88	0.13	0.42
E	0.15-0.4	n.d.	0.37	6.5	73.7	4.2	1.2	1.0	18	5	0.5	2.0	4.04	0.10	0.48
Btg	0.4-0.7	57 (4)	0.14	36.3	43.9	3.7	8.9	7.6	14	13	0.6	10.8	24.88	0.12	0.19
C/Btg1	0.7-1.0	31 (6)	0.07	23.6	59.3	3.6	8.0	6.3	22	20	1.6	12.2	25.25	0.19	0.21
C/Btg2	1.0-1.3	15 (6)		9.3	73.2	3.8	7.1	5.0	29	26	2.6	18.9			
C/Btg3	1.3-1.6	7 (2)	0.04	8.4	73.7	3.8	7.8	4.6	41	36	1.8	10.5	23.78	0.14	0.17
C/Btg4	1.6-1.9	7 (3)		9.5	70.0	3.9	7.8	3.9	49	40	1.8	13.7			

*Percentage of one cm^2 cells that contained roots, standard error (n=3) reported in parentheses.

†Effective cation exchange capacity (ECEC) calculated as the sum of Mehlich-III extractable base cations (Ca, Mg, K, and Na) and exchangeable acidity.

§Effective Base Saturation (EBS) calculated by dividing the sum of Mehlich-III extractable base cations (Ca, Mg, K, and Na) by effective cation exchange capacity.

**Effective exchangeable sodium percentage (EESP) calculated by dividing the Mehlich-III extractable Na by effective cation exchange capacity (ECEC).

††n.d. = not determined

Table B.2: Estimates of $\Delta^{14}C$ (‰) in the paired soil redoximorphic features.

Horizon	Depth (m)	Fe-Enriched	Gley	Fe-Depleted
Grass				
Btg	0.2-0.5	-272	-79	-
C/Btg1	0.5-0.8	-508	-227	-244
C/Btg2	0.8-1.1		-281	
C/Btg3	1.1-1.4	-636	-392	-456
C/Btg4	1.4-1.7		-260	
Forest				
Btg	0.4-0.7	-211	-13	-
C/Btg1	0.7-1.0	-507	-107	-458
C/Btg2	1.0-1.3		-164	
C/Btg3	1.3-1.6	-552	-262	-466
C/Btg4	1.6-1.9		-151	

Notes: Samples graphitized in the Houghton Carbon Water and Soils Lab, USDA-FS. $\Delta^{14}C$ is corrected for fractionation by $\delta^{13}C$ measurements on each sample (Stuiver and Pollach 1977).

Table B.3: Iron and zirconium concentrations in the paired soil redoximorphic features.

		--------$Fe_{sro\text{-}oxide}$ (mg/g)--------			--------$Fe_{cryst\text{-}oxide}$ (mg/g)--------			--------Total Fe* (mg/g)--------			--------Total Zr* (mg/g)--------		
Horizon	Depth (m)	Fe-Enriched	Gley	Fe-Depleted	Fe-Enriched	Gley	Fe-Depleted	Fe-Enriched	Gley	Fe-Depleted	Fe-Enriched	Gley	Fe-Depleted
Grass													
Btg	0.2-0.5	0.82	0.11	-	25.32	3.24	-	n.d.†	n.d.	-	n.d.	n.d.	-
C/Btg1	0.5-0.8	3.08	0.09	0.11	45.96	2.85	1.31	n.d.	n.d.	n.d.	n.d.	n.d.	n.d.
C/Btg2	0.8-1.1	2.39	0.09	0.11	22.09	2.55	2.10						
C/Btg3	1.1-1.4	3.25	0.05	0.11	17.36	1.74	1.96	n.d.	n.d.	n.d.	n.d.	n.d.	n.d.
C/Btg4	1.4-1.7	2.88	0.03	0.05	14.75	1.72	1.31						
Forest													
Btg	0.4-0.7	0.90	0.12	-	28.75	3.97	-	40.66	18.68		0.24	0.26	-
C/Btg1	0.7-1.0	2.64	0.18	0.20	17.31	2.65	2.25	27.13	14.85	14.05	0.23	0.17	0.22
C/Btg2	1.0-1.3	2.89	0.09	0.13	13.95	2.28	2.63						
C/Btg3	1.3-1.6	3.41	0.14	0.14	13.03	2.34	1.37	27.25	18.66	9.77	0.21	0.17	0.18
C/Btg4	1.6-1.9	3.59	0.06	0.15	17.60	2.81	2.48						

*Total Zr, Mn, and Fe in unweathered granite equal to 14.42, 0.32, and 0.15 mg/g respectively.

†n.d. = not determined

Table B.4: Iron stable isotope ratios of bulk soil and redoximorphic features in the paired soils

		----------$Fe_{sro\text{-}oxide}$ ($\delta^{56}Fe_{IRMM\text{-}14}$)*----------				----------$Fe_{cryst\text{-}oxide}$ ($\delta^{56}Fe_{IRMM\text{-}14}$)*----------			
Horizon	Depth (m)	Bulk	Fe-Enriched	Gley	Fe-Depleted	Bulk	Fe-Enriched	Gley	Fe-Depleted
Grass									
A	0.0-0.08	-1.27 (0.28)	-	-	-	-0.04 (0.05)	-	-	-
E	0.08-0.2	-0.16 (0.26)	-	-	-	-0.21 (0.08)	-	-	-
Btg	0.2-0.5	-0.53 (0.06)	-0.49 (0.20)	0.33 (0.06)	-	-0.40 (0.05)	-0.62 (0.02)	0.04 (0.03)	-
C/Btg1 & C/Btg2	0.5-1.1	-0.28 (0.55)	-0.32 (0.55)	-0.85 (0.07)	0.21 (0.06)	-0.29 (0.06)	-0.77 (0.08)	-0.04 (0.08)	0.19 (0.02)
C/Btg3 & C/Btg4	1.1-1.7	-0.17 (0.04)	-0.12 (0.56)	-0.93 (0.11)	-1.74 (0.21)	-0.40 (0.03)	-0.47 (0.05)	0.03 (0.03)	0.22 (0.06)
Forest									
A	0.0-0.15	-1.92 (1.12)	-	-	-	-0.14 (0.07)	-	-	-
E	0.15-0.4	-0.72 (0.25)	-	-	-	-0.15 (0.03)	-	-	-
Btg	0.4-0.7	-0.10 (0.10)	-0.37 (0.02)	-1.98 (0.28)	-	-0.31 (0.03)	-0.36 (0.10)	0.03 (0.00)	-
C/Btg1 & C/Btg2	0.7-1.3	-0.10 (0.03)	-0.18 (0.05)	-1.67 (0.15)	0.01 (0.06)	-0.29 (0.03)	-0.42 (0.11)	0.17 (0.08)	0.25 (0.04)
C/Btg3 & C/Btg4	1.3-1.9	-0.98 (0.21)	-0.34 (0.04)	-0.75 (0.05)	0.05 (0.07)	-0.32 (0.06)	-0.64 (0.06)	0.04 (0.03)	0.31 (0.04)

* 95% confidence interval from replicate MC-ICP-MS measures reported in parentheses.

References

Agrawal, S. G., K. W. King, J. F. Moore, P. Levison, and J. McDonald. 2010. Use of industrial byproducts to filter phosphorus and pesticides in golf green drainage water: Journal of Environmental Quality 40:1273-1280.

Alban, D. H. 1982. Effects of nutrient accumulation by aspen, spruce, and pine on soil properties. Soil Science Society of America Journal 46:853-861.

Amundson, R. and H. Jenny. 1991. The place of humans in the state factor theory of ecosystems and their soils. Soil Science 151:99-109.

Bazilevskaya, E., M. Lebedeva, M. Pavich, G. Rother, D.Y. Parkinson, D. Cole, and S. L. Brantley. 2013. Where fast weathering creates thin regolith and slow weathering creates thick regolith. Earth Surface Processes Landforms 38: 847-858.

Beard, B. L., C. M. Johnson, L. Cox, H, Sun, and K. H. Nealson. 1999. Iron Isotope Biosignatures. Science 285:1889-1892.

Berner, R. A., A. C. Lasaga, and R. M. Garrels. 1983. The carbonate-silicate geochemical cycle and its effect on atmospheric carbon-dioxide over the past 100 million years. American Journal of Science 283: 641-683.

Berthrong, S. T. E. G. Jobbágy, and R. B. Jackson. 2009. A global meta-analysis of soil exchangeable cations, pH, carbon, and nitrogen with afforestation. Ecological Applications 19:2228-2241.

Billings, W. D. 1938. The structure and development of olf field shortleaf pine stands and certain assosciated physical properties of the soil. Ecological Monographs 8:437-500.

Billings, S.A. and D. deB. Richter. 2006. Changes in stable isotopic signatures of soil nitrogen and carbon during 40 years of forest development. Oecologia 148:325–333.

Binkley, D. 2002. Ten-year decomposition in a loblolly pine forest. Canadian Journal of Forest Researarch 32:2231-2235.

Binkley. 2006. Soils In Ecology and Ecology In SOils. Pages 259-278 in B. P. Warkentin, editor. Footprints in the Soil. Elsevier, New York.

Binkley, D. and R. Fisher, R. 2012. Ecology and Mangement of Forest Soils. Wiley-Blackwell, New York.

Birkeland, P. W. 1999. Soils and Geomorphology. Oxford University Press, New York

Bormann, F. H., G. E. Likens, and J. M. Melillo. 1977. Nitrogen budget for an aggrading northern hardwood forest ecosystem. Science 1967:981-983.

Bouchez, J., F. von Blanckenburg, and J. A. Schuessler. 2013. Modeling Novel Stable Isotope Ratios in the Weathering Zone. American Journal of Science 313:267-308.

Brady, N. C. and R. R. Weil. 2010. Elements of the nature and properties of soils. Pearson Prentice Hall, Upper Saddle River, New Jersey.

Brantley, S. L., L. Liermann, and T. D. Bullen. 2001. Fractionation of Fe Isotopes by Soil Microbes and Organic Acids. Geology 29:535-538.

Brantley, S. L., L. J. Liermann, R. L. Guynn, A. Anbar, G. A. Icopini, and J. Barling. 2004. Fe Isotopic Fractionation during Mineral Dissolution with and without Bacteria. Geochimica et Cosmochimica Acta 68:3189-3204.

Brantley, S. E. and M. Lebedeva. 2011. Learning to read the chemistry of regolith to understand the Critical Zone. Annual Review of Earth and Planetary Sciences 39:387-416.

Brimhall, G. H. and W. E. Dietrich. 1987. Constitutive mass balance relations between chemical composition, volume, density, porosity, and strain in metasomatic hydrochemical systems: Results on weathering and pedogenesis. Geochimica et Cosmochimica Acta 51:567-587.

Brown, E. T., J. M. Edmond, G. M. Raisbeck, D. L. Bourles, F. Yiou, and C. I. Measures. 1992. Beryllium isotope geochemistry in tropical river basins. Geochimica et Cosmochimica Acta 56:1607-1624

Buol, S., R. J. Southard, R. C. Graham, and P. A. McDaniel. 2003. Soil Genesis and Classification. Iowa State Press, Ames, Iowa.

Buss, H. L., R. Mathur, A. F. White,and S. L. Brantley. 2010. Phosphorus and Iron Cycling in Deep Saprolite, Luquillo Mountains, Puerto Rico. Chemical Geology 269:52-61.

Carter, M. R. 1993. Soil Sampling and Methods of Analysis. Lewis Publishers, Boca Raton, Florida.

Chmeleff, J., F. von Blanckenburg, K. Kosser, and D. Jakob. 2010. Determination of the 10Be half-life by multicollecter ICP-MS and liquid scintillation counting. Nuclear Instruments & Methods in Physics Research, Section B, Beam Interactions with Materials and Atoms 268:192-199.

Cleland, T. M. 2004. A Practical Description of the Munsell Color System and Suggestions for Its Use 1937. Kessinger Publishing, Whitefish, Montana.

Cline, M. G. 1961. The changing model of soil. Soil Science Society of America Journal. 25:442-446.

Coile, T. S. 1940. Soil changes assosciated with loblolly pine succession on abandoned agricultural land of the Piedmont Plateau. Duke University School of Forestry Bulletin 5.

Cowles, H. C.1928. Persistence of prairies. Ecology 9:380-382.

Crosby, H. A., C. M. Johnson, E. E. Roden, and B. L. Beard. 2005. Coupled Fe(II)−Fe(III) Electron and Atom Exchange as a Mechanism for Fe Isotope Fractionation during Dissimilatory Iron Oxide Reduction. Environmental Science and Technology 39:6698-6704.

Dadgari, F. 1983. Pedogenesis of Na+-and Mg2+-affected Sedgefield Soils (fine, Mixed, Thermic, Aquultic Hapludalfs) in the North Carolina Piedmont. North Carolina State University (Ph.D. Dissertation), Raleigh, North Carolina.

Dane, J. H., and G. C. Topp. 2002. Methods of soil analysis-physical methods. Soil Science Society of America, Madison, Wisconsin.

Darwin, C. 1892. The formation of vegetable mould, through the action of worms, with observations on their habits, University of Chicago Press, Chicago, Illinios.

Delcourt, P. A., H. R. Delcourt, D. F. Morse, and P. A. Morse. 1993. History, evolution, and organization of vegetation and human culture. Pages 47-79 in W. H. Martin, S. G. Boyce, and A.

Devine, S., D. Markewitz, P. Hendrix, and D. Coleman. 2011. Soil Carbon Change through 2 m during Forest Succession Alongside a 30-Year Agroecosystem Experiment. Forest Science 57:36-50.

Dixon, J. L. and F. von Blanckenburg. 2012. Soils as pacemakers and limiters of global silicate weathering. Comptes Rendus Geoscience 344:597-609.

Dokuchaev, V. 1883. Russian Chernozem. Moscow Israel Program for Scientific Translations Ltd, Jerusalem, Isreal.

Dudal, R., F. Nachtergaele, and M. Purnell. 2002. The human factor of soil formation. 17th World Congress of Soil Science, Thailand.

Dunscomb, J. K. 1992. Forest Soil Recovery after Agriculture: land use change on the Southern Piedmont. Duke University (Master's Thesis), Durham, North Carolina.

Ellert, B. H. and J. R. Bettany. 1995. Calculation of organic matter and nutrients stored in soils under contrasting management regimes. Canadian Journal of Soil Science 75:529-538.

Emmanuel, S., Y. Erel, A. Matthews, and N. Teutsch. 2005. A Preliminary Mixing Model for Fe Isotopes in Soils. Chemical geology 222:23-34.

Eriksson, H. M. and K. Rosen. 1994. Nutrient distribution in a Swedish tree species experiment. Plant and Soil 164:51-59.

Esternacht, C., editor. Biodiversity of the Southeastern United States. John Wiley, New York.

Eswaran, H. 2002. Soil under a Microscope: Evaluating Soils in Another Dimension. United States Department of Agriculture, http://soils.usda.gov/use/worldsoils/microscope/ (last accessed June 2011).

Fantle, M. S. and D. J. DePaolo. 2004. Iron Isotopic Fractionation during Continental Weathering. Earth and Planetary Science Letters 228:547-562.

Fekiacova, Z., S. Pichat, S. Cornu, and J. Balesdent. 2013. Inferences from the Vertical Distribution of Fe Isotopic Compositions on Pedogenetic Processes in Soils. Geoderma 209:110-118.

Fett, J. P., K. LeVier, and M. L. Guerinot. 1998. Soil Microogranisms and Iron Uptake by Higher Plants. Pages 187-208 in A. Sigel and H. Sigel, editors. Metal Ions in Biological Systems; iron transport and storage in microogranisms, plants, and animals. Marcel Dekker, New York.

Fimmen, R. L., D. deB. Richter, D. Vasudevan, M. A. Williams, and L. T. West. 2008. Rhizogenic Fe-C redox cycling: A hypothetical biogeochemical mechanism that drives crustal weathering in upland soils. Biogeochemistry 87:127-141.

Franzluebbers, A. J., J. A. Stuedemann, H. H. Schomberg, and S. R. Wilkinson. 2000. Soil organic C and N pools under long-term pasture management in the Southern Piedmont USA. Soil Biology and Biochemistry 32:469-478.

Golley, F. B. 1993. A history of the ecosystem concept in ecology: more than the sum of the parts. Yale University Press, New Haven, Connecticut.

Graham, R. C. and H. B. Wood. 1991. Morphologic development and clay redistribution in lysimeter soils under chaparral and pine. Soil Science Society of America Journal 55:548-551.

Graly, J. A., P. R. Bierman, L. J. Reusser, and M. J. Pavich. 2010. Meteoric 10Be in soil profiles-A global meta-analysis. Geochimica et Cosmochimica Acta 74:6814-6829.

Graly, J. A., L. J. Reusser, and P. R. Bierman. 2011. Short and long-term delivery rates of meteoric 10Be to terrestrial soils. Earth and Planetary Science Letters 302:329-336.

Guelke, M., and F. von Blanckenburg. 2007. Fractionation of Stable Iron Isotopes in Higher Plants. Environmental Science and Technology 41:1896-1901.

Guelke, M., F. von Blanckenburg, R. Schoenberg, M. Staubwasser, and H. Stuetzel. 2010. Determining the Stable Fe Isotope Signature of Plant-Available Iron in Soils. Chemical Geology 277:269-280.

Guelke-Stelling, M. and F. von Blanckenburg. 2012. Fe isotope fractionation caused by translocation of iron during growth of bean and oat as models of strategy I and II plants. Plant and soil 352:217–231.

Hesterberg, D., M. C. Duff, J. B. Dixon, and M. J. Vepraskas. 2011. X-Ray Microspectroscopy and Chemical Reactions in Soil Microsites. Journal of Environment Quality 40.3:667-678.

Hilgard, E. W. 1860. Report on the geology and agriculture of the state of Mississippi. State Printer, East Barksdale, Mississippi.

Icopini, G. A., A. D. Anbar, S. S. Ruebush, M. Tien, and S. L. Brantley. 2004. Iron Isotope Fractionation during Microbial Reduction of Iron: The Importance of Adsorption. Geology 32:205–208.

Jacobs, P. M., L. T. West, and J. N. Shaw. 2002. Redoximorphic features as indicators of seasonal saturation, Lowndes County, Georgia. Soil Science Society of America Journal 66:315-323.

Jenny, H. 1941. Factors of soil formation: A system of quantitative pedology. Dover Publications, New York.

Johnson, D. L. 1990. Biomantle evolution and the redistribution of earth materials and artifacts. Soil Science 149:84-102.

Johnson, M. S. and J. Lehmann. 2006. Double-Funneling of Trees: Stemflow and Root-Induced Preferential Flow. Ecoscience 13:324-333.

Jones, D. L., C. Nguyen, and R. D. Finlay. 2009. Carbon Flow in the Rhizosphere: Carbon Trading at the Soil–root Interface. Plant Soil 321:5-33.

Kaste, J. M. and M. Baskaran. 2011. Meteoric 7Be and 10Be as process tracers in the environment. Pages 61-87 in M. Baskaran, editor. Handbook of Environmental Isotope Geochemistry. Springer-Verlag, Berlin.

Kiczka, M., J. G. Wiederhold, S. M. Kraemer, B. Bourdon, and R. Kretzschmar. 2010. Iron Isotope Fractionation during Fe Uptake and Translocation in Alpine Plants. Environmental Science and Technology 44:6144-6150.

Kiczka, M., J. G. Wiederhold, J. Frommer, A. Voegelin, S. M. Kraemer, B. Bourdon, and R. Kretzschmar. 2011. Iron Speciation and Isotope Fractionation during Silicate Weathering and Soil Formation in an Alpine Glacier Forefield Chronosequence. Geochimica et Cosmochimica Acta 75:5559-5573.

Lal, D. and B. Peters. 1967. Cosmic ray produced radioactivity on Earth. Pages 61-87 in K. Sitte, editor. Handbuch der Physik. Springer-Verlag, New York.

Lefler, H. T. 1967. A New Voyage to Carolina: John Lawson. University of North Carolina Press, Chapel Hill, North Carolina.

Li, J., D. deB. Richter, A. Mendoza, and P. R. Heine. 2008. Four-decade response of soil trace elements to an aggrading old-field forest. Ecology 89:2911–2923.

Li, J. and D. deB. Richter. 2012. Effects of Two-Century Land Use Changes on Soil Iron Crystallinity and Accumulation in Southeastern Piedmont Region, USA. Geoderma 173:184-191.

Lindsey, W. L. 1979. Chemical Equilibria in Soils. Blackburn Press, Caldwell, New Jersey.

Maizel, M., R. D. White, R. Root, S. Gage, S. Stitt, L. Osborne, G. Muehlbach. 1998. Historical Interrelationships Between Population Settlement and Farmland in the Conterminous United States, 1790 to 1992. Pages 5-13 in T. D. Sisk, editor. Perspectives on Land Use History of North America: A context for Understanding our Changing Environment. United State Geological Survey Technical Report, Springfield, Virginia.

Mansfeldt, T., S. Schuth, W. Häusler, F. E. Wagner, S. Kaufhold, and M. Overesch. 2012. Iron Oxide Mineralogy and Stable Iron Isotope Composition in a Gleysol with Petrogleyic Properties. Journal of Soils and Sediments 12:97-114.

Markewich, H. W., M. J. Pavich, and G. R. Buell. Contrasting soils and landscapes of the Piedmont and Coastal Plain, eastern United States. Geomorphology 3: 417-447.

Markewitz, D., D. deB. Richter, H. L. Allen, and J. B. Urrego. 1998. Three decades of observed soil acidification in the Calhoun Experimental Forest: Has acid rain made a difference?. Soil Science Society of America Journal 62:1428-1439.

Markewitz, D. and D. deB. Richter. 2000. Long-term soil potassium availability from a Kanhapludult to an aggrading loblolly pine ecosystem. Forest Ecology and Management 130:109-129.

Markewitz, D., F. Sartori, and C. Craft. 2002. Soil Change and Carbon Storage in Longleaf Pine Stands Planted on Marginal Agricultural Lands. Ecological Applications 12:1276-1285.

Marschner, H., V. Römheld, and M. Kissel. 1986. Different Strategies in Higher Plants in Mobilization and Uptake of Iron. Journal of Plant Nutrition 9:695-713.

McIntosh, R. P. 1985. The background of ecology: concert and theory. Cambridge University Press, Caimbridge, United Kingdom.

Mehra, O. P. and M. L. Jackson. 1958. Iron oxide removal from soils and clays by a dithionite-citrate system buffered with sodium bicarbonate. Clays and Clay Minerals 7:317-327.

Metz, L. 1958. The Calhoun Experimental Forest. USDA Southeastern Forest Experiment Station. Asheville, North Carolina.

Metz, L. J. and J. E. Douglass. 1959. Soil Moisture Depletion under Several Piedmont Cover Types. United States Department of Agriculture Forest Service, Washington, D. C.

Mobley, M. L. 2011. An Ecosystem Approach to Dead Plant Carbon over 50 years of Old-Field Forest. Duke University (Ph.D. Dissertation), Durham, North Carolina.

Mobley, M. L., D. deB Richter, and P. R. Heine. 2014. Accumulation and decay of woody detritus in a humid subtropical secondary pine forest. Canadian Journal of Forest Research 43:109-118.

Monaghan, M. C., S. Kreshnaswami, and J. H. Thomas. 1983. 10Be concentrations and the long-term fate of particle-reactive nuclides in five soil profiles from California. Earth and Planetary Science Letters 65:51-60.

Montgomery, D. R. 2012. Dirt: The erosion of civilizations. University of California Press, Ewing, New Jersey.

Murty, D., M. U. F. Kirschbaum, R. E. Mcmurtrie, and H. Mcgilvray. 2002. Does conversion of forest to agricultural land change soil carbon and nitrogen? a review of the literature. Global Change Biology 8:105-123.

Nelson, D. W. and L. E. Sommers, L. E. 1996. Total Carbon, Organic Carbon, and Organic Matter. Pages 961-1011 in D. L. Sparks, A .L. Page, P. A. Helmke, R. H. Loeppert, P. N. Soltanpour, M. A. Tabatabai, C. T. Johnson, and M. E. Sumner, editors. Methods of Soil Analysis Part 3: Chemical Methods. Soil Science Society of America, Madison, Wisconson.

NRCS, 2012, Technical Resources: MLRA 153A, 136, and 133A Resource Report. United States Department of Agriculture, Washington, D.C.

O'Halloran, I. P. and B. J. Cade-Menum. 2008. Total and Organic Phosphorus. Pages 265-292 in Y. K. Soon and W. H. Hendershot, editors. Soil Sampling and Methods of Analysis. Canadian Society of Soil Science, Boca Raton, Florida.

O'Neill, J. S. 1985. Cenozoic fluctuations in biotic parts of the global carbon cycle. Pages 377-396 in E. T. Sundquist and W. S. Broeke, editors. The Carbon Cycle and Atmospheric CO2: Natural Variations Archean to Present. American Geophysical Union, Washington, D.C.

O'Brien, R. G. and M. K. Kaiser. 1985. MANOVA method for analyzing repeated measures designs: an extensive primer. Psychological bulletin 97:316-333.

Odum, E. P. 1969. The Strategy of Ecosystem Development. Science 164:262-270.

Oh, N. H. and D. deB.. Richter. 2004. Soil acidification induced by elevated atmospheric CO2. Global Change Biology 10:1936-1946.

Oh, N. H. and D. deB. Richter. 2005. Elemental translocation and loss from three highly weathered soil-bedrock profiles in the southeastern United States. Geoderma 126:5-25.

Oosting, H. J. 1942. Ecological Analysis of the plant communities of Piedmont, North Carolina. American Midland Naturalist 28:1-126.

Owen, W. 2002. The History of Native Plant Communities in the South. Pages 61-87 in D. N. Wear and J. G. Greis, editors. Southern Forest Resource Assesment. United States Department of Agriculture Forest Service, Washington, D. C.

Pavich, M. J., L. Brown, J. Klein, and R. Middleton. 1984. 10Be accumulation in a soil chronosequence. Earth and Planetary Science Letters 68:198-204.

Pavich, M. J., L. Brown, J. N. Valette-Silver, J. Klein, and R. Middleton. 1985. 10Be analysis of a Quaternary weathering profile in the Virginia Piedmont. Geology 13:39:41.

Pavich, M. J. 1986. Processes and rates of saprolite production and erosion on a foliated granite rock on the Virginia Piedmont. Pages 551-590 in S. M. Coleman, and C. P. Dethier, editors. Rates of Chemical Weathering of Rocks and Minerals. Academic Press, Orlando, Florida.

Pavich, M. J., L. Brown, J. Harden, J. Klein, and R. Middleton. 1986. 10Be distribution in soils from Merced River terraces, California. Geochimica et Cosmochimica Acta 50: 1727-1735.

Pavich, M. J. 1989. Regolith residence time and the concept of surface age of the Piedmont "peneplain". Geomorphology 2:181-196.

Pedersen, H. D., D. Postma, R. Jakobsen, and O. Larsen. 2005. Fast Transformation of Iron Oxyhydroxides by the Catalytic Action of Aqueous Fe(II). Geochimica et Cosmochimica Acta 69:3967-3977.

Peebles, C. S. 1978. Determinants of Settlement Size and Location in the Moundville Phase. Pages 369-416 in B. D. Smith, editor. Mississippian Settlement Patterns. Academic Press, Waltham, Massachusetts.

Peet, R. K. and N. L. Christensen. 1987. Competition and tree death, BioScience 37:586-595.

Piatek, K, B. and H. L, Allen. 2001. Are forest floors in mid-rotation stands of loblolly pine (Pinus taeda) a sink for nitrogen and phosphorus?. Canadian Journal of Forest Research 31:1164-1174.

Piccolo, A., G. Pietramellara, and J. S. Mbagwu. 1997. Use of Humic Substances as Soil Conditioners to Increase Aggregate Stability. Geoderma 75:267-277.

Poitrasson, F. J. Viers, F. Martin, and J. J. Braun. 2008. Limited Iron Isotope Variations in Recent Lateritic Soils from Nsimi, Cameroon: Implications for the Global Fe Geochemical Cycle. Chemical Geology 253:54-63.

Raymo, M. and W. F. Ruddiman. 1992. Tectonic forcing of late Cenozoic climate. Nature 359: 117-122

Raymond, P. A., N. H. Oh, R. E. Turner, and W. Broussard. 2008. Anthropogenically enhanced fluxes of water and carbon from the Mississippi River. Nature 451: 449-452.

Renders, P. J. and G. M. Anderson. 1987. Solubility of kaolinite and beryl to 573 K. Applied Geochemistry 2:193-203.

Reséndiz-Paz, M. L., M. D. Gutiérrez-Castorena, E. Gutiérrez-Castorena, C. Ortiz-Solorio, L. Cajuste-Bontempts, and P. Sánchez-Guzmán. 2013. Local soil knowledge and management of Anthrosols: A case study in Teoloyucan, Mexico. Geoderma 193:41-51.

Richter, D. deB., D. W. Johnson, and K. H. Dai. 1992. Cation Exchange Reactions in Acid Forest Soils: Effects of Atmospheric Pollutant Deposition. Pages 341-357 in D. L. Johnson and S. E. Lindberg, editors. Atmospheric Deposition and Forest Nutrient Cycling. Springer-Verlag, New York.

Richter, D. deB., D. Markewitz, C. G. Wells, H. L. Allen, R. April, P. R. Heine, B. Urrego. 1994. Soil chemical change during three decades in an old-field loblolly pine (Pinus Taeda L.) ecosystem. Ecology 75:1463-1473.

Richter, D. deB. and D. Markewitz. 1995. How deep is soil?. Bioscience 45:600-609.

Richter, D. deB., D. Markewitz, P. R. Heine, V. Jin, J. Raikes, K Tian, and C. G. Wells. 2000. Legacies of agriculture and forest regrowth in the nitrogen of old-field soils. Forest Ecology and Management 138:233-248.

Richter, D. deB. and D. Markewitz. 2001. Understanding Soil Change: Soil Sustainability over Millennia, Centuries, and Decades. Cambridge University Press. New York.

Richter, D. deB., H. L. Allen, J. Li, D. Markewitz, and J. Raikes. 2006. Bioavailability of slowly cycling soil phosphorus: major restructuring of soil P fractions over four decades in an aggrading forest. Oecologia, 150:259-271.

Richter, D. deB. 2007. Humanity's transformation of Earth's soil: Pedology's new frontier. Soil Science. 172:957-967.

Richter, D. deB. and D. Yaalon. 2012. "The changing model of soil" revisited. Soil Science Society of America Journal 76:766-778.

Ryan, M. G., D. Binkley, and J. H. Fownes. 1997. Age-related decline in forest productivity. Advances in Ecological Research 27:213-262.

Schaetzl, R. J. and Anderson. 2005. Soils: Genesis and Geomorphology. Cambridge University Press, New York.

Schlesinger, W. H. 1990. Evidence from chronosequence studies for a low carbon-storage potential of soils. Nature 348:232-234.

Schoenberg, R. and F. von Blanckenburg. 2005. An Assessment of the Accuracy of Stable Fe Isotope Ratio Measurements on Samples with Organic and Inorganic Matrices by High-Resolution Multicollector ICP-MS. International Journal of Mass Spectrometry 242:257-272.

Schoenberg, R. and F. von Blanckenburg. 2006. Modes of Planetary-Scale Fe Isotope Fractionation. Earth and Planetary Science Letters 252:342-359.

Schoeneberger, P. J. 2013. Field Book for Describing and Sampling Soils, Version 3.0. Government Printing Office, Washington, D.C.

Schwertmann, U. and R. M. Taylor. 1989. Iron Oxides. Pages 379-427 in J. B. Dixon and S. B. Weed, editors. Minerals in Soil Evironments. Soil Science Society of America, Madison, Wisconson.

Sheldon, J. and D. F. Ritter. 1964. Rates of regional denudation in the United States. Journal of Geophysical Research 69:3395-3401.

Sparks, D. L. 2002. Methods of soil analysis-Chemical methods. Soil Science Society of America, Madison, Wisconsin.

Sparks, D. L. 2003. Environmental Soil Chemistry: Academic Press, London.

Steefel, C. I. and P. A. Van Cappellen. 1990. A new kinetic approach to modeling water-rock interaction: The role of nucleation, precursors, and Ostwald ripening. Geochimica et Cosmochimica Acta 54:2657-2677.

Stone, J. 1998. A rapid fusion method for separation of beryllium-10 from soils and silicates. Geochimica et Cosmochimica Acta 62:555-561.

Suarez, D. L. 1996. Beryllium, Magnesium, Calcium, Strontium, and Barium. Pages 575-603 in D. L. Sparks, A .L. Page, P. A. Helmke, R. H. Loeppert, P. N. Soltanpour, M. A. Tabatabai, C. T. Johnson, and M. E. Sumner, editors. Methods of Soil Analysis Part 3: Chemical Methods. Soil Science Society of America, Madison, Wisconson.

Switzer, G. L. and L. E. Nelson. 1972. Nutrient Accumulation and Cycling in Loblolly Pine (Pinus taeda L.) Plantation Ecosystems: The First Twenty Years. Soil Science Society of America Journal 36:143-147.

Takahashi, Y., Y. Minai, S. Ambe, Y. Makide, and F. Ambe. 1999. Comparison of adsorption behavior of multiple inorganic ions on kaolinite and silica in the presence of humic acid using the multitracer technique. Geochimica et Cosmochimica Acta 63:815-836.

Targulian, V. and I. Sokolov. 1978. Structural and functional approaches to the soil: Soil-memory and soil-moment. Pages 17-33 in A. M. Molchanov, editor. Mathematical modeling in ecology. Nauka, Moscow.

Targulian, V. 2001. Pedogenesis and the lithosphere. Eurasian Soil Science 34: S21-S27

Thompson, A., J. Ruiz, O. A. Chadwick, M. Titus, and J. Chorover. 2007 Rayleigh Fractionation of Iron Isotopes during Pedogenesis along a Climate Sequence of Hawaiian Basalt. Chemical Geology 238:72-83.

Tollner, E. W., W. L. Hargrove, and G. W. Langdale. 1984. Influence of conventional and no-till practices on soil physical properties in the southern Piedmont. Journal of Soil and Water Conservation 39:73-76.

Trimble, S. W. 2008. Man induced soil erosion on the Southern Piedmont. United States Soil and Water Conservation Society. Ankey, Iowa.

Trodick Jr., C. D. 2011. In situ and meteoric 10Be concentrations of fluvial sediment collected from the Potomac River Basin. University of Vermont (Master's Thesis), Burlington, Vermont.

Tsai, H., Y. Maejima, and Z. Y. Hseu. 2008. Meteoric 10Be dating of highly weathered soils from fluvial terraces in Japan. Quaternary International 188:185-196.

Turner, B. L., A. Wells, K. M. Andersen, and L. M. Condron. 2012. Patterns of tree community composition along a coastal dune chronosequence in lowland temperate rain forest in New Zealand. Plant Ecology 213: 1525-1541.

Urrego, J. B. 1993. Nutrient accumulation in biomass and forest floor of a 34-year-old loblolly pine plantation. North Carolina State University (Master's Thesis), Raleigh, North Carolina.

Valette-Silver, J. N., F. Tera, J. Klein, and R. Middleton. 1986. 10Be in geothermal systems. Geothermal Resources Council Transactions 10:161-166.

Van Lear, D. H. and P. R. Kapeluck. 1995. Above- and below-stump biomass and nutrient content of a mature loblolly pine plantation. Canadian Journal of Forest Research 25:361-367.

Vepraskas, M. J. and Lindbo, D. L. 2012. Redoximorphic Features as Related to Soil Hydrology and Hydric Soils. Pages 143-172 in H. Lin, editor. Hydropedology: synergistic integration of soil science and hydrology. Academic Press, London.

Vitousek, P. M. and W. A Reiners. 1975. Ecosystem Succession and Nutrient Retention: A Hypothesis. BioScience 25:376-381.

Walker, L.R., D. A. Wardle, R. D. Bardgett, and B. D. Clarkson, B.D. 2010. The use of chronosequences in studies of ecological succession and soil development Journal of Ecology 98:725-736.

Wardlaw, J. F. and J. B. Passioura. 1976. Transport and Transfer Processes in Plants. Academic Press, New York.

Wardle, D. A., L. R. Walker, and R. D. Bardgett. 2004. Ecosystem properties and forest decline in contrasting long-term chronosequences. Science 305: 509-513.

Watts, W. A. The Late Quaternary Vegetation History of the Southeastern United States. Annual Review of Ecology and Systematics 11:387-409.

Wear, D. 2002. Land Use. Pages 153-173 in D. N. Wear and J. G. Greis, editors. Southern Forest Resource Assesment. United States Department of Agriculture Forest Service, Washington, D. C.

Wear, D. N. and J. G. Greis. 2002. Southern Forest Resource Assesment. United States Department of Agriculture Forest Service, Washington, D. C.

Wendt, J. W. and S. Hauser. 2013. An equivalent soil mass procedure for monitoring soil organic carbon in multiple soil layers. European Journal of Soil Science 64:58-65.

West, L. T., F. H. Bienroth, M. E. Sumner, and B. T. Kang. 1997. Ultisols: Characteristics and impacts on society. Advances in Agronomy 63:179-236.

West, N., E. Kirby, P. R. Bierman, and D. H. Rood. 2011. Preliminary estimates of regolith generation and mobility in the Susquehanna Shale Hills Critical Zone Observatory, Pennsylvania, using meteoric 10Be. Applied Geochemistry 26:S146–S148.

White, P. J, and M. R. Broadley. 2003. Calcium in plants. Annals of botany 92:487-511.

Whitehead, D. R. 1973. Late-Wisconsin Vegetational Changes in Unglaciated Eastern North America. Quaternary Research 3:621-631.

Wiederhold, J. G., S. M. Kraemer, N. Teutsch, P. Borer, A. N. Halliday, and R. Kretzschmar. 2006. Iron Isotope Fractionation during Proton-Promoted, Ligand-Controlled, and Reductive Dissolution of Goethite. Environmental Science and Technology 40:3787-3793.

Wiederhold, J. G., N. Teutsch, S. M. Kraemer, A. N. Halliday, and R. Kretzschmar. 2007a. Iron isotope fractionation in oxic soils by mineral weathering and podsolization. Geochimica et Cosmochimica Acta 71:5821-5833.

Wiederhold, J. G., N. Teutsch, S. M. Kraemer, A Halliday, and R. Kretzschmar. 2007b. Iron Isotope Fractionation during Pedogenesis in Redoximorphic Soils. Soil Science Society of America Journal 71:1840-1850.

Willenbring, J. K. and F. von Blanckenburg. 2010. Meteoric cosmogenic Beryllium-10 adsorbed to river sediment and soil: Applications for Earth-surface dynamics. Earth-Science Reviews 98:105-122.

Wolfe, J. A. 1985. Distribution of major vegetational types during the Tertiary. Pages 357-375 in E. T. Sundquist and W. S. Broeke, editors. The Carbon Cycle and Atmospheric CO2: Natural Variations Archean to Present. American Geophysical Union, Washington, D.C.

Wuest, S. B. 2009. Correction of Bulk Density and Sampling Method Biases Using Soil Mass per Unit Area. Soil Science Society of America Journal 73:312-316.

Yamaguchi, K. E., C. M. Johnson, B. L. Beard, N. J. Beukes, J. Gutzmer, and H. Ohmoto, H. 2007. Isotopic Evidence for Iron Mobilization during Paleoproterozoic Lateritization of the Hekpoort Paleosol Profile from Gaborone, Botswana. Earth and Planetary Science Letters 256:577-587.

Yanai, R.D., M. A. Arthur, T. G. Siccama, and C. A. Federer. 2000. Challenges of measuring forest floor organic matter dynamics-repeated measures from a chronosequence. Contributions to Mineralogy and Petrology 149:129-140.

Yesavage, T., M. S. Fantle, J. Vervoort, R. Mathur, L. Jin, L. J. Liermann, and S. L. Brantley. 2012. Fe Cycling in the Shale Hills Critical Zone Observatory, Pennsylvania: An Analysis of Biogeochemical Weathering and Fe Isotope Fractionation. Geochimica et Cosmochimica Acta 99:18-38.

Biography

Allan Roy Bacon was born in Cottonwood, Arizona on October 26, 1982. He was raised in central Arizona, on the banks of the Verde River in the town of Clarkdale. He earned his Bachelor of Science degree (summa cum laude) in Forestry from Northern Arizona University in May of 2009, under the tutelage of Dr. Stephen C. Hart. Allan's publications include "Estimating historical atmospheric mercury concentrations from silver mining and their legacies in present-day surface soil in Potosi, Bolivia" (Atmospheric Environment 2010); "Human-soil relations are changing rapidly: proposals from SSSA's new working cross-divisional working group on soil change" (Soil Science Letters 2011); "Estimations of historical atmospheric mercury concentrations from mercury refining and present day soil concentrations of total mercury in Huancavelica, Peru" (Science of the Total Environment 2012); "Coupling meteoric ^{10}Be with pedogenic losses of ^{9}Be to improve estimates of soil residence time on an ancient North American interfluve" (Geology 2012); "Evolution of soil and ecosystem research at the Calhoun Experimental Forest" (in Research for the Long Term 2013); and "Priority research questions for soil science in the 21st century" (Soil Science Society of America Journal 2013). Allan has received The Dwight D. Billings Fellowship (Duke UPE); a Graduate Student Research Grant (GSA); an International Mentorship Grant (NSF-CZEN); a Doctoral Dissertation Improvement Grant (NSF-DEB); a Conference Travel Award (ESF); and an Honorable Mention for Outstanding Student Manuscript (Duke NSOE).